



## UNITED TECHNOLOGIES RESEARCH CENTER

(NASA-CR-159747) STUDY OF THE EFFECTS OF  
GASEOUS ENVIRONMENTS ON THE HOT CORROSION OF  
SUPERALLOY MATERIALS Final Report (United  
Technologies Research Center) 93 p  
HC A05/MF A01

N80-18155

CSCL 11F G3/26

Unclass  
47248



NASA CR-159747

**UNITED TECHNOLOGIES  
RESEARCH CENTER**



East Hartford, Connecticut 06108

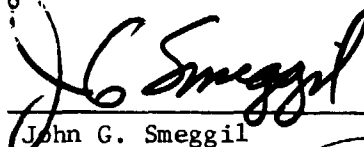
Study of The Effects of Gaseous  
Environments on The Hot  
Corrosion Of Superalloy Materials

This work was performed for

NASA-Lewis Research Center  
Contract No. NAS3-21376

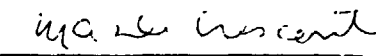
FINAL REPORT

REPORTED BY

  
John G. Smeggil

  
Norman S. Bornstein

APPROVED BY

  
M. A. DeCrescente

DATE January 1980

NO. OF PAGES \_\_\_\_\_

COPY NO. \_\_\_\_\_

1. Report No. NASA CR-159747		2. Government Accession No.		3. Recipient's Catalog No.	
4. Title and Subtitle Study of the Effects of Gaseous Environments on The Hot Corrosion of Superalloy Materials				5. Report Date November 1979	
				6. Performing Organization Code	
7. Author(s) J. G. Smeggil and N. S. Bornstein				8. Performing Organization Report No. R79-914387-4	
9. Performing Organization Name and Address United Technologies Research Center East Hartford, Connecticut 06108				10. Work Unit No.	
				11. Contract or Grant No. NAS3-21376	
12. Sponsoring Agency Name and Address National Aeronautics and Space Administration Washington, DC 20546				13. Type of Report and Period Covered <u>Contractor Report</u>	
				14. Sponsor's Agency Code	
15. Supplementary Notes NASA-Lewis Research Center, Materials and Structures Division, Cleveland, Ohio 44135. Final Report. Project Manager, Carl A. Stearns					
16. Abstract <p>Studies have been conducted to examine the effect of the gaseous corrodent NaCl on the high temperature oxidation and sodium sulfate-induced hot corrosion behavior of alumina formers, chromia formers, and the superalloy B-1900. Isothermal experiments were conducted at 900°C and 1050°C in air in the presence and absence of NaCl vapors. Microstructural changes in oxide morphology and increased rates of oxidation were observed when NaCl(g) was present. It is hypothesized that the accelerated rates of oxidation are the result of removal of aluminum from the scale-substrate interface and the weakening of the scale-substrate bonds. The aluminum removed was redeposited on scale surfaces in the form of alumina whiskers. For the superalloy B-1900, alumina whiskers are also formed, and the alloy oxidizes at catastrophic rates. In the case of Ni-25Cr alloy, NaCl vapors interact with the scale depleting it of chromium.</p> <p>With respect to sulfidation corrosion, the interactions between NaCl vapors and Na<sub>2</sub>SO<sub>4</sub> are quite complex. NaCl dissolved in the fused salt attacks alumina formers. For the chromia formers sodium sulfate limits the rates of reactions between sodium chloride and chromia.</p> <p>The overlay coating CoCrAlY subjected to thermal transients, char, and sodium sulfate deposits produced corrosion microstructures similar to those observed in Naval gas turbine engines. In the absence of the fused salt, thermal transients combined with NaCl(g) produce an alloy depleted zone with internal precipitates.</p>					
17. Key Words (Suggested by Author(s)) Corrosion, oxidation, sodium chloride, sodium sulfate, chromium, aluminum oxide, superalloys, thermogravimetry, corrosion growth morphology, low power corrosion			18. Distribution Statement Unclassified--unlimited STAR Category 26		
19. Security Classif. (of this report) Unclassified		20. Security Classif. (of this page) Unclassified		21. No. of Pages	
				22. Price*	

Study of The Effects of Gaseous  
Environments on The Hot  
Corrosion of Superalloy Materials

TABLE OF CONTENTS

	<u>Page</u>
I. INTRODUCTION . . . . .	1
II. BACKGROUND . . . . .	3
III. EXPERIMENTAL APPROACH . . . . .	6
A. Materials . . . . .	6
B. Procedures . . . . .	6
IV. EXPERIMENTAL RESULTS AND DISCUSSION. . . . .	8
A. Oxidation - Air Alone . . . . .	8
B. Oxidation - Gaseous NaCl. . . . .	8
1. Alumina Formers . . . . .	9
2. Chromia Formers . . . . .	10
3. The Superalloy B-1900 . . . . .	11
C. Hot Corrosion . . . . .	13
1. Alumina Formers . . . . .	13
2. Chromia Formers . . . . .	14
3. The Superalloy B-1900 . . . . .	16
D. Low Power Corrosion . . . . .	18
V. SUMMARY AND CONCLUDING REMARKS. . . . .	26
VI. APPENDIX I. A PROPOSED MECHANISM TO ACCOUNT FOR THE GROWTH OF CHROMIA CRYSTALS BY MOLTEN SALTS . . . . .	28
VII. ACKNOWLEDGEMENTS . . . . .	32
VIII. REFERENCES . . . . .	33
IX. TABLES and FIGURES . . . . .	37



## I. INTRODUCTION

The accelerated corrosion of gas turbine materials due to the presence of condensed salts is commonly called hot corrosion. Sulfidation attack is a form of hot corrosion in which the principle component of the condensed salt is sodium sulfate. Sulfidation corrosion has been intensively studied for more than a decade and it is realized that a solution to the sulfidation problem requires a basic understanding of the corrosion mechanism(s) so that appropriate corrective action can be taken. It is important to also realize that, based upon current knowledge, the sulfidation problem currently encountered will be a major problem for machines using coal-derived synthetic fuel oils and gases because corrodents are formed from naturally occurring impurities in the coal (Ref. 1). Furthermore, these impurities are not readily removed by current processing techniques. Corrosive compounds that are likely to be found in the hot section of turbines operating in marine and industrial environments include  $\text{Na}_2\text{SO}_4$  as well as  $\text{NaCl}$  (e.g. Ref. 2-4).

The critical step in the corrosion phenomenon, sulfidation attack, is the destruction of the normally protective oxide layer which separates the fused salt from the substrate. Thus an understanding of the various mechanisms by which the normally protective scales are rendered ineffectual is a prerequisite for the attenuation of and/or prevention of corrosion. In laboratory tests it has been shown that one means by which the normally protective layer is rendered ineffectual is by dissolution of the oxide as a result of interaction between the scale and oxide ions present in the melt. Other means by which the normally protective scale can be compromised include (a) local reducing conditions, (b) mechanical erosion, (c) mechanical faults accompanying oxide growth, (d) thermal stresses, (e) superimposed operating stresses, and (f) mechanical disruption resulting from chemical reactions (Refs. 5-11). However, the mechanism which relates to scale breakdown as a result of chemical reactions with various chemical species present in the gas phase has received little attention and is little understood even though it is potentially as important as any other mechanism. Hence the main thrust of this work is directed toward understanding the mechanism(s) by which the protection normally afforded by alumina and chromia scales is compromised as a result of chemical reactions involving reactants present in the gas phase.

Accelerated corrosion has been reported to occur in some Navy gas turbines that operate at reduced power levels (Ref. 12). An explanation offered to account for such corrosion involves the acidic fluxing of protective alumina scales by molten salts in the presence of  $\text{SO}_3$  ( $\text{SO}_2/\text{O}_2$ )-containing atmospheres at temperatures of about  $1300^\circ\text{F}$  ( $704^\circ\text{C}$ ) (Ref. 12). However, in addition to lowered metal temperatures, low power engine operation also implies reduced air flows and burner temperatures. Under such conditions, the deposition

of salts and combustion products are altered as compared with those experienced during engine operation at normal power levels (Ref. 2). Hence experiments were conducted to determine the effects of such exposure to protective CoCrAlY coatings without  $\text{SO}_3(\text{SO}_2/\text{O}_2)$  additions to test atmospheres.

This work was supported by the NASA-Lewis Research Center under Contract No. NAS3-21376; Mr. Carl A. Stearns, NASA Project Manager.

Three previous quarterly reports were issued under this contract:

1. Smeggil, J. G.: Study of the Effects of Gaseous Environments on the Hot Corrosion of Superalloy Materials, First Quarterly Report, R78-914387-1, work conducted for NASA-Lewis Research Center, Contract No. NAS3-21376, December, 1978.
2. Smeggil, J. G.: Study of the Effects of Gaseous Corrodants on the Hot Corrosion of Superalloy Materials, Second Quarterly Report, R79-914387-2, work conducted for NASA-Lewis Research Center, Contract No. NAS3-21376, March, 1979.
3. Smeggil, J. G.: Study of the Effects of Gaseous Environments on the Hot Corrosion of Superalloy Materials, Third Quarterly Report, R79-914387-3, work conducted for NASA-Lewis Research Center, Contract No. NAS3-21376, July, 1979.

## II. BACKGROUND

All structural alloys are, with respect to the high temperature oxidizing environments, thermodynamically unstable and react to form surface layers or scales. The composition and the adherence of such scales depends in part upon substrate and environmental compositions as well as the parameters time and temperature.

Oxidation is the general term used to describe the formation and growth of the surface oxide layer(s) that develops on structural materials. Hot corrosion is the phrase used to describe the accelerated oxidation associated with the presence of molten salts. The principle constituents of such salts found on hot gas path turbine component surfaces are the alkali sulfates. Moreover, discrete sulfide particles are commonly observed near surfaces of materials which have undergone hot corrosion effects resulting from sodium sulfate deposits. Thusly, the terms "hot corrosion" and "sulfidation" are frequently used interchangeably. Moreover, because sea salt crystals are ever present in the air and inadvertently present in liquid fuels, hot corrosion (or sulfidation) is a major concern to both users and producers of gas turbine engines.

In investigating sulfidation corrosion, researchers have studied both the chemical reactions that occur between fused alkali salts and metallic substrates and the mechanisms by which salts deposit onto turbomachinery. It is generally agreed that the source of the corrosive alkali is sea salt crystals and that the condensed salt always associated with sulfidation corrosion is primarily sodium sulfate. Many mechanisms have been proposed to account for the deposition of salts onto turbomachinery. However, in addition to condensed salt deposits, gas turbine components will also be exposed to atmospheres containing low partial pressures of chloride-bearing species. Stearns et al. (Ref. 3) and Kohl et al. (Ref. 4) have reported that gaseous NaCl is expected to be the major sodium-bearing species in the hot section of the gas turbine.

In previously reported studies aimed at defining the role of gaseous corrodents, the United Technologies Research Center, undertook to examine the effects of gaseous environments on the sulfidation attack of superalloys (Ref. 13). The results of that study are succinctly summarized thusly:

1. Gaseous NaCl and HCl interact with and modify the oxide scale that forms on the intermetallic compound NiAl. Specifically, it was shown that, during isothermal oxidation in the presence of such gaseous halides, the oxide scale was covered with numerous alumina whiskers. The size and density of such whiskers are NaCl(g) concentration dependent. It was also shown that increasing the concentration of NaCl(g) increases the number of whiskers while the individual whisker size is decreased.

2. Experiments were conducted to determine if the  $\text{Al}_2\text{O}_3$  whiskers were formed by rearrangement of the surface  $\text{Al}_2\text{O}_3$  or if they originated from aluminum at the metal-oxide interface. Neither impure nor high purity dense alumina developed  $\text{Al}_2\text{O}_3$  whiskers on exposure to  $\text{NaCl(g)}$ -bearing atmospheres. Thus, it was concluded that the aluminum source for the  $\text{Al}_2\text{O}_3$  whisker formation is not at the surface, i.e., the gas-scale interface. It was proposed that a halogen-containing species reacts with the alloy substrates to form an "Al-NaCl" vapor moiety which diffuses through the alumina scale and reacts with oxygen at the free surface to form alumina whiskers. The precise nature of this "Al-NaCl" species is as yet unknown. Such a transport mechanism is consistent with the observation of isothermal rupture, spallation, and reformation of protective alumina scales.
3. At the 10 ppm level, the concentration of NaCl is sufficient to rupture protective alumina scales. In this study it was found that the NaCl concentration in a laboratory box furnace atmosphere was about 20 ppm.
4. In the presence of sodium sulfate deposits and with NaCl vapors in test atmospheres, alumina whiskers are produced. At  $1050^\circ\text{C}$  in the presence of  $\text{NaCl(g)}$  vapors, incubation periods associated with sulfidation are prolonged. To account for this observation, it was proposed that the "Al-NaCl" species removes oxygen from  $\text{Na}_2\text{SO}_4$  to form alumina whiskers. Furthermore, the newly formed alumina reacts with sodium oxide present in the condensed salt to further delay the sulfidation-initiation process.
5. NaCl vapors were also shown to interact with chromia-rich scales. At  $900^\circ\text{C}$   $\text{NaCl(g)}$  was shown to react with chromia-rich scales to produce "S" shaped curves. An "S" shaped curve is indicative of "breakaway" oxidation where the rate of oxygen pickup is noticeably increased as a result of scale rupture. Based upon metallographic and x-ray diffraction studies, the oxide scale formed in the presence of  $\text{NaCl(g)}$  is composed of both the spinel,  $\text{NiCr}_2\text{O}_4$ , and  $\text{Cr}_2\text{O}_3$ . Moreover, areas are observed where chromia depletion is markedly evident. The formation of the spinel and the loss of chromium is consistent with the formation of volatile chromium-containing species. Stearns et al., and Fryburg et al., have shown that the vapor species responsible for the loss of chromium from the alloys primarily are  $(\text{NaCl})_x\text{CrO}_3(\text{g})$ ,  $x = 1, 2, 3$ , and  $(\text{NaOH})_x\text{CrO}_3(\text{g})$ ,  $x = 1, 2$  (Refs. 14, 15). When Ni-25Cr and chromium specimens are coated with  $\text{Na}_2\text{SO}_4$  and subsequently exposed to air and gaseous NaCl, "S" shaped oxidation

curves are not observed. It appeared as if  $\text{Na}_2\text{SO}_4$  mitigates the deleterious effect of  $\text{NaCl(g)}$  although the mechanism by which this occurs was not known.

6. Lastly, the role of reducing agents was examined and it was found that finely divided carbon co-deposited with  $\text{Na}_2\text{SO}_4$  onto  $\text{NiAl}$  decreased the rate of corrosion at  $900^\circ\text{C}$ , but exhibited no effect at  $1050^\circ\text{C}$ . For the chromia-forming  $\text{Ni-25Cr}$  alloy, the data suggested that carbon influenced isothermal scale breakage, but the cause was not known.

Accelerated corrosion has been observed to occur in some Navy gas turbine engines that operate predominantly at reduced power (Ref. 12). Because low power operation implies reduced air flows, burner temperatures, and metal temperatures, the concentration of  $\text{NaCl(g)}$  in the environment and rate of deposition of salts and combustion products are changed. Amplifying briefly on this, the anticipated effects of low power engine operation include carbon formation during initial engine ignition and shutdown. Furthermore unlike operation at normal power levels, carbon-enriched atmospheres and the production of fuel chars have been reported for Naval gas turbines during operation at reduced power levels (Ref. 2). Thus, for a gas turbine operated in a cyclic mode, frequent opportunities exist for either unburnt fuel or fuel chars to impact turbine hardware and locally burn. Moreover such carbon, unlike the quickly burning powders used in the prior study (Ref. 13), can exist for prolonged durations at elevated temperatures. Burn-off rates for carbon have been previously reported to strongly depend on the form in which it is present (Ref. 16). Although the effect of strictly reducing atmospheres on corrosion processes has been reported (Ref. 17), the effect of alternating oxidizing/reducing conditions on  $\text{Na}_2\text{SO}_4/\text{NaCl(g)}$ -induced hot corrosion has been largely overlooked.

The objectives of the study reported herein are to confirm that the conclusions based upon the initial short term experimental data (Ref. 13) are also valid for long term tests; to investigate the role of reactive additions; and to determine effects of alternating oxidizing/reducing conditions on  $\text{Na}_2\text{SO}_4\text{-NaCl(g)}$  hot corrosion.

### III. EXPERIMENTAL APPROACH

#### A. Materials

The composition of the alloys employed in this study are listed in Table I. The NiAl and CoCrAl specimens were prepared by arc-melting buttons under an argon atmosphere which were then annealed at 1300°C (2370°F) for 24 hours in flowing hydrogen. The Ni-25Cr and Ni-40Cr specimens were prepared by induction melting the metals in an alumina crucible for 20 minutes under an argon atmosphere after which time the specimens were annealed for 24 hours at 1100°C (2010°F) in hydrogen.

The nominal composition for the B-1900 alloy used here is 64.0 w/o Ni; 8.0 w/o Cr, 10.0 w/o Co, 6.0 w/o Mo, 4.0 w/o Ta, 2.0 w/o Nb, 4.5 w/o Al, 2.0 w/o Ti, 0.13 w/o C, 0.018 w/o B, and 0.06 w/o Zr (Ref. 18). The CoCrAlY (IM6250) coating used is nominally 18-24 w/o Cr, 12-14 w/o Al, 0.5-0.75 w/o Y, balance Co, applied over a Mar-M509 substrate (10.0 w/o Ni, 23.5 w/o Cr, 55.0 w/o Co, 7.0 w/o W, 3.5 w/o Ta, 0.2 w/o Ti, 0.60 w/o C, and 0.50 w/o Zr) (Ref. 18). The coating was applied by physical vapor deposition (PVD) techniques and subsequently given a standard heat treatment (4 hours at 1079°C [1975°F] in argon).

The pure chromium used in limited tests was supplied by Mr. C. A. Stearns, NASA-Lewis Research Center. The 4N+ purity material did contain trace levels of calcium as determined by energy dispersive analyses.

All specimens were machined to approximately 2.5 cm x 1.0 cm x 0.2 cm (6.4 cm sq. surface area) and ground with 600 grit SiC. A platinum support wire was used to suspend all specimens, and prior to insertion into the experimental apparatus they were washed and degreased; the final rinse was absolute ethanol.

The air used in all experiments was passed over anhydrous calcium sulfate (Drierite) to reduce water vapor levels. The average air flow was 300 scc/min. which corresponds to a flow velocity of 0.19 cm/sec. The sodium chloride, sodium sulfate, sodium chromate and ammonium chromate used in the study were ultrapure or analytical reagent grade, or the highest purity obtainable, and were obtained from the Alfa-Ventron Products. Lastly, the HCl gas used in this program was purchased commercially as primary standard HCl-N<sub>2</sub> mixtures.

#### B. Procedures

All oxidation experiments were conducted using an Ainsworth type RV-AU-1 balance which is readable to 0.01 milligrams and reproducible to  $\pm 0.03$

milligrams. The specimens were introduced into a quartz tube (2.5" O.D.) which was heated by a three zone Marshall furnace maintained at  $\pm 5^{\circ}\text{C}$  of the set temperature by a Leeds and Northrup proportional controller series 60.

The sodium chloride vapors were generated from the fused salt held in a platinum crucible on a movable pedestal within the quartz tube. The temperature of the crucible was measured by thermocouples lying immediately adjacent to the pedestal. The concentration of sodium chloride gas was determined from the differences in weights of the platinum crucible before and after each experiment and the mass flow of air. The weight change data for the samples exposed to the sodium chloride vapors were corrected for condensation of the salt onto the platinum suspension wires. At the 10 and 100 ppm sodium chloride levels, the correction factors are  $1 \times 10^{-3}$  and  $3.98 \times 10^{-2}$  milligrams per hour respectively.

Sodium sulfate was applied onto preheated specimens from an air aerosol spray of the aqueous solutions. The quantity of salt applied was determined by weighing the test specimen before and after the coating application. Chromia coatings were formed by the thermal conversion of ammonium chromate to chromia which occurs during exposure at elevated temperatures. The sodium sulfate deposits examined here corresponded to  $1.0 (\pm 10\%) \text{ mg/cm}^2$  of the calculated specimen's surface area. For mixed sodium sulfate-chromia deposits, an aqueous solution of 1 part by weight  $\text{Na}_2\text{SO}_4$  to 2.2 parts by weight  $(\text{NH}_4)_2\text{CrO}_4$  was used to effect deposits of  $3.2 (\pm 10\%) \text{ mg/cm}^2$ . The sodium sulfate component of such a deposit mixture would correspond to  $1.0 (\pm 10\%) \text{ mg/cm}^2$ .

In experiments designed to simulate low power gas turbine operation, thermal spikes were used to simulate the effect of char deposits forming and burning off in situ on turbine hardware surfaces. The laboratory test involved inserting CoCrAlY-coated test specimens into a box furnace preheated to  $1300^{\circ}\text{C}$  ( $2370^{\circ}\text{F}$ ) for durations up to 30 seconds. Char particles were formed when salt-coated specimens were exposed with 5 to 3 cc of Diesel No. 2 fuel. Unlike the commercially available carbon, the chars formed as described above burn slowly and survive for several hours at  $700^{\circ}\text{C}$  ( $1290^{\circ}\text{F}$ ). Lastly, the quantity of char in some tests was increased by the addition of 5 cc of Stycast-1260A\*, an epoxy resin which contains approximately 0.1 w/o chloride. Subsequent to the brief exposure in the high temperature furnace, specimens were aged in air for several hours at  $700^{\circ}\text{C}$  ( $1290^{\circ}\text{F}$ ) to simulate turbine operation under steady state conditions.

\* An epoxy used for mounting specimens for metallographic examination and produced by Emerson & Cuming, Incorporated, Canton, Massachusetts.



#### IV. EXPERIMENTAL RESULTS AND DISCUSSION

##### A. Oxidation-Air Alone

In order to establish a base-line from which meaningful comparisons were made, the alloys described in Table 1 were isothermally oxidized in air at 700°, 900° and 1050°C. Moreover, experiments involving NiAl, Ni-25Cr and B-1900 at 900° and 1050°C were conducted for 100 hour test periods while all other experiments were performed at 700°C and for durations of approximately twenty-four hours.

The NiAl and NiAl-base alloys as well as the CoCrAlY compositions formed, upon exposure at elevated temperatures, thin dense alumina scales, e.g., Fig. 1. The oxidation kinetics for the various NiAl and CoCrAl compositions modified by yttrium and hafnium addition were similar to that of NiAl alone, cf. Fig. 2.

The oxidation behavior of the various Ni-Cr alloys listed in Table I were also well behaved in that the scales formed were as described by numerous investigators (e.g., Refs. 19,20,21). The oxidation kinetics for these alloys were analogous to that for the Ni-25Cr composition, Fig. 3. In general, a chromia scale was observed on the surfaces of the alloys with a wide variation in oxide grain sizes and shapes. At 1050°C the surfaces exhibited a rumpled appearance with numerous mounds protruding from the surface, Fig. 4. Metallographic examination revealed the typical scale morphologies associated with these chromia formers as shown in Fig. 5.

Lastly, the oxidation behavior of the nickel base superalloy B-1900 was quite complex, Fig. 6. At low temperature, 700°C, the oxide formed after 100 hours is rich in chromium. At 900 and 1050°C, a more heterogeneous oxide structure is observed as described by Fryburg et al. (Ref. 22). The surface oxide consists of alternate areas rich in chromium and nickel with areas rich in aluminum. Metallographic examination of the B-1900 alloy specimens shows that the oxide scale is separated from the unaffected matrix by a narrow zone devoid of gamma prime, Fig. 7.

##### B. Oxidation-Gaseous NaCl

It has been previously reported that gaseous NaCl interacts with growing oxide scales on model alumina and chromia formers (Ref. 13). Based upon the limited short term data, simple models were proposed. The results of the present study confirm the previous findings and further increase the knowledge of hot corrosion.

## 1. Alumina Formers

It was previously reported (Ref. 13) that, in the presence of low concentrations of gaseous NaCl and HCl, alumina whiskers are formed on the surface of the oxide scale.

The source of aluminum for whisker growth was experimentally determined to lie below the scale. It was previously proposed that some as yet unidentified halogen-bearing species diffuses through the dense alumina scales, and at the metal-substrate interface, where the oxygen potential is reduced, reacts with the substrate to form an "Al-NaCl" species. This moiety then diffuses back through the dense alumina scale and oxidizes at the free surface to form the alumina whiskers (Ref. 13).

Based on this model, it was hypothesized that the continual transport of aluminum from the alloy-oxide interface would ultimately result in scale rupture. In agreement with previous studies (Ref. 13), the alumina formers upon exposure to gaseous NaCl at 900 and 1050°C formed numerous alumina whiskers on oxide surfaces. Again in agreement with prior results (Ref. 13), EDAX examination confirmed only the presence of aluminum with no traces of sodium or chlorine on external specimen surfaces.

For specimens oxidized in air with NaCl(g) the weight gain data was in agreement with the previously reported behavior (Ref. 13), Figs. 8 and 9. During the first 24 hours, there was no evidence of isothermal scale spallation at either test temperature, Figs. 8 and 9. However, as shown in Figs. 8 and 9, it is apparent, as noted by the discontinuities in the weight gain curves, that during prolonged exposures aperiodic isothermal scale rupture occurred. Moreover, the magnitude of such weight change discontinuities appears to increase with increasing salt concentration.

Examination of the spalled and retained scales by scanning electron microscopy and EDAX techniques reveals the presence of multilayers of essentially pure alumina, Fig. 10. It also is apparent that the external alumina layer is poorly attached to the underlying protection alumina scale, Fig. 10, and both scales are highly faceted. Moreover, such exaggerated faceting of alumina crystals even exists at the scale-substrate interface, Fig. 10. On the other hand, scales produced by exposure to air alone do not exhibit such highly faceted crystals at this interface, cf. Fig. 1.

Additionally, the normal alumina scale is bonded to the NiAl substrate in numerous areas, as shown in Fig. 11a. The density of attachment sites (or metallic pegs) is very high. However, when NaCl(g) is present, the density of such points of attachment is sharply reduced, as shown in Fig. 11b.

Thus, it is concluded that the  $\text{NaCl(g)}$  reacts with the substrate at the metal-oxide interface, removing aluminum and thereby forming voids and reducing the number of attachment sites or pegs, which eventually results in scale cracking or spallation and the attendant increased rates of oxidation.

The oxides of sulfur are commonly present in most gas turbine environments. Because  $\text{NaCl(g)}$  can react with oxides of sulfur to form alkali sulfates, a series of experiments was conducted to determine if the presence of  $\text{SO}_2$  would alter any of the findings previously discussed. Specifically, concern was expressed that the presence of  $\text{SO}_2$  would effectively block the transport mechanism responsible for the production of alumina whiskers. It is realized, however, that  $\text{HCl}$  had produced similar morphological changes on  $\text{NiAl}$  substrates in prior studies (Ref. 13). Furthermore, if any reaction would occur between  $\text{NaCl(g)}$ ,  $\text{SO}_2$ , and  $\text{H}_2\text{O}$ , a likely product would be  $\text{HCl(g)}$ . As shown in Fig. 12, when  $\text{SO}_2$  was admitted into the system, alumina whiskers continued to form on the scales. Thus, sulfur oxides do not inhibit the transport processes responsible for alumina whisker formation.

Lastly, although this discussion has dealt with  $\text{NiAl}$ , alumina whiskers were similarly produced, as expected, when  $\text{CoCrAlY}$  was exposed to oxidation in the presence of  $\text{NaCl}$  vapors, Fig. 13.

## 2. Chromia Formers

The chromia formers listed in Table I are generally well behaved and oxidized at slow and controlled rates. Nevertheless, in the presence of gaseous  $\text{NaCl}$ , the weight gain curves were described as "S" shaped, which are associated with break-away oxidation kinetics (Ref. 13). Because isothermal scale rupture effects occurred only once during the early stages of oxidation, it was hypothesized that, after the gaseous  $\text{NaCl}$  reacts with the protective oxide, the scale that reforms is not a continuous protective chromia scale (Ref. 13).

In the experiments described in the present study, the introduction of gaseous  $\text{NaCl(g)}$  once again promoted the formation of "S" shaped weight gain curves or breakaway oxidation during the early stages of oxidation at both  $900^\circ\text{C}$  and  $1050^\circ\text{C}$ , Fig. 14. At  $900^\circ\text{C}$  the rate of oxidation of the chromia former  $\text{Ni-25Cr}$  is markedly affected by  $\text{NaCl}$ , the magnitude of the weight gain increasing with increasing  $\text{NaCl(g)}$  concentration, Fig. 15. However, at  $1050^\circ\text{C}$ , an inverse relationship is noted, Fig. 16. The effect of  $\text{NaCl(g)}$  is greater at the 12 ppm level than at the 113 ppm level. In order to further examine this apparent anomaly, a series of experiments was conducted in which the concentration of  $\text{NaCl(g)}$  was increased from 113 to 400 ppm. As shown in Fig. 16, the increase in concentration from 113 to 400 ppm caused an increase in the rate of oxidation of the alloy. Therefore, the experiments conducted at the 10 and 100 ppm levels were repeated and the results were the same: that is, at 100 ppm level the magnitude of the final weight gain is less than that for both the 10 ppm and 400 ppm levels.

Metallographic and scanning electron microscopy studies of the surfaces of Ni-25Cr consistently revealed oxide blisters rich in nickel and almost totally void of chromium, Fig. 17. Surprisingly, loose non-adherent chromia crystals were frequently observed on the surfaces of such chromium-poor oxide scales which appeared as surface blisters. Chromium depletion and nickel-enrichment was normally observed on the surface oxides of specimens exposed for twenty-four hours to air with NaCl vapors (Ref. 13). However the extent of such chromium depletion observed here in these localized blistered oxide regions has been markedly increased by prolonged exposure to such conditions.

Lastly, based on extensive scanning electron microscopy and EDAX studies, although large areas of the surface oxide are virtually void of chromium, the oxide at the interface is chromium-rich. Such exaggerated duplex structures were only observed in the case of specimens oxidized in NaCl(g)-containing atmospheres. Thus, during oxidation of the chromia-forming alloys, the composition of the oxide scale exposed to the NaCl vapors continually changed. Based upon the experimental results, it is postulated that the NaCl gas reacts with and removes chromium from the scale, altering the composition from the original protective chromia to that of the spinel and lastly to virtually pure nickel oxide with trace levels of chromium. Thus, unlike systems where the NaCl(g) causes repeated isothermal scale breakage, the initial protective chromia scale, once cracked, does not reform.

### 3. The Superalloy B-1900

B-1900 is a nickel base superalloy and is characteristic of the family of superalloys developed to exhibit exceptionally high temperature strength and good oxidation properties, but unfortunately it has poor hot corrosion resistance. In simple oxidation the alloy forms a variety of oxide scales, the composition of the predominant scale depending upon temperature and duration of exposure.

The effect of gaseous NaCl on the oxidation behavior of the superalloy B-1900 was most unexpected and dramatic. At the low NaCl(g) levels employed in this study, the superalloy oxidized at catastrophic rates. At 900°C at both 10 and 100 ppm NaCl(g) levels, the amount of oxidation of the alloy was comparable to or greater than that observed when the alloy is coated with sodium sulfate and oxidized in air alone, Fig. 18. Although the magnitude of the weight change varied from experiment to experiment, the net result was quite reproducible. In almost all tests, the oxidation of the alloy after prolonged exposure to either 10 or 100 ppm of NaCl(g) was catastrophic. Furthermore, at the end of 100 hour test periods, the rates of oxidation for specimens exposed at 900°C to NaCl(g)-bearing atmospheres were greater than that for specimens coated with Na<sub>2</sub>SO<sub>4</sub> (1 mg/cm<sup>2</sup>). In fact, the amount of weight gain for specimens exposed to 100 ppm NaCl(g) levels was greater than that for specimens coated with Na<sub>2</sub>SO<sub>4</sub> at the end of 100 hour test periods.

Both the rate and the amount of oxidation of the B-1900 alloy exposed at 1050°C to 10 ppm NaCl was comparable to that observed for simple oxidation. However, when the concentration of NaCl(g) was increased to 100 ppm, the alloy oxidized at rapid rates, Fig. 19, but not at the catastrophic rate noted at 900°C.

The oxide scales formed on the surfaces of the nickel base superalloy were examined by scanning electron microscopy and EDAX. Alumina whiskers were noted on the surfaces of the NaCl exposed scale, a surface oxide characteristic similar to that seen on similarly tested NiAl specimens. EDAX analyses of metallographically prepared cross sections of specimens exposed at 900°C revealed the presence of a laminated oxide structure and enrichments of molybdenum near the metal-scale interface, Fig. 20. The surface of selected specimens were immersed in distilled water, and the only cation noted was molybdenum. Molybdenum trioxide is slightly soluble in water (Ref. 23).

On the other hand, B-1900 specimens exposed for 100 hours at 1050°C to NaCl(g) at 100 ppm levels indicated only a few small oxide pits, Fig. 21. EDAX examination of these oxide pits, Fig. 22, revealed enrichments of chromium and aluminum but not molybdenum as was found in specimens tested at 900°C. Metallographic cross-sections of B-1900 specimens tested at 1050°C in air with 10 ppm levels of NaCl(g) were similar to those tested at 1050°C in air alone.

B-1900 was also exposed at 700°C to air with 10 ppm NaCl vapors. Oxidation kinetics were not accelerated and were similar to that found for exposure to air alone. However, examination of the NaCl exposed surfaces indicated structures dramatically different from those formed on exposure to air alone, Fig. 22. The specimen exposed to air alone shows a chromium-enriched oxide layer covering the alloy matrix with localized blooms of tantalum-rich oxides which derived from the MC carbide network in the alloy. In the presence of NaCl vapors, in addition to alumina whiskers, well-formed crystals of nickel-rich oxide, titanium-rich oxides, chromium oxides and probably molybdenum oxides also occur. On the other hand, on surfaces of specimens of B-1900 exposed to temperatures of 900 and 1050°C in NaCl(g)-bearing atmospheres, the only well-formed highly geometric crystals were the alumina whiskers.

The mechanism proposed earlier to account for the formation of alumina whiskers by NaCl vapors can also be used to explain the dramatic increase in oxidation at 900°C of the nickel base superalloy B-1900 in the presence of NaCl vapors. As previously noted during short term exposures, alumina whiskers form on the surfaces of the scale. The formation of these whiskers depletes the alloy of aluminum, weakens the substrate, and cracks form within the scale. The isothermal spallation of the scale would not in itself account for the extremely rapid rates of oxidation. However, as shown by the scanning electron microscopy and EDAX analysis, localized enrichments of molybdenum are observed at the scale-substrate interface. Therefore, it is hypothesized that as a result of aluminum depletion,

the scale cracks, locally oxidizing the substrate alloy which has become enriched in molybdenum and other alloying elements. At elevated temperatures, the liquid  $\text{MoO}_3$  readily reacts with and dissolves oxide scales. The accelerated oxidation of alloys due to the accumulation of molybdenum oxides is not new and has been previously reported by Leslie and Fontana (Ref. 24). At  $1050^\circ\text{C}$  the rates of evaporation of  $\text{MoO}_3$  and the pressures needed to contain the liquid are excessive, hence the reduction in the rates of accelerated oxidation. On the other hand, at  $700^\circ\text{C}$  accelerated attack was not encountered even though substantial interaction between the  $\text{NaCl(g)}$  and the oxide scale did occur. The likely cause of this absence of accelerated oxidation kinetics relates to the melting point of  $\text{MoO}_3$ , which is  $795^\circ\text{C}$  (Ref. 20) or  $95^\circ\text{C}$  above the  $700^\circ\text{C}$  test temperature.

### C. Hot Corrosion

#### 1. Alumina Formers

The sulfidation behavior of the intermetallic compound  $\text{NiAl}$  has been studied by numerous investigators, and the experimental results reported herein are in agreement with the literature. At both  $900^\circ\text{C}$  and  $1050^\circ\text{C}$ , the intermetallic compound reacts with the fused salt to form a nonprotective oxide scale. Metallographic examination revealed the presence of a nonadherent oxide scale and sulfides precipitated in the alloy depletion zone which separates the unaffected matrix from the corrosion product.

It was previously shown (Ref. 13) that at  $900^\circ\text{C}$  the presence of  $\text{NaCl(g)}$  had no effect on the thermogravimetric data of sodium sulfate-coated  $\text{NiAl}$ .

However, at  $1050^\circ\text{C}$  as  $\text{NaCl(g)}$  was admitted into the environment, the rate of oxidation of the  $\text{Na}_2\text{SO}_4$ -coated  $\text{NiAl}$  decreased (Ref. 13). At the 200 ppm level, no sulfidation corrosion was noted for a twenty-four hour test period. A model was proposed in which it was suggested that the reduction in the rates of corrosion of the sodium sulfate-coated  $\text{NiAl}$  is related to the formation of a volatile " $\text{Al-NaCl}$ " species whose stability is oxygen dependent, and at the sodium sulfate-air interfaces reacts with both oxygen and oxide ions to form alumina (Ref. 13).

As shown in Fig. 24, the addition of  $\text{NaCl(g)}$  to the environment prolongs the duration of the incubation period and does markedly reduce the magnitude of the weight gain of sodium sulfate-coated  $\text{NiAl}$  specimens tested at  $1050^\circ\text{C}$ . However, at the end of the 100 hour test period, the rate of weight change is similar for specimens tested in air alone or in air with up to 100 ppm  $\text{NaCl(g)}$ . Thus, the  $\text{NaCl}$  vapors in the concentration range studied here have increased the time until accelerated oxidation kinetics occur but do not prevent their eventual occurrence. Metallographic examination of the specimens removed after 100 hours

exposure show that the NiAl did react with the fused salt; the attack was sporadic, nonuniform, and did produce characteristic alloy depleted zones with sulfide precipitates. In other areas the aluminum content of the alloy was reduced sufficiently to promote the typical Widmanstatten structure associated with nickel-rich NiAl, and areas of gamma prime,  $\text{Ni}_3\text{Al}$ , were also observed, Fig. 25.

Thus, gaseous  $\text{NaCl(g)}$  can postpone the accelerated oxidation kinetics associated with sulfidation corrosion, but the net result is alloy attack. It was previously shown that at  $1050^\circ\text{C}$ , the introduction of  $\text{NaCl(g)}$  decreased the magnitude of the weight gain for  $\text{Na}_2\text{SO}_4$ -coated NiAl. In fact, at the 200 ppm level the rate of weight gain was similar to that observed for simple oxidation. It has been proposed that the rate of evaporation of the fused salt is increased as  $\text{NaCl}$  dissolves in the  $\text{Na}_2\text{SO}_4$ . Increased rates of vaporization of  $\text{Na}_2\text{SO}_4$  due to  $\text{NaCl}$  had been reported by Felten and Pettit (Ref. 25) and Radzavich and Pettit (Ref. 26). However, Stearns et al. (Ref. 27) has shown that this effect is at best minimal. In the current study it is observed that little, if any, of the original salt deposit is present after 100 hours, and alumina crystals are noted on the surface scale. Because the source of the aluminum for whisker formation originated at the scale-metal interface, it is postulated that the increased rate of salt loss is due to reactions between the transient " $\text{NaCl-Al}$ " species and  $\text{Na}_2\text{SO}_4$ ; a product of the reaction is alumina and sulfur oxides.

Lastly, it should be noted that although addition of reactive elements did not influence isothermal oxidation rates, yttrium additions at the 0.2 w/o level significantly increased corrosion rates of the NiAl, Fig. 26. Hafnium additions at the levels tested here similarly worsened the hot corrosion behavior of NiAl. For the various CoCrAl compositions, reactive metal additions did not alter the thermogravimetric behavior exhibited by the CoCrAl composition itself, Fig. 27.

## 2. Chromia Formers

The alloys which form chromia scales are most resistant to sulfidation corrosion. All the Ni-Cr alloys tested here with sodium sulfate deposits yielded similar results. Specifically, specimens tested at  $1050^\circ\text{C}$  show sharp weight gain - weight loss kinetics for brief periods then slow oxidation kinetics, Fig. 28. On the other hand, similar effects also occur at  $900^\circ\text{C}$  but at much slower rates, Fig. 29. In fact, 24 hour experiments do not adequately show the full extent of weight loss behavior. Weight loss behavior is thought to result from volatilization effects involving principally sulfur oxides and sodium chromate. These results are in agreement with thermogravimetric data presented by Wright et al. (Ref. 28), Bornstein and DeCrescente (Ref. 9), and our previous studies (Ref. 13).

Moreover, as shown by Stearns et al. (Ref. 14), and Fryburg et al. (Ref. 15), gaseous  $\text{NaCl}$  reacts with and transports chromium as the vapor species  $(\text{NaCl})_{1,2,3}$ ,  $\text{CrO}_3(\text{g})$ , and  $(\text{NaOH})_{1,2} \text{CrO}_3(\text{g})$ .  $\text{NaOH}$  here derives from the hydrolysis of  $\text{NaCl}$ .



Both prior studies (Ref. 13) and our current results have shown that continual exposure of chromia formers to oxidizing atmospheres with NaCl vapor present results in the depletion of chromium from the oxide scale and breakaway kinetics.

It was previously shown (Ref. 13) that the detrimental effects of the gaseous corrodents appears, in the limited 24 hour tests, to be mitigated by sodium sulfate. It is known that chromia acts with and lowers the oxide ion content of sodium sulfate thereby imparting sulfidation inhibition. In the process, chromate salts are formed which lead to the growth of chromia crystals in the form of well-formed platelets on the surface of the oxide scale (Refs. 13, 28). The mechanism by which such crystals are formed is independent of the presence of sodium chloride vapors and so will not be discussed further here, cf. Appendix I.

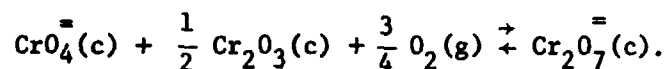
The production, however, of such crystals is highly temperature dependent, occurring rapidly at 1050°C and much more slowly at 900°C. Moreover, clusters of such Cr<sub>2</sub>O<sub>3</sub> platelets have a much higher surface area than the nominal surface area of the test specimen itself. Consequently, these crystals offer an additional or alternative source of chromia with which the sodium chloride vapors can interact. Thus in the presence of chloride vapors a protective scale can be formed and maintained.

Thusly, the two reactions - one involving gaseous chloride interactions with chromia, the other involving the production of Cr<sub>2</sub>O<sub>3</sub> crystal platelets by the action of the molten salt - occur simultaneously and independently of each other. The thermogravimetric data then reflects the net effects of these two parallel reactions as well as volatilization effects.

Amplifying on this, in the 100 hour experiments conducted in this study at 900°C, the rate of weight change for the 100 ppm NaCl(g) is shown in Fig. 29. In both the presence and absence of NaCl(g), the salt-coated specimens initially gain weight, and within a short time, lose weight, the loss being associated with vaporization of reaction products. Of significance, however, is the observation that the rates of weight loss are slower in the presence of the NaCl(g), inferring that the substrate is oxidizing at rates faster than that in air alone. Thus, the production rate of Cr<sub>2</sub>O<sub>3</sub> crystals is insufficient at 900°C in the presence of 91 ppm NaCl(g) to minimize the amount of NaCl(g) available at the oxide surface to react with protective scales, and clearly enhanced oxidation rates occur. However, at 1050°C, the rate of formation of such crystals is sufficiently high to afford sacrificial protection yielding oxidation behavior similar to that found for exposure to air alone, Fig. 28 and Ref. 13. However, it must be noted that any such apparent protection will only be temporary. The duration of this protection will depend on how long such chromia crystals survive volatilization effects. The volatilization of these chromia crystals will result both from the vaporization of Cr<sub>2</sub>O<sub>3</sub>(c) as CrO<sub>3</sub>(g) and from the formation of volatile species such as (NaCl)<sub>x</sub> CrO<sub>3</sub>(g), x = 1, 2, 3 (Ref. 14).

Moreover, it is observed, based upon scanning electron microscopy studies, that for surfaces of the specimens exposed at 1050°C the oxide scale has been significantly enriched in nickel, Fig. 30. Similar observations were observed when the chromia formers are exposed to only gaseous NaCl, as if the fused salt was absent. The chromium-deficient oxide scale shown in Fig. 30 is not the virtually chromium-free oxide blister discussed earlier, cf. Fig. 17.

In summary, in the presence of Na<sub>2</sub>SO<sub>4</sub>, the Ni-Cr alloys developed well-formed chromia platelets, whose growth is strongly temperature dependent. It is postulated that the mechanism responsible for the development and growth of the crystals is related to oxygen transport (cf. Appendix I):



Oxygen reacts with chromia in regions of high oxygen activity and is transported through the molten salt to regions of lower activity. These crystals with their higher surface areas are more reactive with respect to NaCl. Thus, it appears that Na<sub>2</sub>SO<sub>4</sub> mitigates the deleterious effect of NaCl(g).

### 3. The Superalloy B-1900

The hot corrosion behavior of Na<sub>2</sub>SO<sub>4</sub>-coated B-1900 has been described by many investigators. In general, during oxidation of the salt-coated specimens, an induction period is observed; the duration is dependent upon temperature among other things. Of notable interest is the observation that, during prolonged exposures at 900°C, the rates of oxidation of the salt-coated specimens (1 mg/cm<sup>2</sup> Na<sub>2</sub>SO<sub>4</sub>) did not continuously increase, but, as shown in Fig. 31, after approximately 40 hours from the initiation of corrosion, slowed down and continually decreased with increasing time. Based upon metallographic examination, approximately 40 percent of the cross sectional area had been consumed. Based upon wet chemical analysis, sodium sulfate was consistently present at levels of 0.04 mg/cm<sup>2</sup> on samples after exposure for 100 hours at 900°C to air either alone or with 10 ppm levels of NaCl(g).

The presence of NaCl(g) markedly affected the sulfidation corrosion of B-1900 at 900°C. In the presence of 95 ppm NaCl(g) the duration of the incubation period was decreased, Fig. 31. Linear oxidation kinetics ensued with total consumption of the specimen after 60 hours exposure.

In fact, at the 100 ppm NaCl(g) level at both 900°C and 1050°C, Na<sub>2</sub>SO<sub>4</sub>-coated B-1900 specimens were completely consumed, Figs. 31 and 32. At 1050°C, the sodium sulfate-coated B-1900 specimens exhibited similar oxidation kinetics with and without 10 ppm levels of NaCl(g) present, namely very rapid initial oxidation kinetics followed by net weight loss effects, Fig. 32. On the other hand, on

exposure at 900°C at the 11 ppm NaCl(g) level, the specimens were not completely consumed, but as shown in Fig. 31, the rate of weight gain is constant or increasing, and total consumption of the alloy is anticipated. Thus, a major difference between the 900°C sulfidation corrosion of B-1900 in the presence of NaCl(g) is the observation that NaCl(g) (1) reduces or removes the incubation period, and (2) continually promotes the accelerated corrosion of the alloy. In the absence of the NaCl(g), the rate of oxidation of the salt-coated specimen eventually decreased. But this decrease was not due to either the complete consumption of the specimen or the complete loss of sodium sulfate from specimen surfaces before the end of the experiment.

It was previously shown that NaCl(g) markedly accelerates the rate of oxidation of B-1900 in the absence of salt deposits. Therefore, because both current and prior studies (Ref. 13) have indicated that NaCl vapors cause scale rupture effects irrespective of the presence of Na<sub>2</sub>SO<sub>4</sub> deposits, it would be anticipated that the presence of NaCl vapors would result in decreasing incubation periods for B-1900 specimens coated with Na<sub>2</sub>SO<sub>4</sub>, as was experimentally observed.

In previous studies of the accelerated oxidation of nickel base superalloys, it was shown that the eventual decrease in rates of oxidation of salt-coated alloys could be related to the consumption of oxide ions in the melt and the gradual reformation of a protective oxide scale forming beneath the loose, non-protective corrosion product (Refs. 9, 10, 11). In the current study it was shown that the rates of oxidation at 900°C of sodium sulfate-coated B-1900 exposed to gaseous NaCl do not eventually decrease but continually accelerate.

It has been established that externally applied chromia deposits attenuate sulfidation corrosion (e.g., Ref. 29). The objective of the next series of experiments was to determine the role of NaCl(g) in the presence of chromia additions on the surface with respect to hot corrosion processes. In the absence of externally applied chromia deposits, sodium sulfate-coated B-1900 specimens undergo accelerated corrosion after approximately four hours at 900°C, Fig. 31. In the presence of Cr<sub>2</sub>O<sub>3</sub>, the incubation period has been extended to about 40 hours, Fig. 33. The cause for the eventual accelerated oxidation kinetics is unclear. It can be suggested that total inhibition is not observed due to the presence of discontinuities in the oxide scale which eventually allow the salt to contact the substrate. The subsequent formation of sulfides and excess oxide ions overpowers the chromia, and accelerated oxidation occurs. However, this explanation may not be complete because NiAl specimens similarly tested failed to show any effects of hot corrosion for 100 hour test periods. Moreover, because chemical reactions are temperature dependent, rates are very rapid at 1050°C. Thus, at 1050°C no inhibition was observed for either B-1900 or NiAl substrates.

The addition of 10 ppm NaCl into the gaseous environment did not significantly alter the eventual occurrence of accelerated oxidation kinetics, Fig. 33; however, at the 100 ppm level, significant differences occurred.

As indicated in Fig. 33, at the 100 ppm NaCl(g) level, the salt coated ( $\text{Na}_2\text{SO}_4 + \text{Cr}_2\text{O}_3$ ) specimens did not undergo classical hot corrosion in that (a) no incubation period was observed, and (b) the apparent rate of oxidation was a linear function of time. Based upon visual observation, the principle salt appeared to be the chromate, with its characteristic yellow color. Close examination revealed the presence of small nodules and surface discolorations which are indications of areas of localized corrosion.

In view of the fact that with 100 ppm additions of NaCl(g) to test atmospheres B-1900 specimens have been aggressively attacked, the behavior reported here is not readily understood.

#### D. Low Power Corrosion

Field experience and laboratory experiments have shown that, when molten deposits composed primarily of sodium sulfate,  $\text{Na}_2\text{SO}_4$ , are present on hot gas path turbine components, accelerated corrosion can occur. Because the melting point of sodium sulfate is  $884^\circ\text{C}$  ( $1623^\circ\text{F}$ ), engine operation resulting in turbine metal surface temperatures below  $750\text{--}800^\circ\text{C}$  ( $1380\text{--}1470^\circ\text{F}$ ) has been generally considered "safe" (Refs. 30, 31).

It has been reported that as a result of extended low power operation, accelerated corrosion of gas turbine components had occurred (Refs. 12, 32). Low power is associated with low first stage turbine blade metal temperatures, and the overlay CoCrAlY coating exhibited significant attack in engines operating in the 12,000 horsepower range, which is associated with metal temperatures in the range of  $593\text{--}732^\circ\text{C}$  ( $1100\text{--}1350^\circ\text{F}$ ) as compared to normal power levels (20,000 hp), which reportedly are associated with metal temperatures in the range of  $816\text{--}899^\circ\text{C}$  ( $1500\text{--}1650^\circ\text{F}$ ) (Refs. 2, 12, 32, 33). The fuel in all cases was a marine distillate with 0.7 percent sulfur (Ref. 12, 32).

The morphology associated with the accelerated corrosion resulting from low power engine operation is described to be principally characterized by a pitting attack of the CoCrAlY coating with little evidence of  $\beta$ -CoAl depletion (Refs. 12, 32, 33). This microstructure is in contrast to the  $\beta$ -depletion zone and attendant internal sulfides commonly seen in CoCrAlY overlay coatings which have undergone classical hot corrosion attack (Refs. 12, 32), e.g., Fig. 2 in Ref. 33. Moreover, this corrosion morphology occurs principally on the pressure (or concave) surfaces of turbine airfoils (Ref. 33).

The oxides associated with the low temperature corrosion pits are enriched in both chromium and aluminum and are depleted in cobalt although the outer oxide layer is most often enriched in cobalt (Refs. 12, 32, 33). Reduced chromium levels are frequently detected in the CoCrAlY adjacent to these oxide pits, and regions at

the interface between the CoCrAlY and the oxide pit are often sulfur-rich although distinct chromium-, aluminum-, or cobalt-rich sulfides have not been identified (Refs. 12, 32). Lastly, water-soluble cobalt is associated with the corrosion product (Ref. 33). This corrosion morphology has been labeled "B2", and investigators currently working in this area frequently use this notation alone to describe this corrosion microstructure.

The accelerated attack associated with low power operation had been thought to be associated with enhanced salt deposition which was believed to be a consequence of the "lower flow rate through the demisters at low power settings" (Refs. 32, 33). A concurrent Navy report also cites turbine deposits and filter efficiency with corrosion (Ref. 34). In a subsequent report, Wortman, Fryxell, and Bessen related both low power operation and the observation that this pitting corrosion, which occurs primarily on the pressure or concave surfaces of the blades, with the comparative efficiency of the "shower head-film cooling" scheme used to control blade temperature (Ref. 33). According to these authors, the convex blade surfaces are thought to be "effectively wiped" with cooling air from the leading edge to trailing edge, while the concave surfaces are subjected to much more gas turbulence which minimizes the establishment of protective (cooling air) gas films that would hinder the delivery of injurious species (Ref. 33). Therefore, it is inferred that the corrosive salt does not readily deposit on the convex surfaces. According to these investigators, the pitting corrosion morphology is associated with the presence of low melting  $\text{Na}_2\text{SO}_4$ - $\text{CoSO}_4$  mixtures (Ref. 33). At elevated temperatures the sulfates of the transition metals are less stable and decompose.

This picture is incomplete and deals only with the propagation and says nothing about the initiation of failure of the protective alumina scales on the overlay coating.

Jones and Gadomski (Ref. 31) reported that the pitting corrosion morphology seen on overlay-coated hardware removed from marine service can be simulated in the laboratory by depositing mixtures of  $\text{Na}_2\text{SO}_4$  and the sulfates of nickel, iron, zinc, cobalt, and lead onto CoCrAlY coatings and exposing them within the temperature range of 649-760°C (1200-1400°F). According to Jones and Gadomski, the pitting attack results from the acidic dissolution of the protective scales as first described by Goebel, Pettit, and Goward (Ref. 35).

It is well established that liquid sodium pyrosulfate and  $\text{SO}_3$ -rich sodium sulfate melts will readily flux alumina scales (Refs. 12, 32, 36). However, an inconsistency associated with the description of the formation of the "B2" microstructure is the observation that, although corrosion associated with this microstructure occurs primarily on concave (or pressure) airfoil surfaces, salt deposits are noted on all surfaces (Ref. 33). Moreover, it is reported that within the destroyer duty cycle the engine briefly drops to idle (Ref. 2), and as reported

by Bessen and Fryxell, the concentration of unburnt hydrocarbons and carbon monoxide can be as high as 0.1 percent. Also particulate char formation occurs (Ref. 2). Moreover, the corrosion is associated primarily with the surface exposed to line of sight effects and because carbonaceous deposits are reported to be present on the turbine surfaces (Refs. 33, 34, 37), the simultaneous presence of these deposits and the formation of  $\text{SO}_3$ -rich compounds is thermodynamically not favored. Lastly, it has been reported that CoCrAlY overlay coatings have performed exceptionally well in the temperature range of  $704^\circ\text{C}$  ( $1300^\circ\text{F}$ ) with fuels containing almost 3 percent sulfur (3 percent  $\text{H}_2\text{S}$ ), even though based upon chemical analysis, sodium sulfate was found on the airfoil surfaces (Ref. 38).

The observations that the corrosion can be related to (a) salt deposition and filter efficiency, (b) impaction phenomena since the pitting attack occurs only on the concave or pressure surface, and (c) the presence of carbonaceous deposits led us to conduct the study described herein to determine if an alternative mechanism exists whereby such oxide microstructures ("B2") can be formed.

In previous studies (Ref. 13), the role of carbon had been studied by applying mixtures of  $\text{Na}_2\text{SO}_4$  and lampblack onto specimens and exposing them at elevated temperatures. In general, the carbon quickly oxidized. Because carbon formation is favored during initial engine operation and can exist for prolonged durations at elevated temperatures (Ref. 16), the effect of carbon, temperature, and gaseous environment on corrosion was reinvestigated.

In order to determine the role of gaseous chloride as it affects the corrosion morphology, a series of experiments were conducted in which uncoated and  $\text{Na}_2\text{SO}_4$ -coated CoCrAlY specimens were exposed as described in the test schedule below. The CoCrAlY tested here was in the form of CoCrAlY (IM 6250) coatings on MAR-M509 substrates.

#### TEST SCHEDULE

<u><math>\text{Na}_2\text{SO}_4</math></u>	<u>Thermal Spike</u>	<u>Test Conditions</u>
No	No	Age at $700^\circ\text{C}$
No	Yes	Spike, then age at $700^\circ\text{C}$
Yes	Yes	Daily coated with $\text{Na}_2\text{SO}_4$ , then $700^\circ\text{C}$ Age
Yes	Yes	Daily washed, then coat with $\text{Na}_2\text{SO}_4$ , then spike, then $700^\circ\text{C}$ age
Yes	Yes	Daily washed, then spike, then coat with $\text{Na}_2\text{SO}_4$ , then $700^\circ\text{C}$ age

The thermal spike here involved placing the specimen into a furnace preheated to 1300°C for 30 seconds. In one series of experiments involving the entire test schedule shown above, specimens aged in the 700°C furnace were exposed to air alone. In a second series of experiments again involving the entire test schedule shown above, test specimens aged at 700°C were exposed to NaCl vapors. These vapors were provided by NaCl contained in a platinum crucible placed into a 700°C aging furnace. Based on reported vapor pressure data, the anticipated NaCl(g) concentration in this furnace was 100 ppm (Ref. 39). No attempt was made to artificially increase the NaCl(g) composition in the 1300°C furnace above normal background values. These experiments were conducted over a period of 3000 hours.

CoCrAlY coatings aged at 700°C alone with or without NaCl vapors present formed thin oxide scales which protected the specimens from further oxidation, Fig. 34.

When the CoCrAlY coatings were thermally spiked, unique microstructures can be produced. The microstructure of as processed CoCrAlY is shown in Fig. 35. The coatings consists of two phases, the intermetallic beta phase (CoAl) and the solid solution matrix phase (Co-Cr-Al). As a result of the thermal excursion-aging cycle, a phenomenon called discontinuous precipitation occurs, Fig. 36. The magnitude of the effect is dependent upon time and temperature. The morphological changes can be explained as follows. In the binary Co-Al system the solubility of cobalt in the  $\beta$ -CoAl phase increases with temperature, Fig. 37 (Ref. 40). On cooling down after such a heat treatment, the excess  $\alpha$ -cobalt in solution in the  $\beta$ -CoAl thermodynamically wants to precipitate out. If the low temperature aging temperature is too low, kinetically this precipitation either does not occur or occurs on a scale too fine to be seen by ordinary optical metallographic techniques, Fig. 38. However, if an appropriate temperature is chosen, the discontinuous precipitation phenomenon can effect a lamellar-like microstructure as seen in Fig. 36. Of course, the excess aluminum in the  $\alpha$ -cobalt resulting from such increased temperature exposure similarly would like to precipitate as  $\beta$ -CoAl. However, because less aluminum dissolves in  $\alpha$ -cobalt than does  $\alpha$ -cobalt in  $\beta$ -CoAl with increases in temperature, the  $\beta$ -CoAl precipitation phenomenon, though present in the  $\alpha$ -cobalt grains, is less pronounced. Thus, the presence of discontinuous precipitation in coatings normally free of this lamellar-type morphology is indicative of thermal spiking. However, the absence of this morphology does not mean thermal spiking did not occur. If the duration of the spike is too long or the aging temperature is too high, severe coarsening and interdiffusion occurs in the lamellar microstructures which can reestablish the original microstructure, Fig. 38.

Moreover, such heat treatments can alter the distribution of chromium in the coating because the solubility of chromium in  $\beta$ -CoAl is less than that in  $\alpha$ -cobalt (Ref. 41). Therefore, during the excursion to high temperatures, the  $\alpha$ -cobalt unites with the  $\beta$ -CoAl to form  $\beta$ -CoAl (Co-rich) and precipitated chromium. On



cooling, the  $\beta$ -CoAl (Co-rich) disproportionates to form  $\beta$ -CoAl and  $\alpha$ -cobalt (Cr deficient). The previously precipitated chromium could equilibrate with the  $\alpha$ -cobalt or react to form  $\sigma$ -CoCr or chromium carbide phases.

Experiments involving thermal spikes in the absence of sodium sulfate deposits and sodium chloride vapors produced little attack looking similar to that seen in Fig. 34. In experiments designed to investigate the role of  $\text{Na}_2\text{SO}_4$ , in the absence of NaCl vapors with or without thermal spikes, based upon metallographic examination, the amount of attack is minimal with depths of attack no more than a few microns. However, when thermally spiked specimens were aged in the furnace with the NaCl-containing crucible, the results were completely different.

As shown in Fig. 39, in the presence of NaCl(g), a severe broad attack is noted. Based upon metallographic examination the alloy affected zone has been depleted of aluminum, and internal oxidization effects within this zone are apparent. Of particular significance is the depth of attack. In as little as fifty thermal cycles, almost half of the coating has been penetrated. The addition of sodium sulfate deposits to experiments involving exposure to thermal transients and NaCl vapors did not significantly increase or alter the severity of the attack. That is, the formation of the depleted zone with the internally-oxidized "banded" appearance predominated. When specimens were coated with sodium sulfate and subjected both to thermal spikes and to NaCl vapors in the aging furnace, this corrosion microstructure was not significantly altered. The major contribution of the sodium sulfate was the formation of a few small sulfur-rich precipitates that were observed within the depleted zone.

Thus, when CoCrAlY-coated test specimens were subjected in the laboratory to brief thermal excursions ( $\sim 30$  sec), and aged at low temperatures in the absence of NaCl(g), no significant oxidation was observed. Furthermore, no significant microstructural changes were evident in the CoCrAlY coating itself. However, with NaCl(g) present, severe alloy depletion was noted even though no significant microstructural changes were observed in the coating. Moreover, within relatively short durations, approximately half of the coating thickness is depleted of the active elements that impart oxidation and sulfidation resistance. Thus, in the presence of both thermal excursions and NaCl(g), significant reactions occur, and the effect is most deleterious to the coating. This type of microstructure has been observed in components removed from gas turbines used in marine environments, cf. Fig. 8 in Ref. 2.

In order to investigate the role of carbon,  $\text{Na}_2\text{SO}_4$ -coated specimens were placed within a platinum crucible along with 5-8 cc of Diesel No. 2 fuel and inserted for no more than 30 seconds into a preheated furnace at  $1300^\circ\text{C}$ . During this time period, the fuel would burn and form char.

After removal from the high temperature furnace, the samples are placed into another furnace operating in air at  $700^\circ\text{C}$  for extended time periods. In general,

the specimens are exposed to two high temperature exposures per day with about seven hours between exposures. Thus, each cycle consists of a brief high temperature exposure followed by an extended period at 700°C (1290°F). No crucible containing NaCl was used here in the 700°C aging furnace. No SO<sub>2</sub> additions are made to test environments, and sodium sulfate deposits ( $\sim 1 \text{ mg/cm}^2$ ) are applied once every 15 cycles. The specimens are not water washed prior to the reapplication of the sodium sulfate. After 58 cycles the specimen was prepared for both metallographic and electron microbeam probe examination. Another series of experiments was conducted differing only in that the quantity of char employed was increased by the addition of 5 cc of epoxy resin.

As shown in Fig. 40, the CoCrAlY coating exhibits a nodular (or a pitting) type of attack, with the visual and microstructural characteristics described for the pitting "B2" corrosion morphology associated with the accelerated corrosion which had occurred in some Navy gas turbine engines (Refs. 12, 32, 33). After 131 test cycles the specimen is severely pitted, and the characteristic features of the attack are more readily seen (Fig. 41).

The microstructures produced by this testing procedure have the following characteristics:

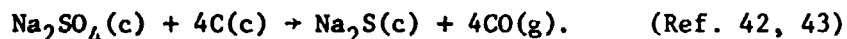
1. an outer cobalt-enriched oxide scale (Fig. 41a),
2. an inner oxide zone enriched in chromium and aluminum and simultaneously depleted in cobalt (Figs. 41b and 41c),
3. little or no  $\beta$ -CoAl depletion zone between the inner oxide zone and the unaffected CoCrAlY coating (Fig. 41).

Furthermore, amplifying on the characteristics of the oxide pits produced by laboratory testing, an enrichment of sulfur is found at the interface between the inner oxide layer and the unaffected CoCrAlY coating, Figs. 41, 41d, 42, 42d. However, no discrete sulfides are found in the oxide or in the CoCrAlY coating below the pit, Figs. 40, 41 and 42. Note that a depletion zone of chromium in the coating adjacent to the oxide pit is also observed, and small islands of  $\alpha$ -cobalt are found in the oxide pit near the unaffected coating, Figs. 40, 41 and 42. Lastly, the microstructure found in the inner oxide zone resembles the original CoCrAlY microstructure, Figs. 40 and 41. Based upon the electron microbeam probe data, one phase in the inner oxide zone is aluminum rich while the other is chromium rich, Fig. 43. Superimposed on this two phase microstructure, oxide striations are observed running parallel to the surface, Figs. 40 and 41. Furthermore, as shown in the above figures, a thin zone slightly enriched in aluminum is observed between the outer cobalt-rich oxide and the inner two phase oxide, Fig. 41c. Lastly, when the corrosion products are placed into water, soluble cobalt is found.

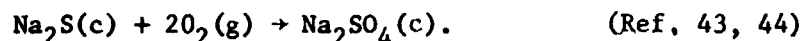
In order to separate the role of the char and the thermal spike, a series of experiments was conducted in which the sodium sulfate-coated CoCrAlY-coated specimens together with fuel with and without epoxy resin were heated at 700°C (1295°F) for seven (7) hours. After 170 cycles, it was observed that no corrosion had occurred. It was also determined that the char formed at 700°C is highly combustible, unlike the char formed at 1300°C which would persist for extended periods (two to four hours).

Lastly, a series of experiments was performed in which the sodium sulfate-coated CoCrAlY specimens and fuel were placed into individual platinum crucibles. Both crucibles were simultaneously inserted into the 1300°C preheated furnace for durations less than 30 seconds. This experiment was then repeated without the fuel. In the absence of the fuel the CoCrAlY specimen is essentially covered with a clear-whitish deposit. When touched with wet litmus paper, the litmus paper remains unchanged in color. When fuel was present, the salt deposit on the CoCrAlY specimen is reddish in appearance; and when touched with wet litmus paper, a distinctly basic response was indicated. When heated at 700°C in air, the reddish deposit slowly turns white.

Because anhydrous sodium sulfide is reported to be red while sodium sulfate is white and because aqueous solutions of sodium sulfide are alkaline while those of sodium sulfate are not, these observations are consistent with the partial conversion of  $\text{Na}_2\text{SO}_4$  to  $\text{Na}_2\text{S}$  which can occur under the transient reducing conditions, i.e.,



At 700°C in the oxidizing environment, the  $\text{Na}_2\text{S}$  phase is converted back to  $\text{Na}_2\text{SO}_4$ , i.e.,



Thus, the anticipated reaction products between  $\text{Na}_2\text{SO}_4$  and carbon, under the conditions described herein, are sodium sulfide,  $\text{Na}_2\text{S}$ , and the oxides of carbon while the release of  $\text{SO}_3$  is not thermodynamically favored (Ref. 43).

The presence of carbon strongly influences both the rate of corrosion and the corrosion morphology. In the presence of carbon, salt, thermal excursions, and subsequent aging, the CoCrAlY coating oxidizes at accelerated rates. It forms an outer cobalt-enriched oxide scale, an inner oxide zone enriched in chromium and aluminum, and simultaneously depleted in cobalt with the corrosion product almost in intimate contact with the unaffected substrate, as if little diffusion had occurred. This microstructure is identical to that described for the accelerated corrosion of CoCrAlY-coated components removed from some Navy gas turbine engines (Refs. 12, 32, 33). Thus, although the "B2" microstructure has been reproduced in

the laboratory by the action of condensed sodium sulfate deposits with  $\text{SO}_3$  ( $\text{SO}_2/\text{O}_2$ ) additions to test atmospheres at relatively low temperatures,  $700^\circ\text{C}$  (Refs. 12, 36), results of experiments described here demonstrate this microstructure can alternately be produced as a result of high temperature  $\text{Na}_2\text{SO}_4$ -induced hot corrosion processes without additions of  $\text{SO}_3$  ( $\text{SO}_2/\text{O}_2$ ) to test environments. Furthermore, this alternative mechanism involves factors which have been reported to be present within the operating profile of gas turbine engines where such corrosion pits have been observed.

Thusly, the corrosion associated with hardware in such engines occurred primarily on the concave surfaces, the surfaces which are "line of sight" with respect to combustion burners. Carbonaceous deposits were reported to be present on turbine surfaces (Refs. 2, 33, 37), and salt deposits were noted on all surface (Ref. 2). Thus, assuming thermal excursions and subsequent low power operation, the conditions investigated in this study had occurred in the field. That is, salt-coated parts were briefly exposed at elevated temperatures in the presence of carbon and subsequently aged at lower temperatures. In the laboratory in the absence of carbon, no accelerated corrosion with the "B2" morphology was observed. In the field, carbon deposition most likely occurs during engine start-up and shut-down. Thus, as had been reported by Schilling et al. (Ref. 38), the CoCrAlY coatings had performed well in engines operating for extended durations on gaseous fuels containing up to 3 w/o sulfur (as  $\text{H}_2\text{S}$ ), even though (based upon chemical analysis) sodium sulfate had been present on high pressure turbine airfoil surfaces. Because the gas turbine engine was reportedly in continuous use, carbon formation would be minimized; and, based upon the model described herein, carbon is an essential ingredient for this type of corrosion.

Sodium chloride was present at low levels in the epoxy used in experiments dealing with carbon which resulted in the production of pits with the "B2" microstructure. However, these experiments do not permit an explicit definition of the role of such sodium chloride in the corrosion process leading to the formation of oxide pits with the "B2" morphology. However, on the basis of other experiments reported here dealing with low levels of  $\text{NaCl}$ , such amounts of sodium chloride are probably not innocuous. Accordingly, further work in this area is needed to define this role.

## V. SUMMARY AND CONCLUDING REMARKS

Sodium chloride gas reacts with the normally protective oxide scales that form on NiAl, Ni-Cr alloys and the nickel base superalloy, B-1900.

With respect to the simple alumina formers, the gas reacts at the metal-oxide interface, transporting aluminum to the free surface where it oxidizes to form  $\text{Al}_2\text{O}_3$  whiskers. The depletion of aluminum at the oxide-metal interface results in the formation of voids, which after prolonged exposure grow and eventually contribute to isothermal scale cracking of sufficient magnitude to be readily detected by thermogravimetric techniques.

In air environments alone, B-1900 exhibited excellent oxidation resistance. However, in the presence of low levels of NaCl vapors, oxidation rates were increased by orders of magnitude. In fact, at the end of 100 hour tests, thermogravimetric curves for specimens exposed to NaCl(g) at 900°C indicated highly positive slopes. On the other hand, sodium sulfate-coated specimens exposed at 900°C to air without NaCl(g) indicated flat or even decreasing oxidation rates, suggesting protective scales had eventually formed there. Moreover, for B-1900 specimens oxidized in air with NaCl vapors, alumina whiskers similar to those found for the simple alumina formers, were evidenced on oxide scales. The attendant isothermal cracking of the protective scale and the enrichment of molybdenum at the scale-alloy interface are contributing factors to the accelerated oxidation of this alloy. Because molybdenum and the other refractory metals are most important alloying elements for the next generation of the aluminum rich (gamma prime strengthened) superalloys, it is most important to understand the mechanism by which gaseous species (such as NaCl vapors) increase the oxidation rates orders of magnitude, so that the proper alloying or metallurgical heat treatments can be performed to improve oxidation resistance to such corrosives. As shown in this study, the deleterious effect of NaCl(g) is also observed when the alloy is coated with molten sodium sulfate.

In this study it was confirmed that NaCl(g) reacts with chromia, and the chromium content of oxide scales can be significantly reduced by gaseous sodium chloride such that oxidation rates are significantly increased. Furthermore, the presence of NaCl vapors in oxidizing atmospheres leads to "S" shaped thermogravimetric curves characteristic of breakaway oxidation kinetics.

During thermal transients, metallurgical transformation can occur in CoCrAlY coatings. In the presence of gaseous NaCl, severe alloy depletion effects and internal precipitation of aluminum and chromium are observed. Such a microstructure has been reported for a gas turbine operating under cyclic conditions in a marine environment. When carbon and  $\text{Na}_2\text{SO}_4$  are present and the alloy is

NASA CR-15974  
R79-914387-4

aged at lower temperatures, accelerated corrosion is observed producing a characteristic microstructure whose features agree with that reported to result from low power operation of some Navy gas turbines, i.e., "B2."

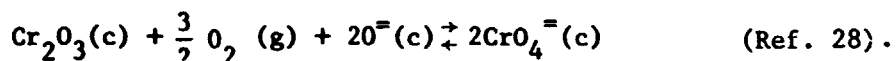
Because NaCl is present in the sodium sulfate at contaminant levels, and was present in the epoxy used to promote char formation, the role of gaseous NaCl in this form of accelerated hot corrosion needs to be further explored.

## VI. APPENDIX I

### A PROPOSED MECHANISM FOR THE GROWTH OF CHROMIA CRYSTALS BY MOLTEN SALTS

Both in the current and in previously reported studies (Ref. 13) pure chromium and Ni-Cr alloys exposed to condensed sodium sulfate deposits develop large platelet-shaped  $\text{Cr}_2\text{O}_3$  crystals (Ref. 13), e.g., Fig. 30. Similar observations have been reported by Wright et al. (Ref. 28). Such platelets develop irrespective of the presence or absence of halogen-bearing vapors.

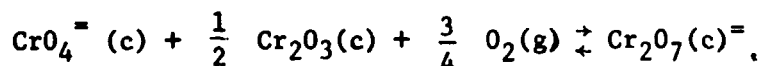
The growth rate of such crystals is slow at  $900^\circ\text{C}$  and rapid at temperatures of  $1000^\circ\text{C}$  (Ref. 28) and  $1050^\circ\text{C}$  (Ref. 13). An explanation previously proposed to account for the growth of such crystals involved oxide ion effects, arising from the reversibility of the reaction:



Based on this interpretation, the dissolution process occurs where the oxide ion level is high, i.e., the oxide-molten salt interface. The precipitation reaction then occurs when the oxide ion level is reduced, i.e., near the molten-salt ambient atmosphere interface (Ref. 28). Such an interpretation, though internally consistent, does not readily explain the distribution of chromia crystals as shown in Fig. 44, cf. Fig. 100 in Ref. 13. Here a number of circular features occur. These structures suggest that a molten salt was transiently present as a droplet on the specimen surface before completely vaporizing because no indication of a molten deposit remains.  $\text{Cr}_2\text{O}_3$  crystals are found both inside and outside such circular structures. However within the delineated perimeters of such features, chromia crystals are either absent or greatly diminished in quantity.

Thus, if such local molten salt droplets existed, the oxide ion level should be lowest at the periphery of such a droplet, i.e., at the gas-salt-oxide interface. Concurrently the oxide ion level should be greatest in the middle of such a droplet in contact with the oxide surface. Hence, according to the above explanation, crystals should appear at the periphery of such structures and be absent in their centers, Fig. 44. On the other hand, observation discloses exactly antithetical microstructures, Figs. 44 and 45.

An alternative explanation to account for the distribution of chromia found in Fig. 44 involves the possibility of an oxygen transport cycle. Thusly, chromia crystals could arise from the reversibility of a reaction such as,





Such a cycle would involve the transport of oxygen from a region of high activity to one of low activity. Thus, chromia scales should dissolve in regions of high oxygen activity in order to transport oxygen across an oxygen gradient. Although sodium dichromate at unit activity is reported to decompose at 400°C (Ref. 23), this does not preclude its existence in a molten salt at some reduced activity.

To evaluate the feasibility of both of these mechanisms, a short series of experiments was conducted. Elemental chromium was used to avoid problems with varying activities such as would occur for an alloy undergoing oxidation. The molten salt involved was sodium chromate. Chromia powder of 99.999% purity obtained from Apache Chemicals Inc., Seward, Illinois was pressed into pellets.

The temperature for the group of tests was 1000°C, a value which was found by Wright et al. to effect the growth of such crystals (Ref. 28). Specimens were maintained in a box furnace for one week and then examined for indications of the attack of chromia scales and/or the formation of large  $\text{Cr}_2\text{O}_3$  crystals.

The first group of experiments involved the absence of either an oxygen or oxide ion sink. Thus pure  $\text{Na}_2\text{CrO}_4$  held for a week in a platinum crucible failed to produce any  $\text{Cr}_2\text{O}_3$  crystals. With the addition of dense alumina pieces to the molten salt, again no chromia crystals were formed. Pressed  $\text{Cr}_2\text{O}_3$  powder pellets held isothermally in air at 1000°C failed to sinter sufficiently to yield large chromia crystals. Furthermore pressed chromia pellets either sprayed with  $\text{Na}_2\text{CrO}_4$  or partially or fully immersed alone in  $\text{Na}_2\text{CrO}_4$  also failed to produce the desired crystals. A small amount of Ostwald ripening, as anticipated, took place for  $\text{Cr}_2\text{O}_3$  pellets specimens partially or fully immersed in  $\text{Na}_2\text{CrO}_4$ ; however this was not the desired effect.

The second group of studies involved the possible action of an oxide ion sink. In the previously reported explanation to account for the growth of these crystals (Ref. 28), the likely and strongest oxide ion acceptor involving Ni-Cr alloys would have been NiO. Thus NiO powders mixed with  $\text{Na}_2\text{CrO}_4$  and held for one week at 1000°C in a platinum crucible failed to produce any chromia crystals. However a stronger oxide ion acceptor than NiO should produce  $\text{Cr}_2\text{O}_3$  crystals. Thus, in an experiment using a glazed porcelain (Coor's) crucible, after a week at 1000°C, both the crucible was attacked and small  $\text{Cr}_2\text{O}_3$  crystals were observed, Fig. 46. The silica used to glaze the crucible likely reacted with the  $\text{Na}_2\text{CrO}_4$  to form various sodium silicates and to produce  $\text{Cr}_2\text{O}_3$  crystals via oxide ion effects.

In the third group of experiments involving an oxygen sink, a specimen of chromium was partially immersed in a pool of sodium chromate contained in a platinum crucible. This experimental design as shown in Fig. 47 emulates the morphology of a molten salt droplet on the surface of a specimen, cf. Fig. 45. After one week, the specimen shows preferential attack at the meniscus where the

molten salt wetted the chromium specimen, Fig. 47. Concomitant with such attack large  $\text{Cr}_2\text{O}_3$  crystals were produced. These crystals are morphologically similar to those reported in the literature (Ref. 28) and observed in prior (Ref. 13) and current studies. The attacked regions of the chromium specimen are where the oxygen activity is highest. Regions of the chromium test piece that were below the surface of the molten salt were not preferentially oxidized. To insure that the effects observed did not result from galvanic interactions with the platinum crucible, the elemental chromium was isolated from the crucible with small alumina blocks with the same results as before, Fig. 47. Similar results were obtained substituting sodium sulfate for the sodium chromate here with the additional presence of a layer of sulfides below the chromia scale.

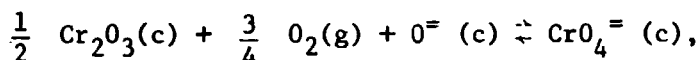
Continuing along these lines, a chromia pellet was partially immersed on an alumina pedestal and a piece of elemental chromium was fully immersed in the  $\text{Na}_2\text{CrO}_4$ , Fig. 48. After testing for one week the region of the pellet covered by the meniscus had largely dissolved, Fig. 48. Thusly it had been partially consumed in transporting oxygen to the submerged chromium specimen. In experiments involving such  $\text{Cr}_2\text{O}_3$  pellets alone and not using the oxygen sink, namely elemental Cr, no comparable effect occurred.

To determine if the transport of oxygen via the dissolution of  $\text{Cr}_2\text{O}_3$  occurred independently of an oxide ion sink, a specimen of elemental chromium was partially immersed in  $\text{Na}_2\text{CrO}_4$  held in a glazed porcelain crucible. After a week at  $1000^\circ\text{C}$ , the crucible showed attack exactly as seen earlier with no elemental chromium present, cf. Fig. 46. However the chromium piece also evidenced attack exactly as seen earlier in experiments with platinum crucibles, cf. Fig. 47.

Thusly the effects reported here are not explained by differences in the solubility of chromia scales in the absence of an oxygen sink (Ref. 28). However they are commensurate with an oxygen transport mechanism involving the dissolution of  $\text{Cr}_2\text{O}_3$  scales that is independent of oxide ion activity. Moreover the rate of attack of chromia scales by this mechanism are significant at temperatures of  $1050^\circ\text{C}$  and  $1000^\circ\text{C}$  (Refs. 13, 28). At the end of weight gain experiments conducted at  $1050^\circ\text{C}$  for 24 hours with Ni-25Cr, Ni-40Cr or elemental chromium coated with molten sodium sulfate (or sodium chromate) deposits, no molten salt is detected on specimen surfaces while prolific amounts of large  $\text{Cr}_2\text{O}_3$  crystals abounded. The morphology of the chromia crystals produced by such thin salt deposit experiments indicates a much larger surface area compared to the usual area calculated from pre-oxidized specimen geometries. Vaporization effects would be enhanced by the greatly enhanced surface areas actually effected by the profuse number of the relatively large crystals produced, cf. Fig. 44. Therefore, if  $\text{Na}_2\text{CrO}_4$  is as reactive as results of experiments conducted here suggest, it should not be surprising to be unable to subsequently find soluble chromium in the case of such experiments.

A recognition of the presence of such a transport process could be important in interpreting results of electrochemical studies of hot corrosion mechanisms. The equations responsible for such transport are independent of oxide ion activity. Moreover, such reactions could affect different areas of the same electrode - the effect appearing as a short circuit within a single electrode.

Rapp and coworkers have presented results of equilibrium solubility studies of  $\text{Cr}_2\text{O}_3$  in molten sodium sulfate melts at  $1000^\circ\text{K}$  for a wide range of  $\text{SO}_2/\text{O}_2$  mixtures (Refs. 45 and 46). These results indicate that for the basic dissolution of  $\text{Cr}_2\text{O}_3$ , i.e.,



at fixed oxide ion activity, the solubility of  $\text{Cr}_2\text{O}_3$  decreases with increased oxygen partial pressure. These results derived from equilibrium studies are contrary to the results presented here for processes involving dynamic transport effects.

## VII. ACKNOWLEDGEMENTS

The authors gratefully acknowledge helpful discussions with Mr. C. A. Stearns, Dr. F. J. Kohl, and Dr. G. C. Fryburg of NASA-Lewis Research Center, Cleveland, Ohio, and with Drs. M. A. Decrescente, R. A. Pike, and G. K. Layden of the United Technologies Research Center, East Hartford, Connecticut. The efforts of Ms. J. Whitehead, Ms. C. Clark, Mr. R. Brown, and Mr. L. Jackman for assistance in conducting the experiments presented herein are also acknowledged.

#### VIII. REFERENCES

1. Ode, W. H.: Coal Analysis and Mineral Matter, Chapter 5, pp. 202-231, in Chemistry of Coal Utilization, Supplementary Volume, ed. by H. H. Lowrey, John Wiley and Sons, Inc., New York (1963).
2. Fryxell, R. E. and I. I. Bessen: Coating Life Assessment in Gas Turbines Operated for Ship Propulsion. In Proceedings of 1974 Gas Turbine Materials in the Marine Environment, held in Castine, Maine, pp. 259-276, ed. by J. W. Fairbanks and I. I. Machlin, MCIC-75-27, publ. by Metals and Ceramics Information Center, Bettelle Laboratories, Columbus, Ohio, July 1974.
3. Stearns, C. A., R. A. Miller, F. J. Kohl and G. C. Fryburg: Gaseous Sodium Sulfate Formation in Flames and Flowing Gas Environments. Presented at Symposium on Corrosion Problems Involving Volatile Corrosion Products. Electrochemical Society Meeting, Philadelphia, Pennsylvania, May 1977; also NASA TM X-73600 (1977); also J. Electrochemical Soc. 124, 1145 (1977).
4. Kohl, F. J., C. A. Stearns and G. C. Fryburg: Sodium Sulfate: Vaporization Thermodynamics and Role in Corrosive Flames, published in Metal-Slag-Gas Reactions and Processes, edited by Z. A. Foroulis and W. W. Smeltzer, Electrochem. Soc., Princeton, New Jersey, page 649 (1975), also NASA TM X-71641 (1975).
5. a) Pilling, N. E. and R. E. Bedworth, J. Inst. Metals 29, 529 (1923).  
b) Hauffe, K.: Oxidation of Metals, Plenum Press, New York, 1965.
6. Ward, G., B. S. Hockenhull, and P. Hancock: Met Trans. 5, 1451 (1974).
7. McKee, D. W. and G. Romeo: Trans. AIME 6A, 101 (1975).
8. Bornstein, N. A. and M. A. DeCrescente: TMS-AIME 245, 1947 (1969).
9. Bornstein, N. S. and M. A. DeCrescente: Investigation of Sulfidation Mechanism in Nickel-Base Superalloys. Final Report conducted for U.S. Naval Ship Research and Development Laboratory, Contract N00600-68-C-0639, April 1969, Annapolis, Maryland.
10. Bornstein, N. S., M. A. DeCrescente, and H. A. Roth: Annual Report on the Effect of Vanadium and Sodium Compounds on Accelerated Oxidation of Nickel-Base Alloys. Contract N00014-70-C-0234, NR 036-089/1-12-70 (471), March 1971, June 1972, and June 1974.

REFERENCES (Cont'd)

11. Bornstein, N. S. and M. A. DeCrescente: TMS-AIME 2, 2875 (1971).
12. Jones, R. L.: A Summary and Review of NAVSEA Funded Low Power Hot Corrosion Studies, NRL Memorandum Report 4072, Naval Research Laboratory, September 24, 1979.
13. Smeggil, J. G. and N. S. Bornstein: Study of the Effects of Gaseous Environments on Sulfidation Attack of Superalloys, NASA CR-135348, Final Contract Report, Conducted for NASA-Lewis Research Center, Contract No. NAS3-20039, November 1977.
14. Stearns, C. A., F. J. Kohl, and G. C. Fryburg: Reactions of Chromium with Gaseous NaCl in an Oxygen Environments. Properties of High Temperature Alloys, ed. by Z. A. Foroulis and F. S. Pettit, Electrochemical Society/AIME, p. 655, (1976); also NASA TM X-73476 (1977).
15. Fryburg, G. C., R. A. Miller, F. J. Kohl, and C. A. Stearns: Volatile Products in the Corrosion of Cr, Mo, Ti and Four Superalloys Exposed to O<sub>2</sub> containing H<sub>2</sub>O and Gaseous NaCl. Presented at Symposium on Corrosion Problems involving Volatile Corrosion Products. Electrochemical Society Meeting, Philadelphia, Pennsylvania, May 1977; also NASA TM X-73599 (1977).
16. McKee, D. W., and D. Chatterji: Corrosive Effects of Pyrolytic Carbon in Gas Turbines in Thirteenth Biennial Conference on Carbon, Irvine, California, July 18-22, 1977.
17. McKee, D. W. and G. Romeo: Met. Trans. 5, 1127 (1974).
18. The Superalloys, Appendix B, Superalloy Data, p. 596, ed. by C. T. Sims and W. C. Hagel, John Wiley and Sons, New York, New York, 1972.
19. Wood, G. C. and T. Hodgkiess: J. Electrochem. Soc. 113, 319 (1966).
20. Giggins, C. S. and F. S. Pettit: TMS-AIME 245, 2495 (1969).
21. Lowell, C. E.: Oxid. of Met. 7, 95 (1973).
22. Fryburg, G. C., F. J. Kohl and C. A. Stearns: Oxidation in Oxygen at 900° and 1000°C of four Nickel-Base Cast Superalloys; NASA-TRW VIA, B-1900, Alloy 713C and IN-738, NASA TN D-8388 (1977).
23. Handbook of Chemistry and Physics 153rd Edition (1972-1973), ed. by R. C. West, The Chemical Rubber Company, Cleveland, Ohio.
24. Leslie, W. C. and M. G. Fontana, Trans of ASM, 41, 1213 (1947).
25. Felten, E. J. and F. S. Pettit, "Degradation of Coating Alloys in Simulated Marine Environments", Pratt and Whitney Quarterly Report, March 1, 1976 May 31, 1976, NRL Contract No. N00173-76-C-0146.

REFERENCES (Cont'd)

26. Radzavich, T. J. and F. S. Pettit, Ibid., Pratt and Whitney Quarterly Report, June 1, 1976-August 31, 1976.
27. Stearns, C. A., F. J. Kohl, G. C. Fryburg, and R. A. Miller: Interaction of NaCl(g) and HCl(g) with Condensed Na<sub>2</sub>SO<sub>4</sub>, NASA TM-73796 (1977), also presented at the Symposium on High Temperature Metal Halide Chemistry sponsored by the electrochemical Society, October 9-14, 1977 in Atlanta, Georgia.
28. Wright, I. G., B. A. Wilcox and R. I. Jaffe: Oxidation and Hot Corrosion of Ni-Cr and Co-Cr Base Alloys Containing Rare Earth Oxides Dispersions, Contract No. N00019-72-C-0190, Final Report, January 30, 1973, Battelle Laboratories, Columbus, Ohio.
29. Bornstein, N. S., M. A. Decrescente and H. A. Roth: Accelerated Corrosion in Gas Turbine Engines, pp. 3-15, Proceedings of Gas Turbine Materials Conference, Washington, D.C., October 1972.
30. Stringer, J.: Hot Corrosion of High Temperature Alloys. Ann. Rev. Mater. Sci. 7, 477-509 (1977).
31. Jones, R. L. and S. T. Gadomski: Mixed Sulfate/SO<sub>3</sub> Reactions in Low Power Hot Corrosion: A Possible Harmful Effect of Platinum Coatings. NRL Letter Report 617-773:RLJ:blr, Naval Research Laboratory, Washington, DC, November 1, 1977.
32. LM 2500 Stage 1 H.P. Turbine Blade Corrosion Evaluation, Second Interim Report to Engineering Program Notice HT-05 LM2500 H.P. Turbine Stage 1 Blade Life, April 26, 1976, Prepared under Contract N00024-76-C-4047. LM2500 Component Improvement Program for Naval Ships Engineering Center, Code 6146, General Electric Company, Maring & Industrial Department, Cincinnati, Ohio 45215.
33. Wortman, D. J., R. E. Fryxell, and I. I. Bessen: A Theory for Accelerated Turbine Corrosion at Intermediate Levels. Report No. R76AEG558, General Electric Company, Aircraft Engine Group, Cincinnati, Ohio. November 10, 1976. Also in the Proceedings of the 3rd Conference on Gas Turbine Materials in a Marine Environment, paper 11 in Session V, held at the University of Bath, England, September 20-23, 1976.
34. Jones, R. L.: SEM/EDAX Analysis of an LM2500 Stage 1 GTP Blade after approximately 3000 Hours at 12,000 hp on the GTS Callaghan. NRL Letter Report 6170-324a: RLJ:blr, Naval Research Laboratory, Washington, DC, April 16, 1976.

REFERENCES (Cont'd)

35. Goebel, J. A., F. S. Pettit, and G. W. Goward: Met. Trans. 4, 261 (1973).
36. Barkalow, R. H. and F. S. Pettit: Degradation of Coating Alloys in Simulated Marine Environments. Final Contract Report, Contract No. N00173-76-C-0146. Pratt and Whitney Aircraft - Commercial Products Division, East Hartford, Connecticut, June 15, 1978.
37. Bessen, I. I. and R. E. Fryxell: Turbine Coatings and Protection in Marine Environments, pp. 73-84 Proceedings of Gas Turbine Materials Conference, Washington, DC, October 1972.
38. Schilling, W. F., H. M. Fox, and A. M. Beltran: Field Testing and Evaluation of Next-Generation Industrial Gas Turbine Coatings. In Proceedings of Conference on Advanced Materials for Alternate Fuel Capable Directly Fired Heat Engines, held at the Marine Maritime Academy, Castine, Maine, July 30-August 3, 1979.
39. Ewing, C. T. and K. H. Stern: J. Phys. Chem. 78, 1998 (1974).
40. Hansen, M.: Constitution of Binary Alloys, Second Edition, McGraw-Hill Book Company, New York (1958).
41. Lemkey, F.: Private communication, 1978.
42. Thorne, P. C. L. and E. R. Roberts: Inorganic Chemistry, publ. by Interscience Publishers, Incorporated, New York (1946).
43. JANAF Tables, Dow Chemical Company, Midland, Michigan.
44. Mellor, I. W.: A Comprehensive Treatise on Inorganic and Theoretical Chemistry Vol. III. F, Cl, Br, I, Li, Na, K, Rb, Cs, publ. by Longman, Green and Company, London, England (1941).
45. Stroud, W. F. and R. A. Rapp: The Solubilities of  $\text{Cr}_2\text{O}_3$  and  $\alpha\text{-Al}_2\text{O}_3$  in Fused  $\text{Na}_2\text{SO}_4$  at  $1200^\circ\text{K}$ , presented at the Electrochemical Society Symposium of Metal-Halide Reactions, Atlanta, Georgia, October, 1977.
46. Rapp, R. A. and K. S. Goto: The Hot Corrosion of Metals by Molten Salts, presented at the Electrochemical Society Symposium on Fused Salts, Pittsburgh, Pennsylvania, October, 1979.



Table I

Analyzed Composition (in wt.%) for Experimental Alloys

<u>Nominal Composition</u>	<u>Analyzed Composition</u>					
	Ni	Co	Al	Cr	Y	Hf
NiAl (70Ni, 30Al)	68.6	----	30.6	----	----	----
NiAl + 0.5Y	68.1	----	31.2	----	0.12	----
NiAl + 1.5Y	69.6	----	29.9	----	0.24	----
NiAl + 1.0Hf	68.9	----	30.9	----	----	1.16
NiAl + 3.0Hf	66.5	----	29.2	----	----	3.62
NiAl + 1.0Cr	67.7	----	31.4	1.27	----	----
Ni-25Cr	75.2	----	----	25.2	----	----
Ni-40Cr	59.9	----	----	39.3	----	----
Ni-40Cr + 0.5Y	58.4	----	----	42.8	0.06	----
Ni-40Cr + 1.5Y	59.3	----	----	41.2	0.93	----
Ni-40Cr + 1.0Hf	59.4	----	----	39.1	----	1.28
Ni-40Cr + 3.0Hf	58.7	----	----	37.7	----	3.16
CoCrAl	----	63.3	13.8	23.9	----	----
CoCrAl + 0.5Y	----	61.6	13.7	24.2	0.50	----
CoCrAl + 1.5Y	----	61.3	13.5	24.2	1.33	----
CoCrAl + 1.0Hf	----	65.3	12.9	25.0	----	0.10
CoCrAl + 3.0Hf	----	61.8	12.9	25.0	----	0.50

PRECEDING PAGE BLANK NOT FILMED

REPRODUCIBILITY OF THE  
ORIGINAL PAGE IS POOR



FIG. 1 NiAl oxidized in air alone at 1050°C for 100 hours.

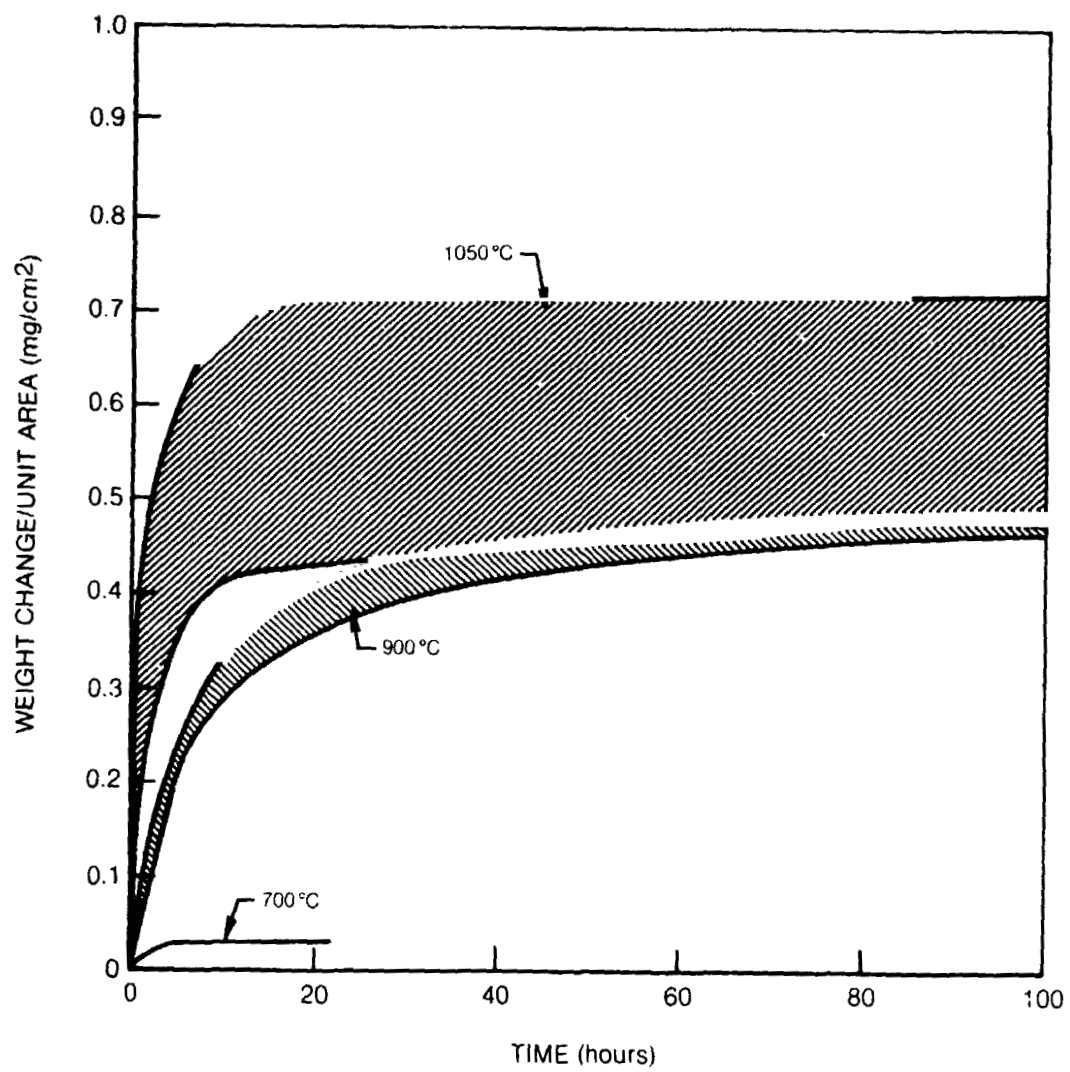


FIG. 2 Thermogravimetric data for NiAl oxidized in air alone.

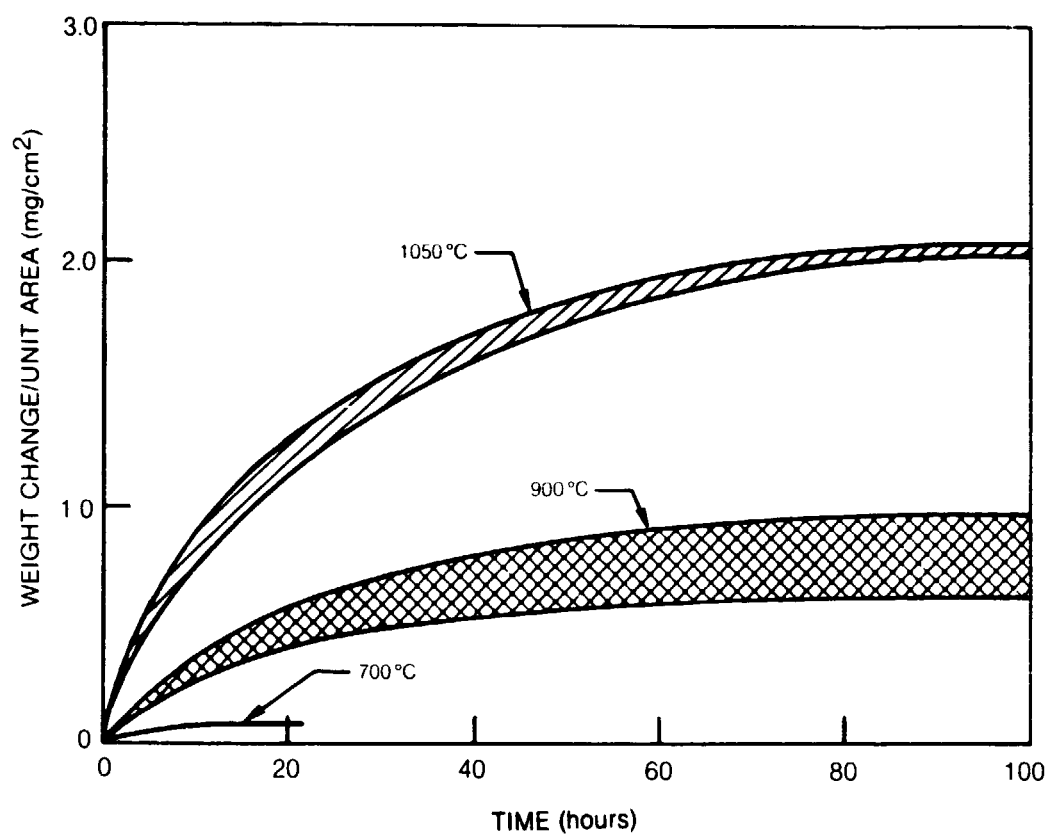


FIG. 3 Thermogravimetric data for Ni-25Cr oxidized in air alone.

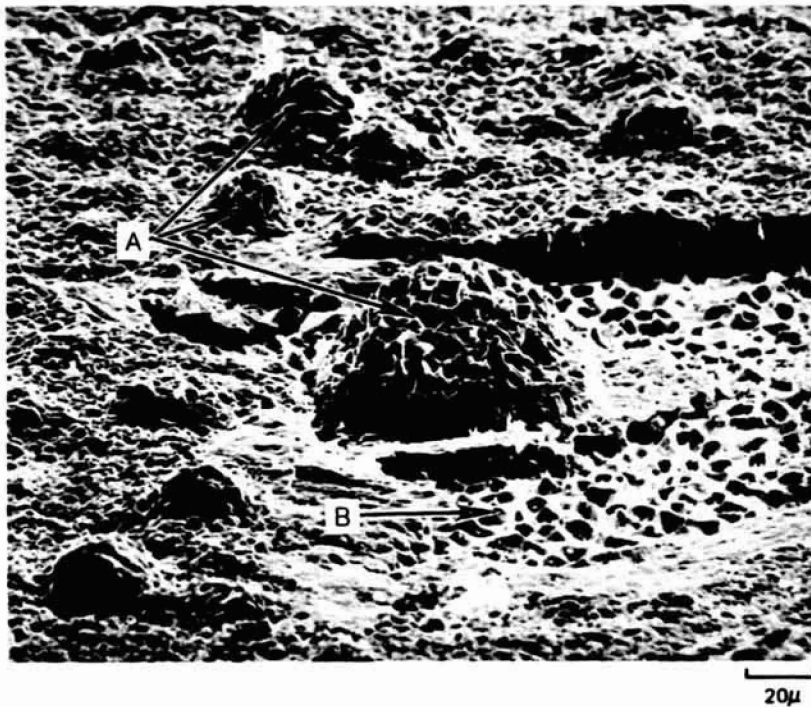


FIG. 4 Oxidation of Ni-25Cr at 1050°C in air alone (100 hours)  
oxide mounds (A) and convoluted oxide on Ni-25Cr surface (B).



A. Dense oxide scale.

20μ



B. Grain boundary attack.

20μ



C. Oxidation loop.

20μ



D. Internal oxidation.

20μ

FIG. 5. Oxidation of Ni-25Cr at 1050 °C in air alone (100 hours).

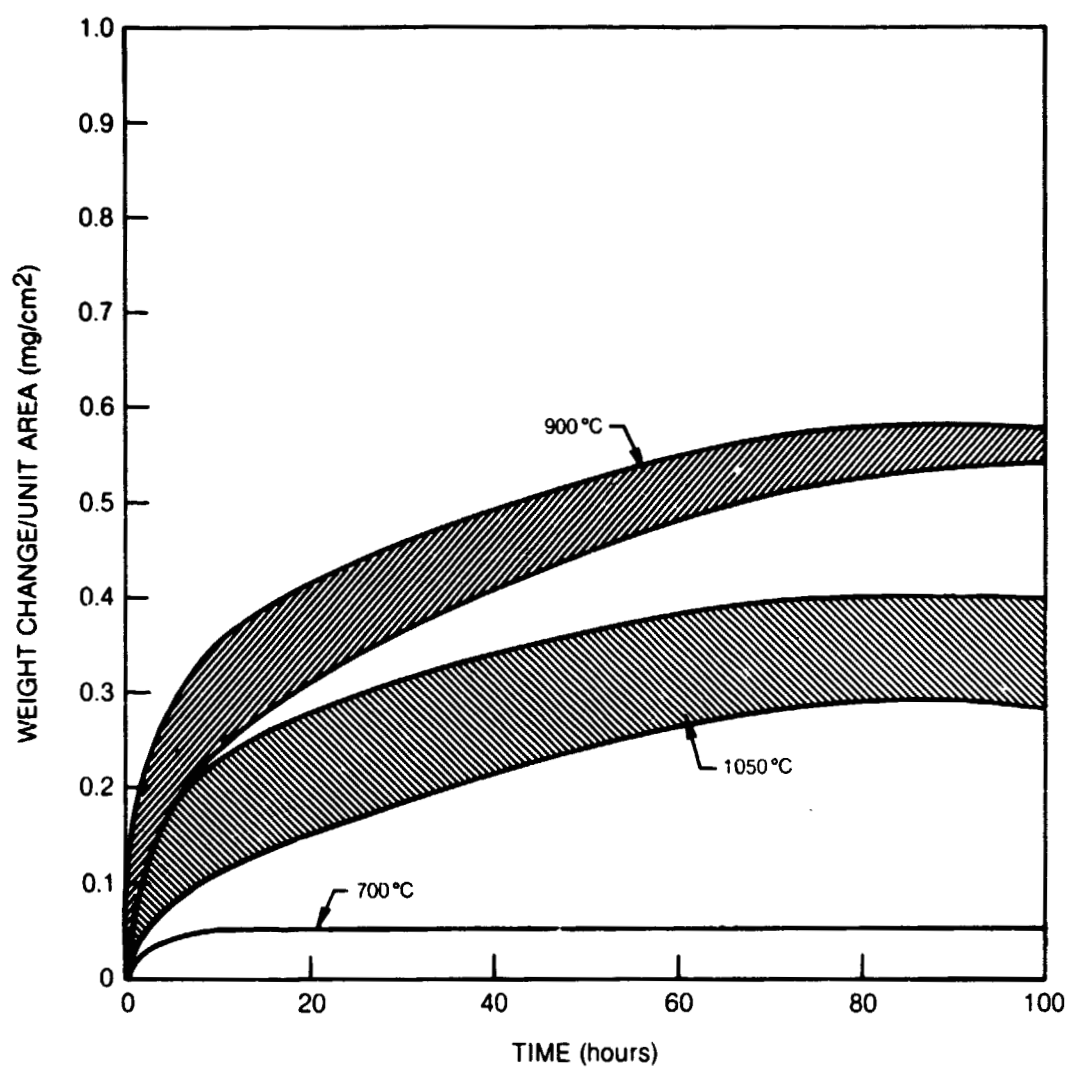


FIG. 6 Thermogravimetric data for B-1900 oxidized in air alone.

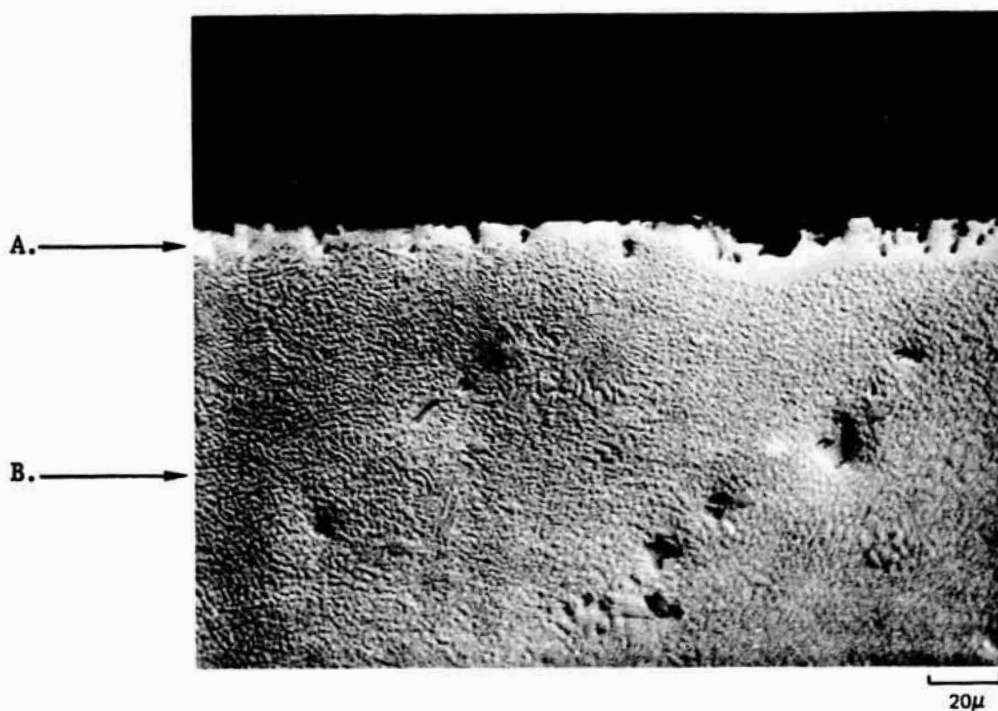


FIG. 7 Oxidation of B-1900 alloy at 1050°C in air alone (100 hours)

A. Thin gamma prime depletion zone (A)

B. Unaffected B-1900 substrate



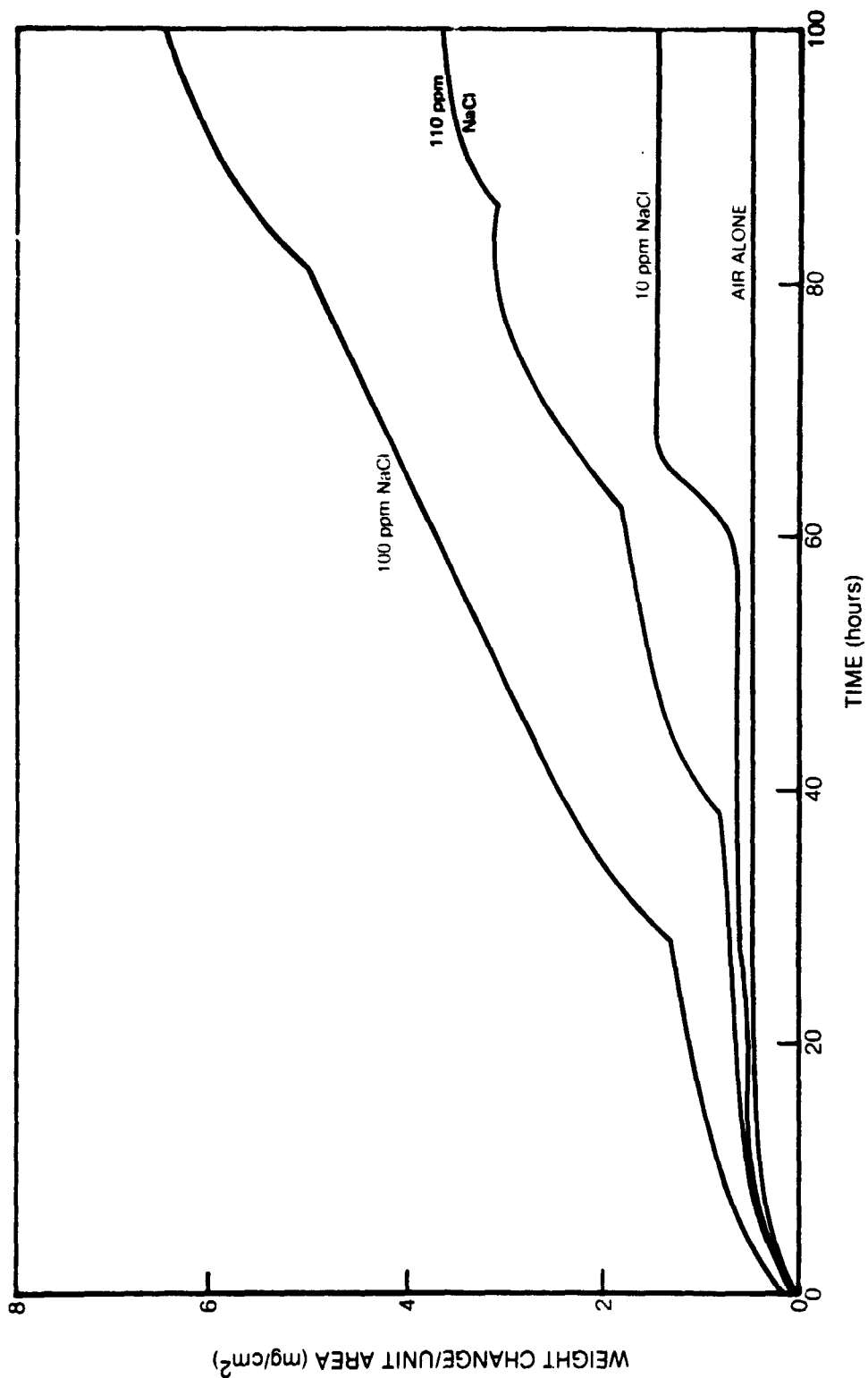


FIG. 8 Thermogravimetric data for NiAl oxidized in air with and without NaCl vapors at 900°C.

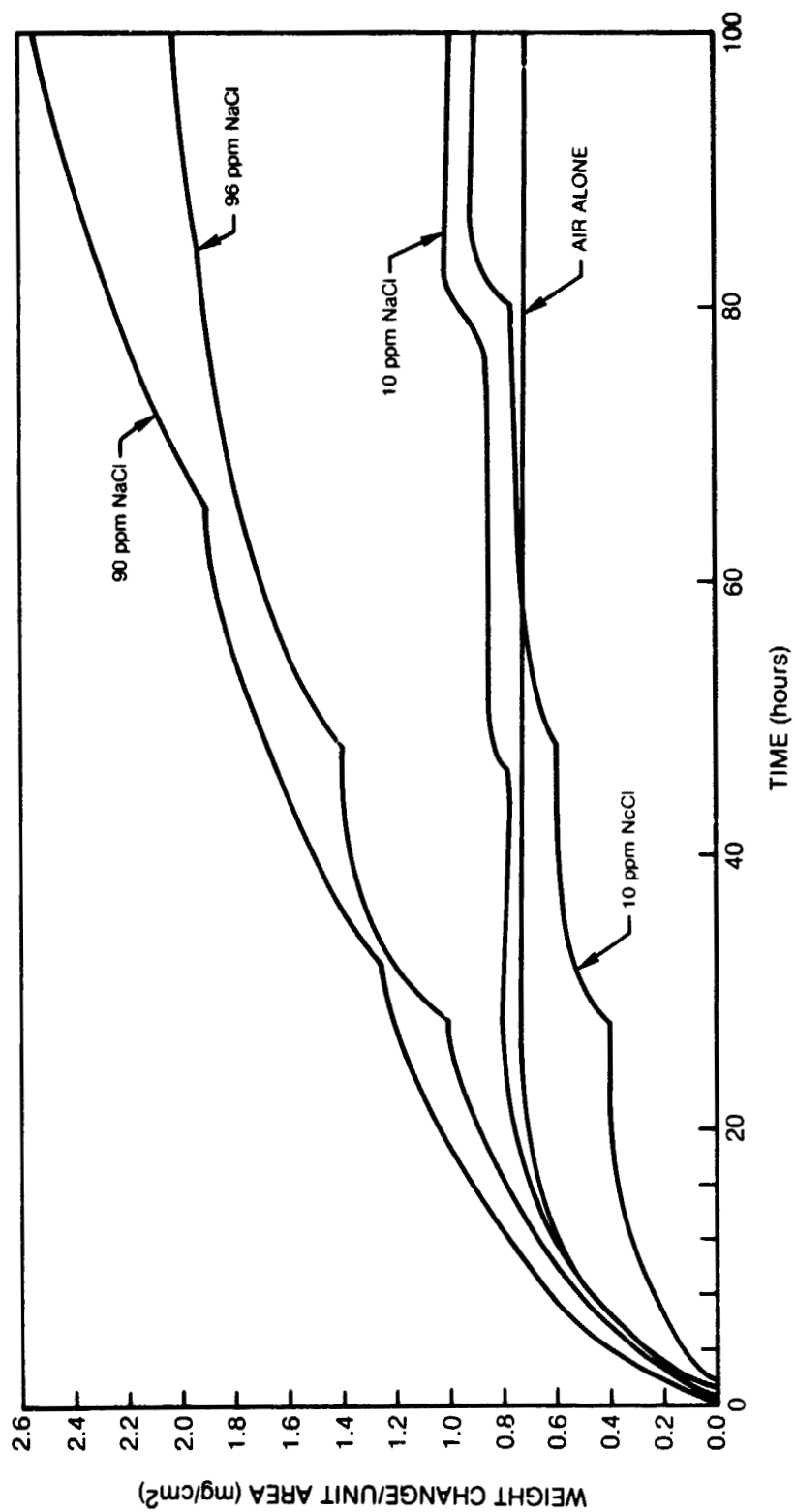


FIG. 9 Thermogravimetric data for NiAl oxidized in air alone with and without NaCl vapors at 1050°C.

- A. Outer oxide scale
- B. Inner oxide scale
- C. NiAl substrate



Note cracks (A) between external (B) and internal scales (C)

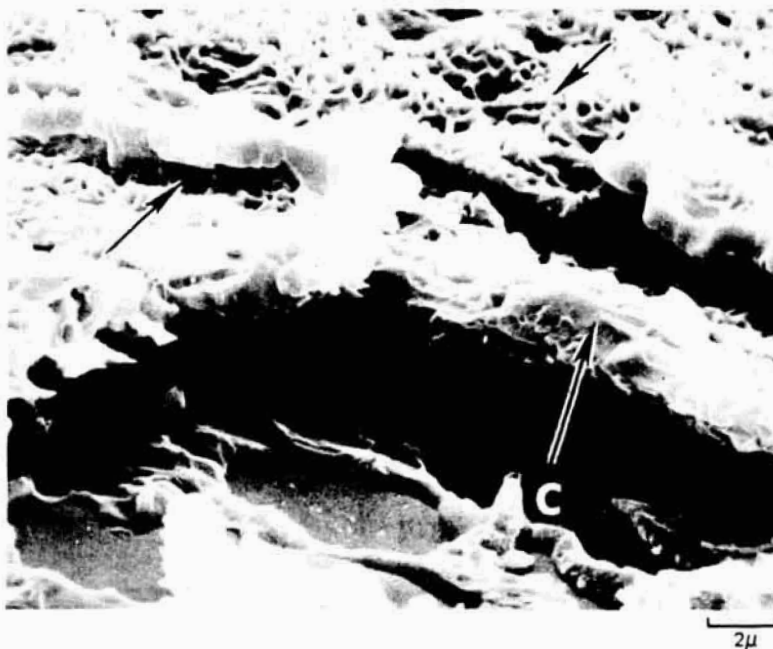
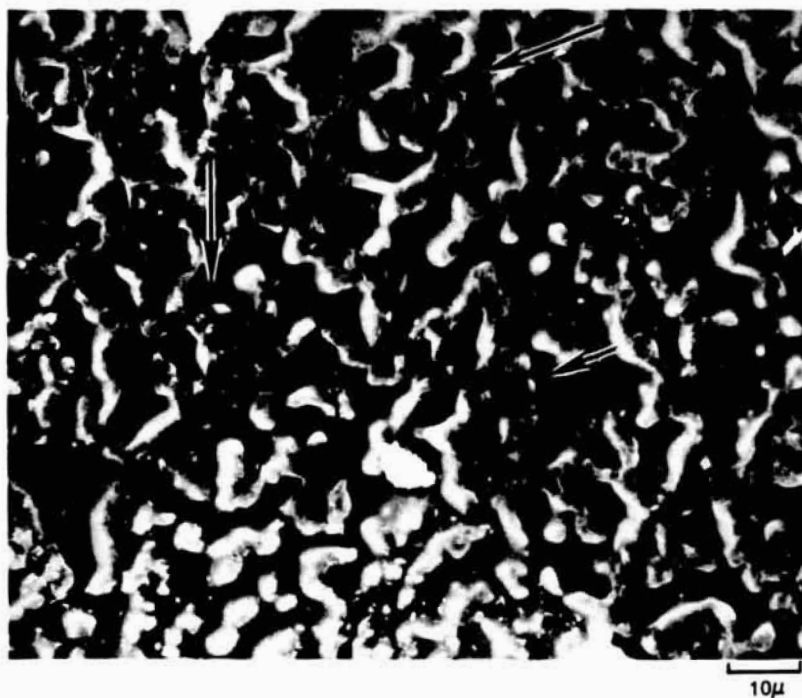


FIG. 10 Microscopy studies--NiAl exposed at 1050°C to air with 10ppm NaCl(g) for 100 hours.

A. Air alone



B. Air with 12ppm NaCl(g)

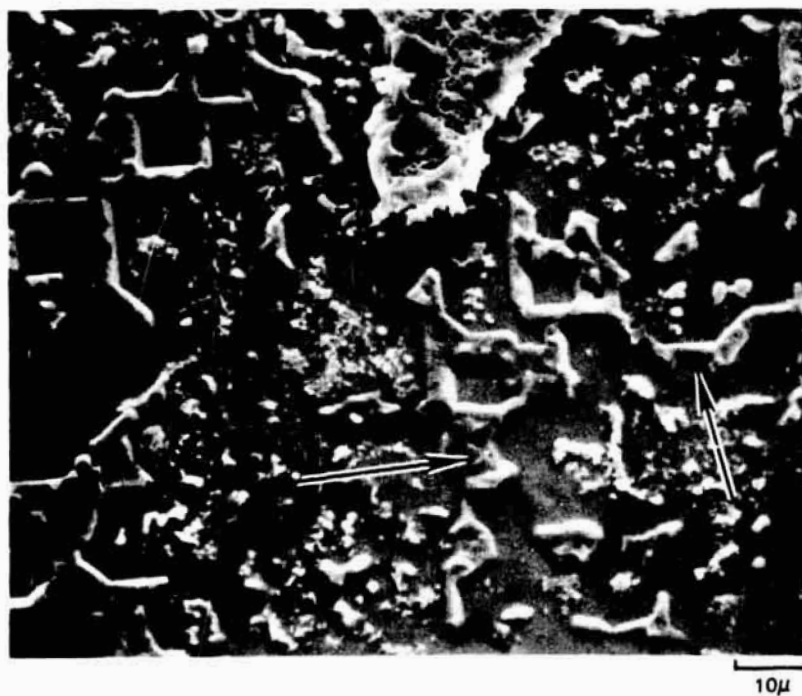


FIG. 11 Microscopy Studies--NiAl exposed at 1050°C for 100 hours. Arrows indicate attachment sites between substrate and scale.

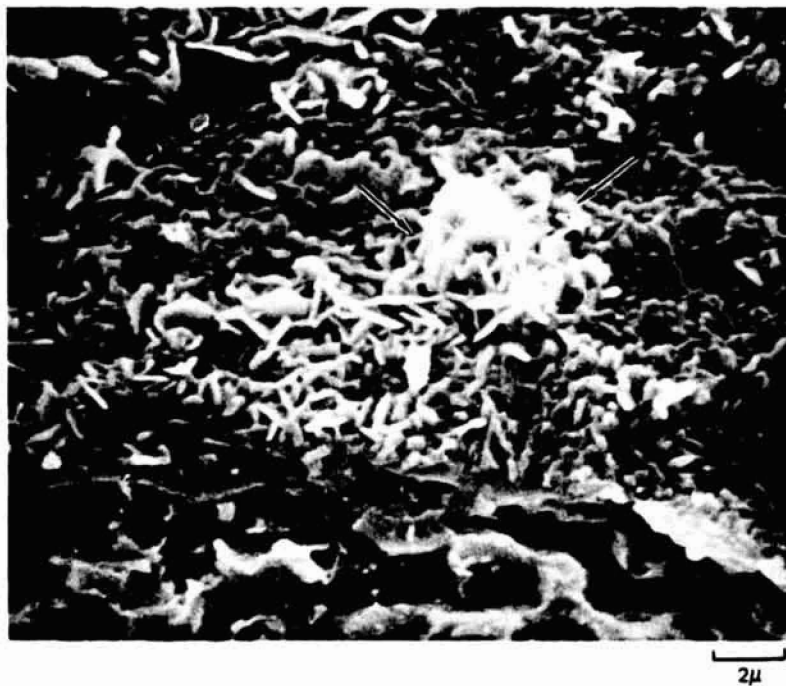


FIG. 12 Microscopy studies--NiAl exposed at 1050°C to air with 100ppm HCl and 0.02v/o SO<sub>2</sub> for 24 hours.

Note the formation of alumina whiskers (arrows).



FIG. 13 Al<sub>2</sub>O<sub>3</sub> whiskers on CoCrAlY oxidized at 1050°C for 24 hours in air with 100ppm NaCl.

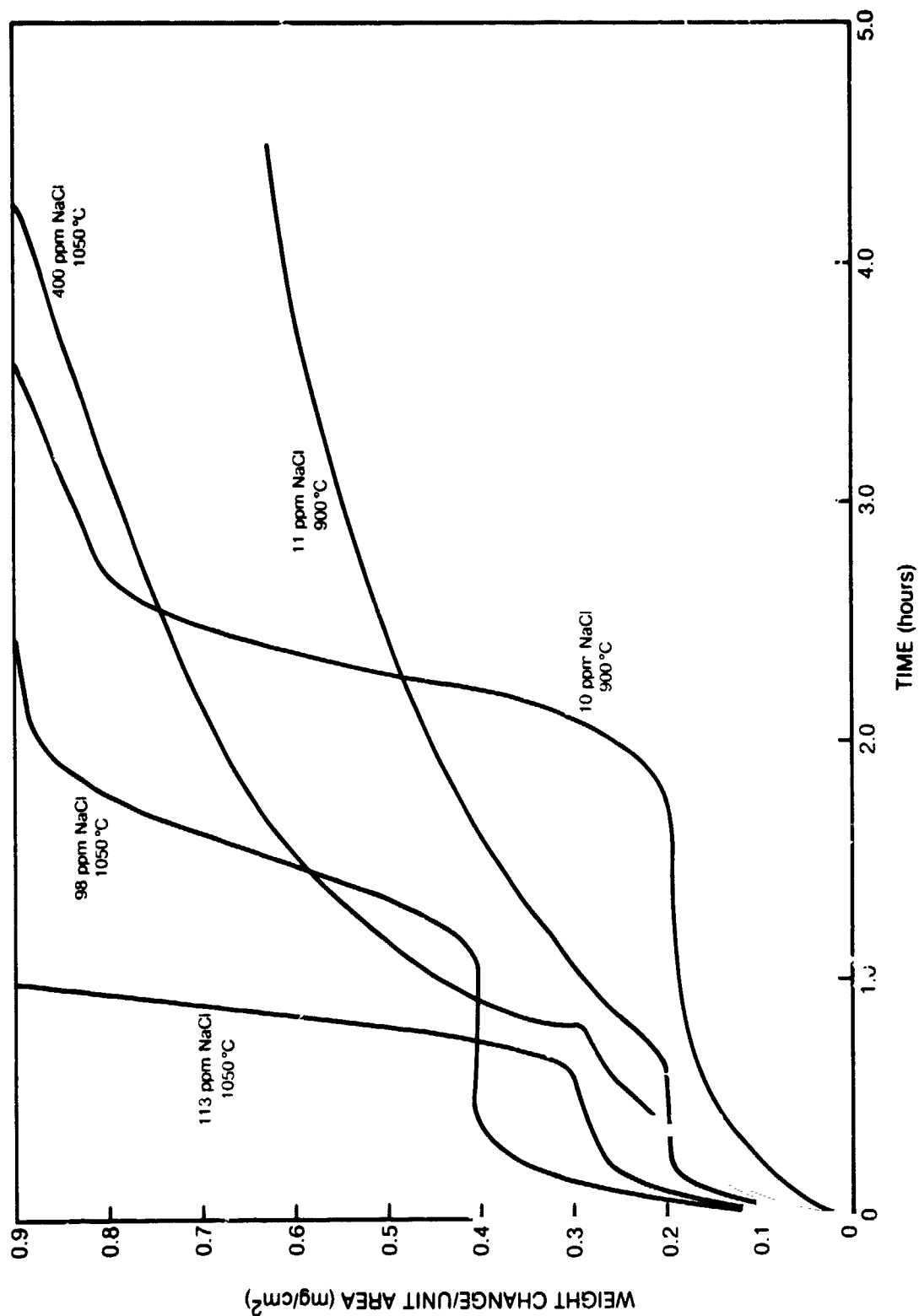


FIG. 14 Early stages in the oxidation of Ni-25Cr oxidized in air with NaCl(g).

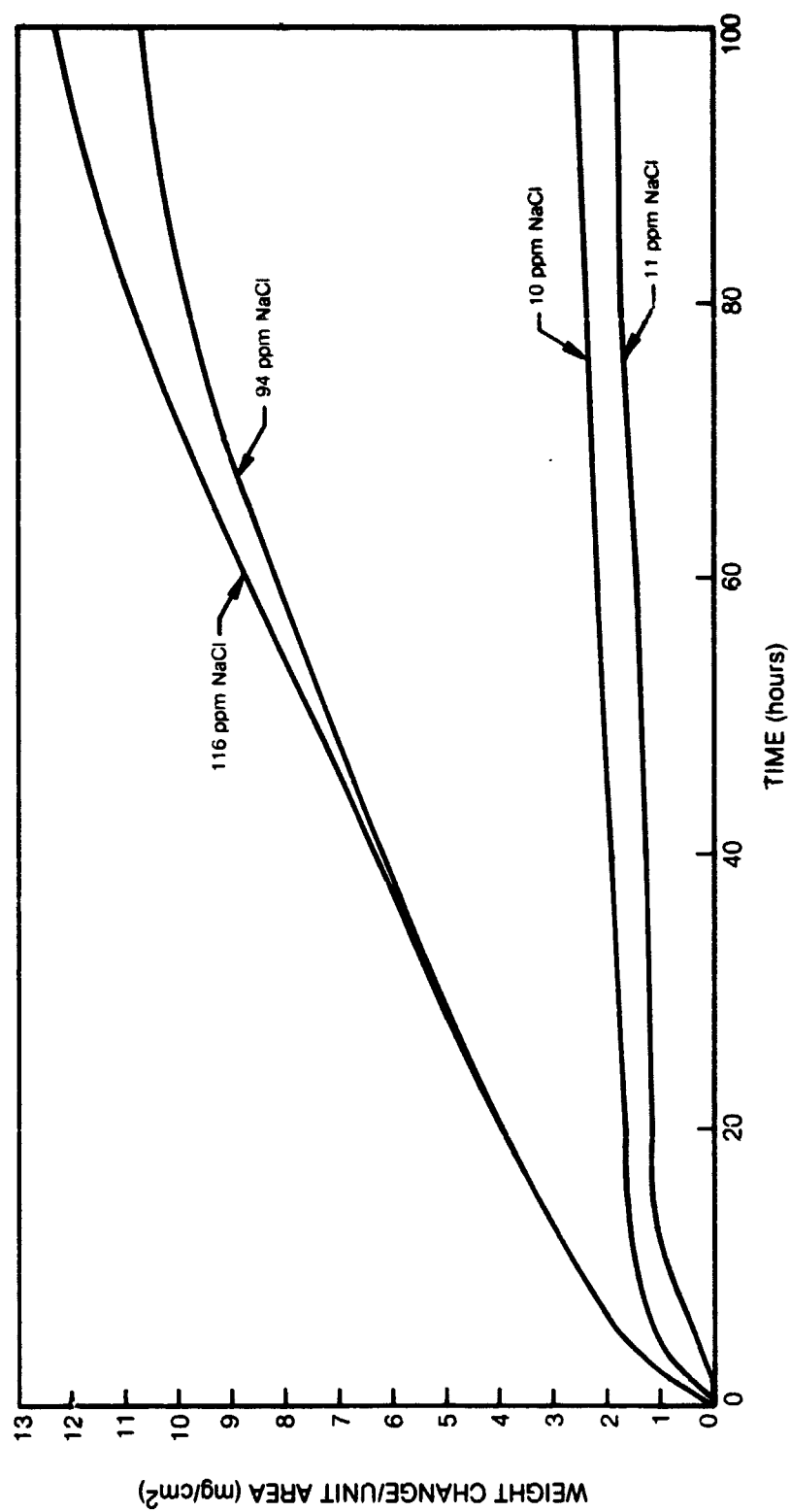


FIG. 15 Oxidization of Ni-25Cr at 900°C in air with NaCl(g).



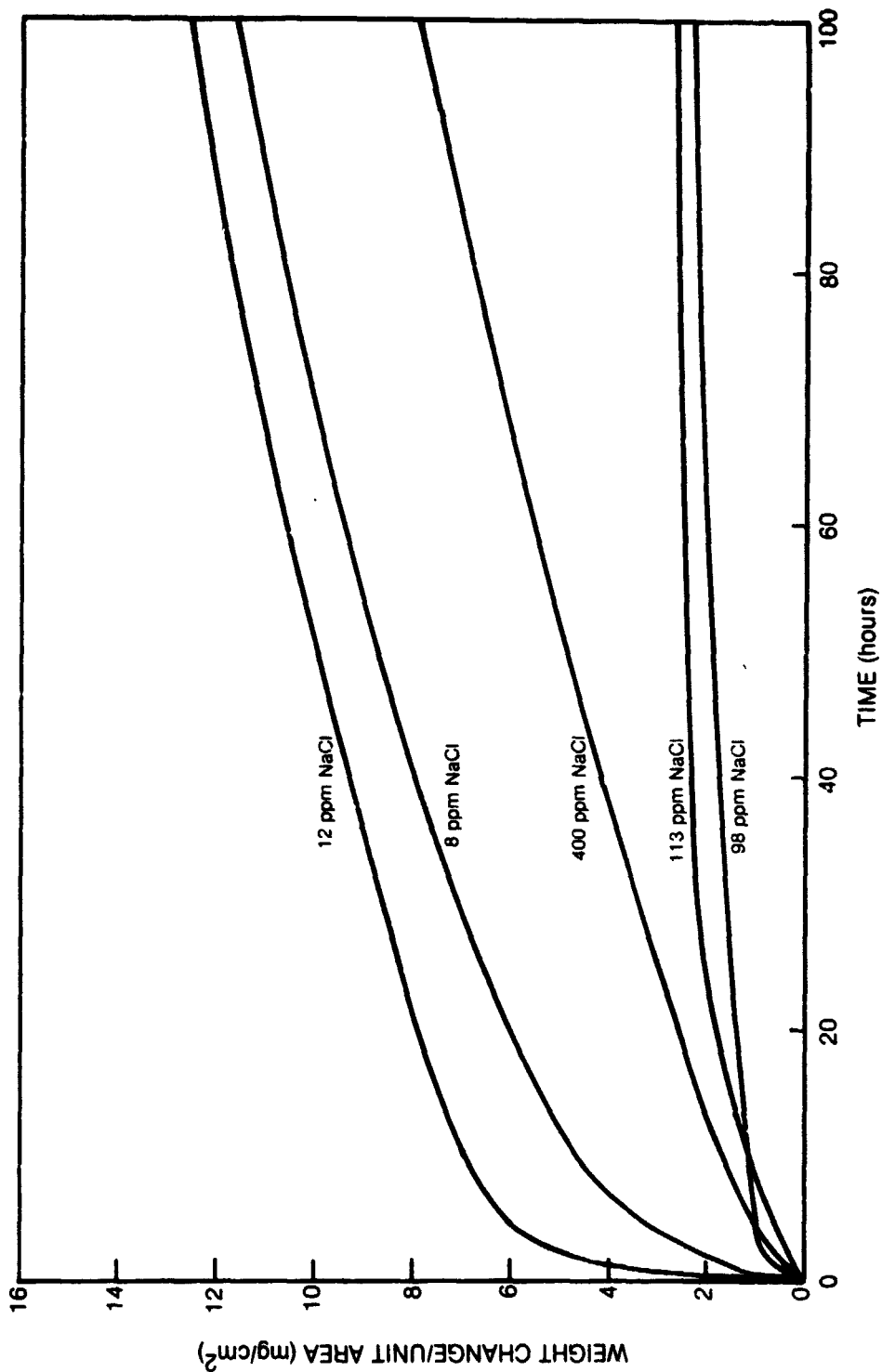
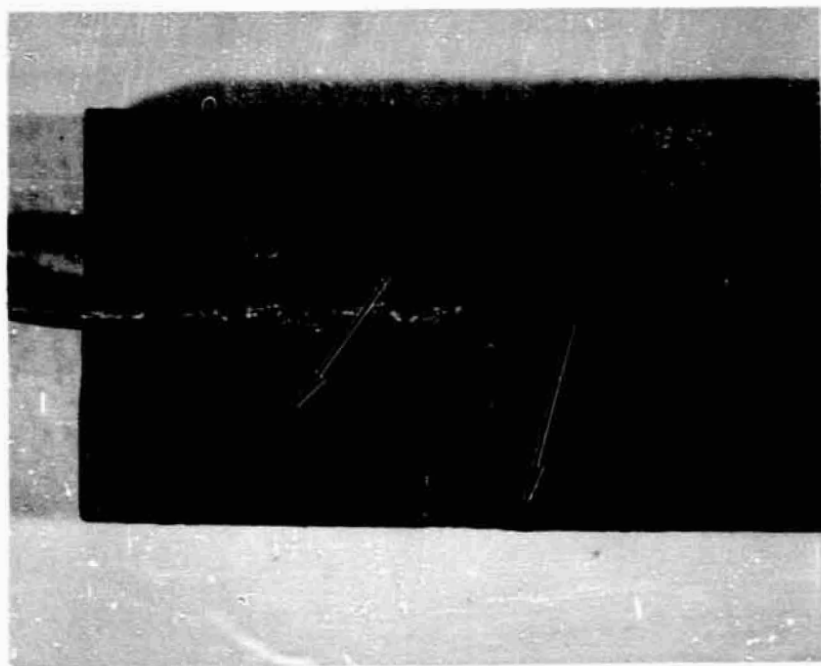


FIG. 16 Oxidation of Ni-25Cr at 1050°C in air with NaCl(g).



1000 $\mu$

FIG. 17 Blister formation (arrows) on Ni-25Cr exposed for 100 hours at 1050°C in air with 8ppm NaCl(g).

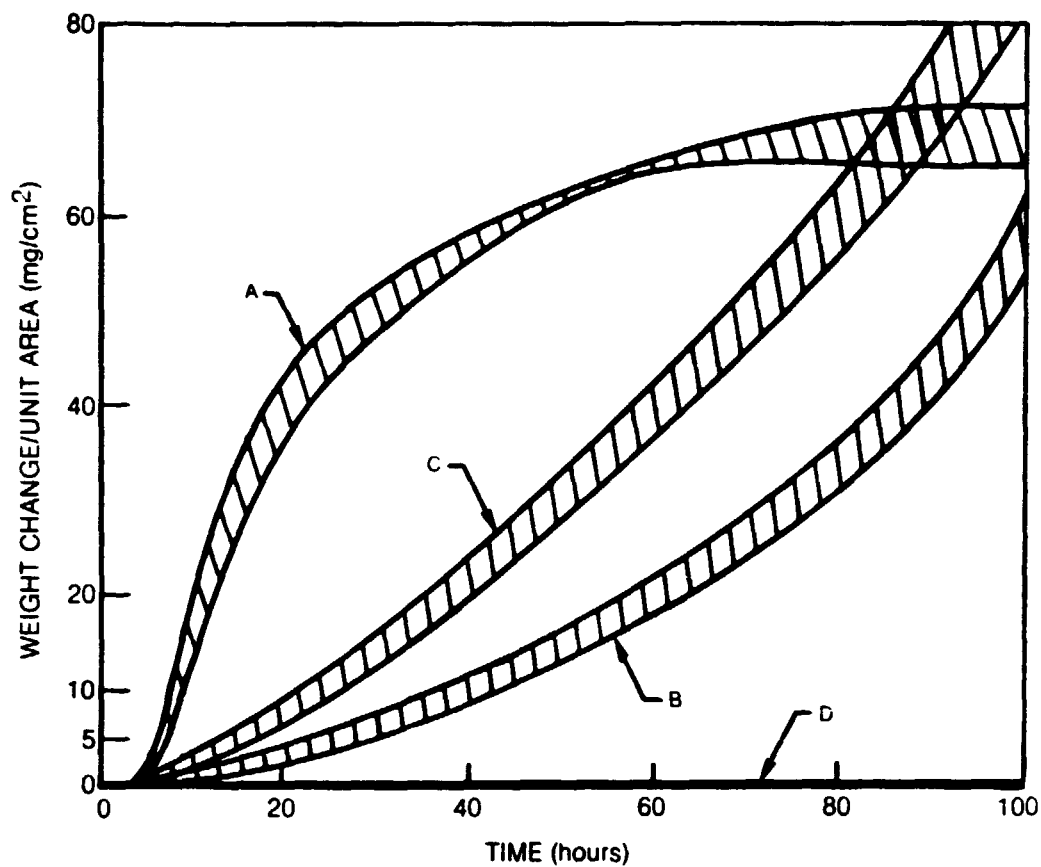


FIG. 18 Oxidation of B-1900 at  $900^\circ\text{C}$

- A.  $\text{Na}_2\text{SO}_4$  coated ( $1 \text{ mg/cm}^2$ )
- B. 10ppm NaCl (no  $\text{Na}_2\text{SO}_4$ )
- C. 100ppm NaCl (no  $\text{Na}_2\text{SO}_4$ )
- D. Air alone (no  $\text{Na}_2\text{SO}_4$ - no NaCl)

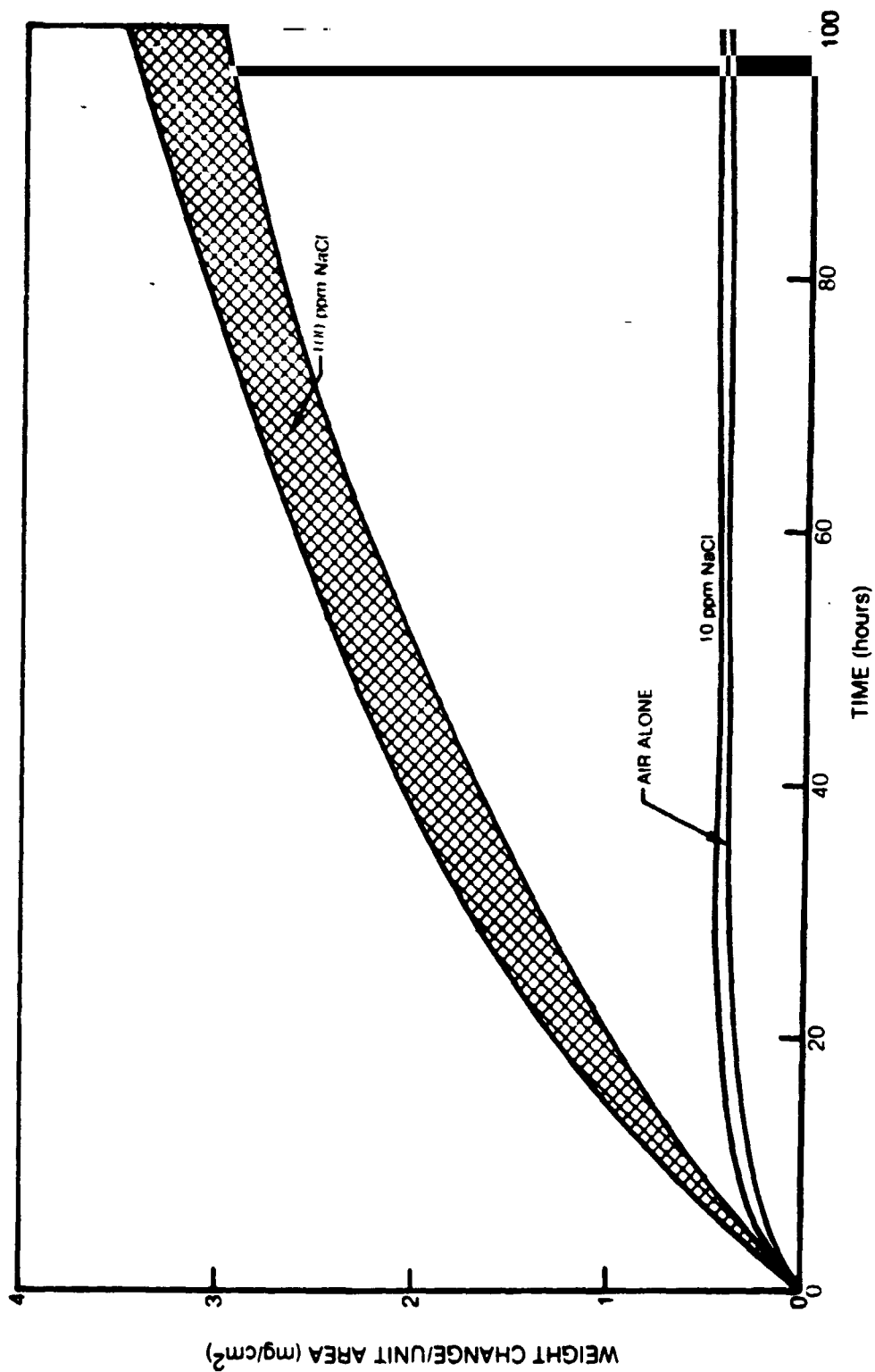
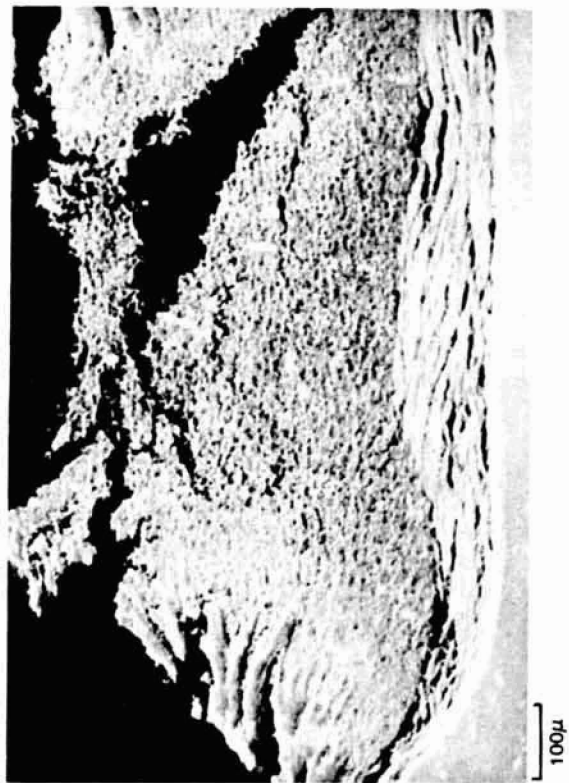


FIG. 19 Oxidation of B-1900 at 1050°C with and without addition of NaCl(g).

Scanning Electron Micrograph



Molybdenum X-ray Map



Nickel X-ray Map



FIG. 20 B-1900 oxidized in air with 11ppm NaCl(g) for 100 hours.

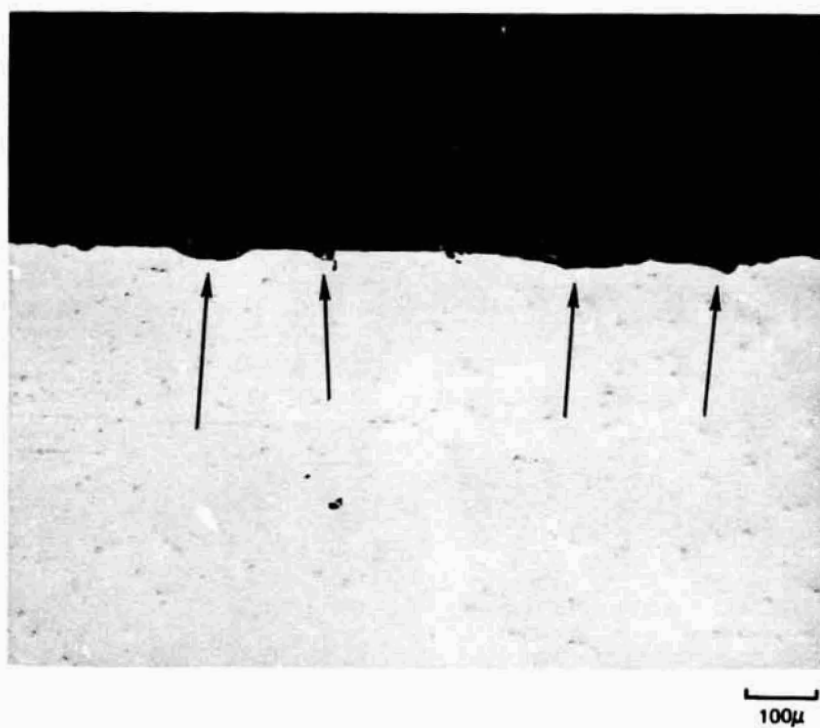
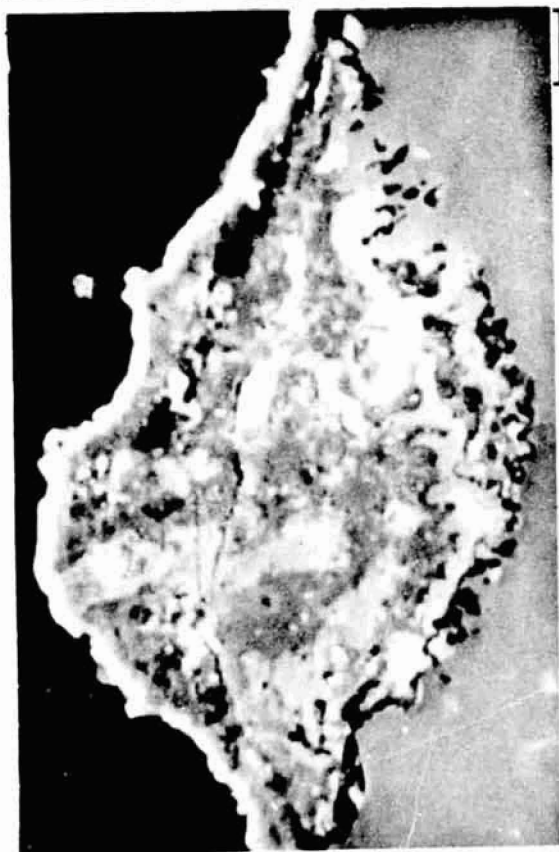


FIG. 21 Pitting attack (arrows) of B-1900 exposed to air with 92ppm NaCl(g) for 100 hours at 1050°C.

Scanning Electron Micrograph



Molybdenum X-Ray Map



Nickel X-ray Map



FIG. 22 B-1900 oxidized in air with 100 ppm NaCl(g) at 1050°C for 100 hours.

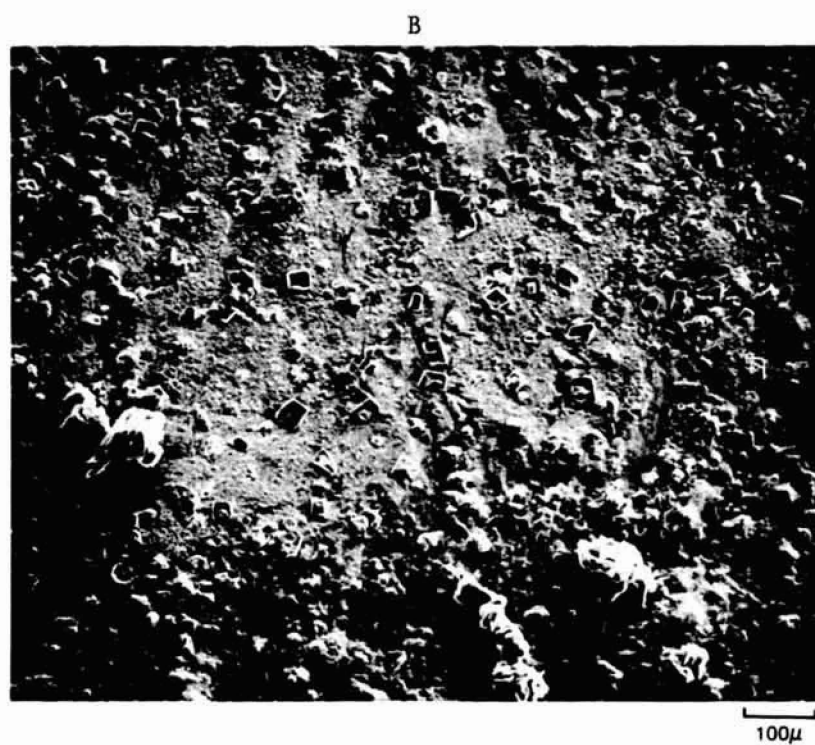
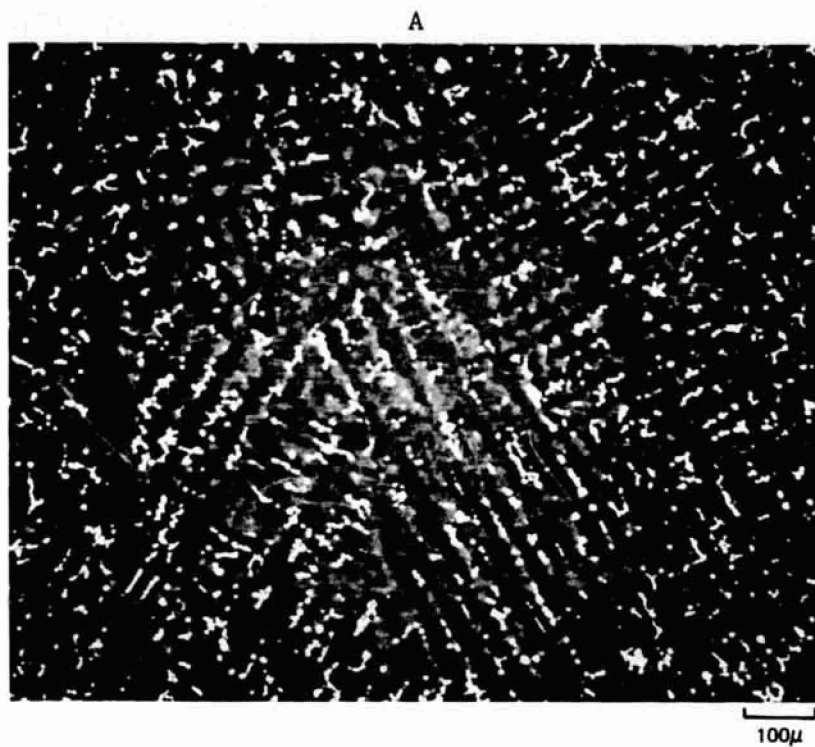


FIG. 23 B-1900 oxidized at 700°C.

A for 100 hours in air alone

B for 60 hours in air with 10ppm NaCl(g)



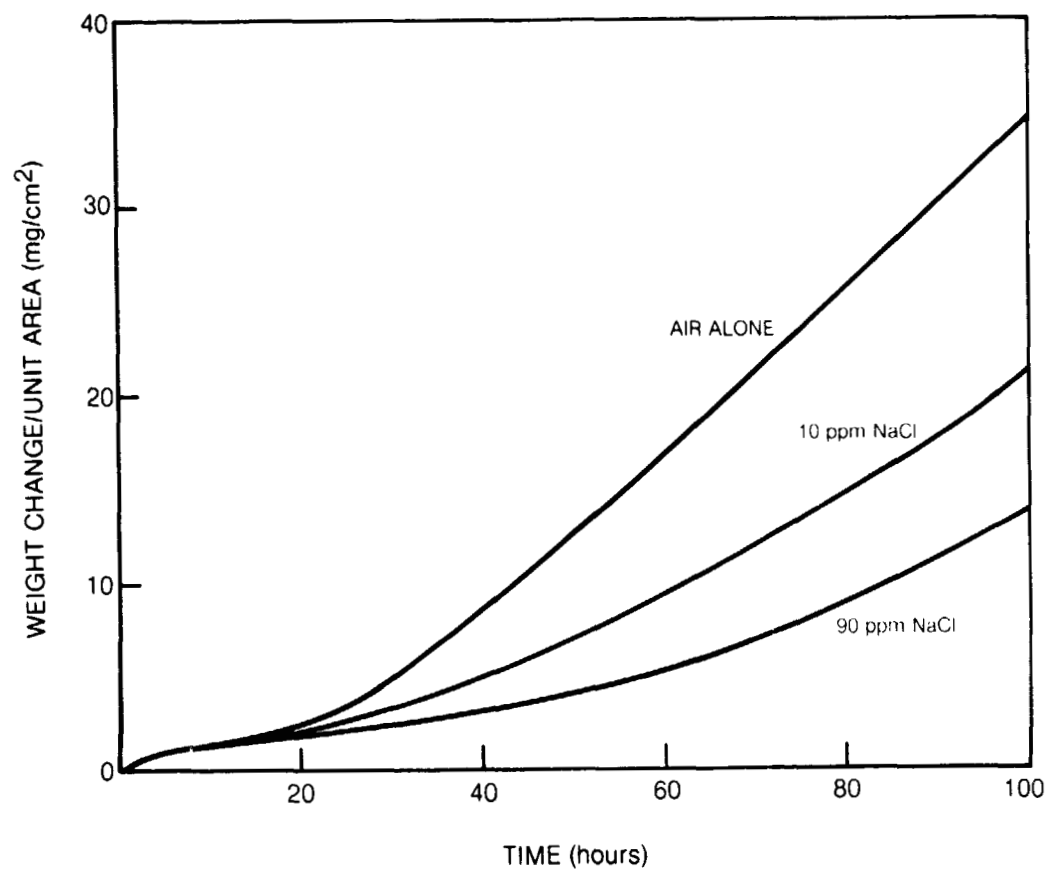


FIG. 24 Oxidation of sodium sulfate-coated (1.0 mg/cm<sup>2</sup>) NiAl at 1050°C.

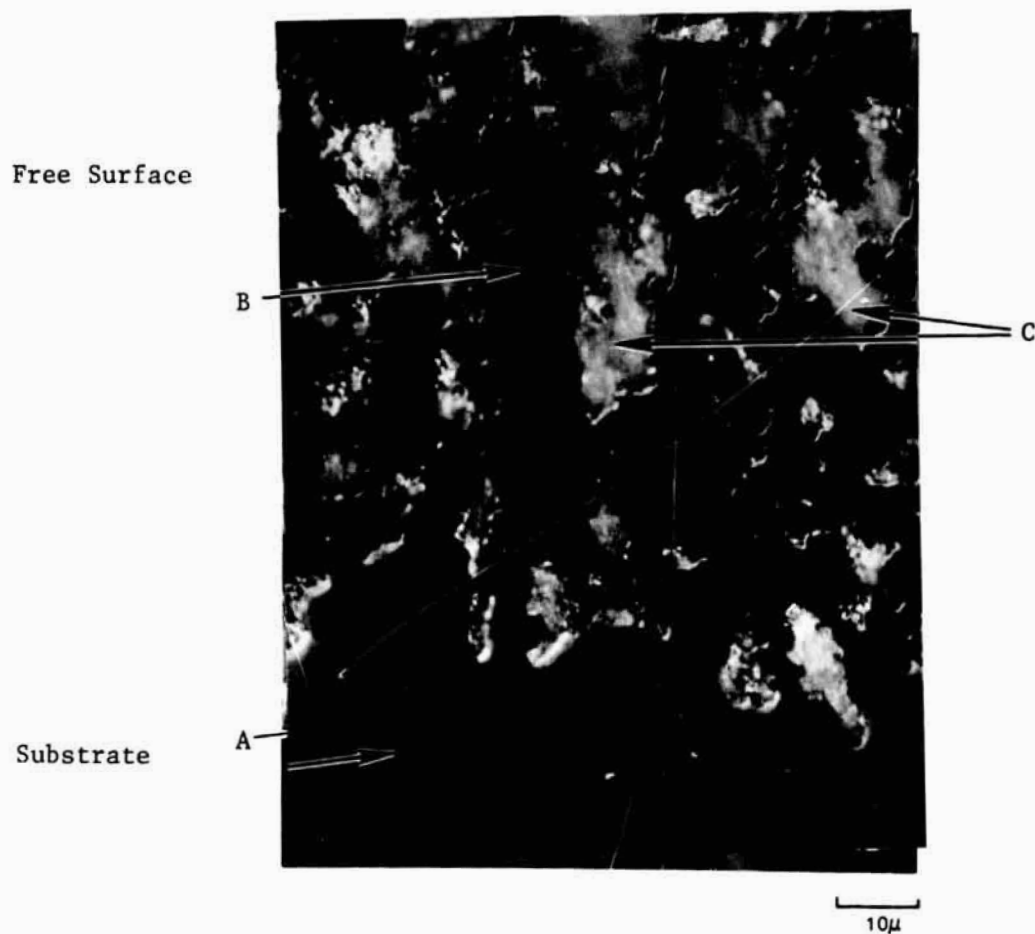


FIG. 25 Sodium sulfate-coated ( $1.0 \text{ mg/cm}^2$ ) NiAl oxidized in air with 90ppm NaCl(g) at  $1050^\circ\text{C}$  for 100 hours. (A) Widmanstätten precipitation and (B)  $\gamma'$  ( $\text{Ni}_3\text{Al}$ ) formation in aluminum depleted NiAl regions containing (C) oxide inclusions.

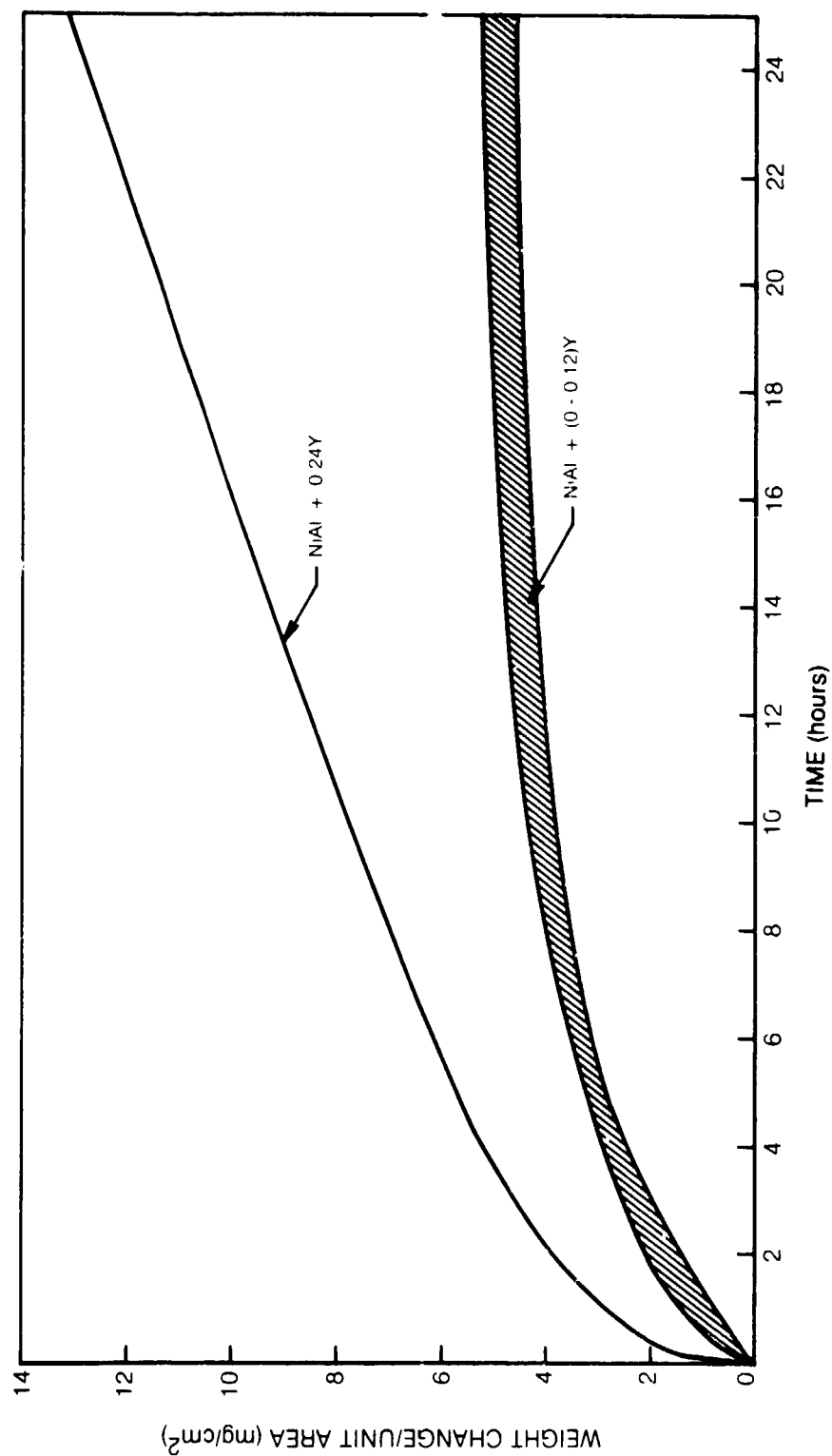


FIG. 26 Oxidation behavior of sodium sulfate-coated ( $1.0 \text{ mg/cm}^2$ )  $\text{NiAl+Y}$  at  $900^\circ\text{C}$  in air alone.

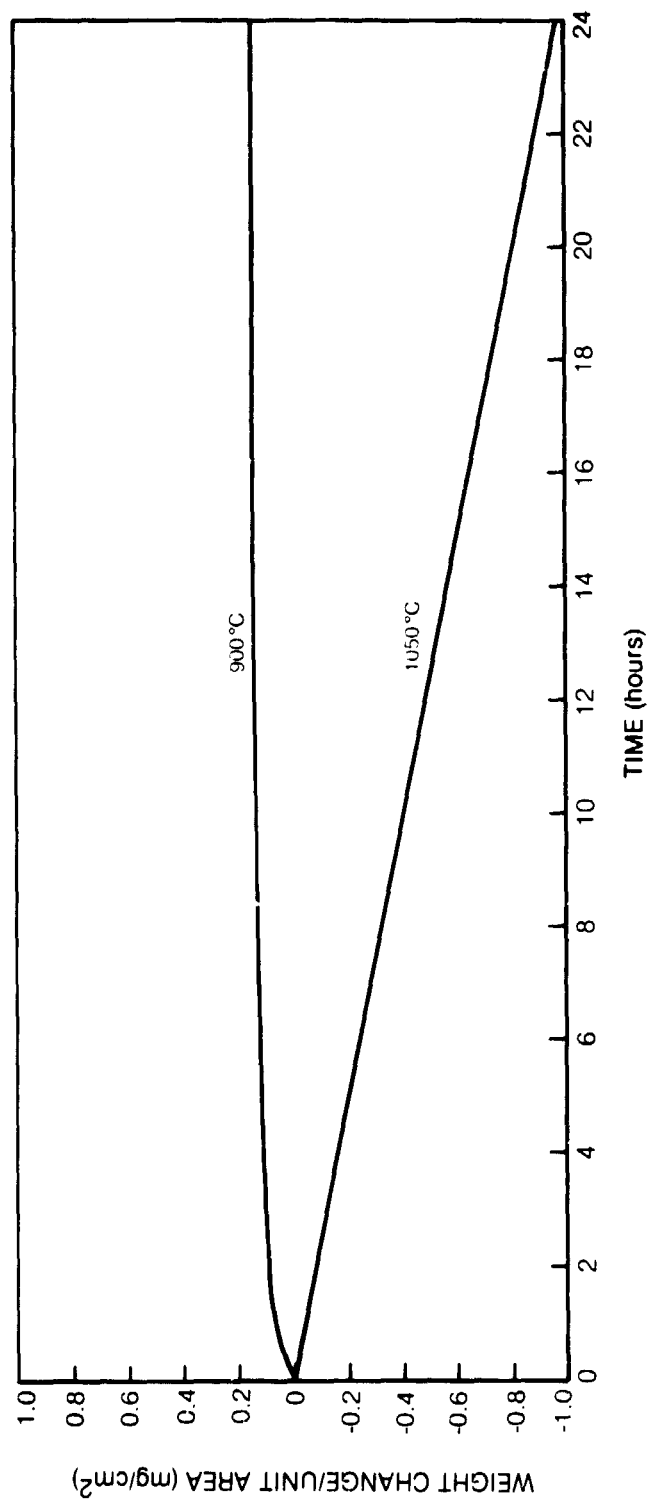


FIG. 27 Oxidation behavior of sodium sulfate-coated (1.0 mg/cm<sup>2</sup>) CoCrAl.

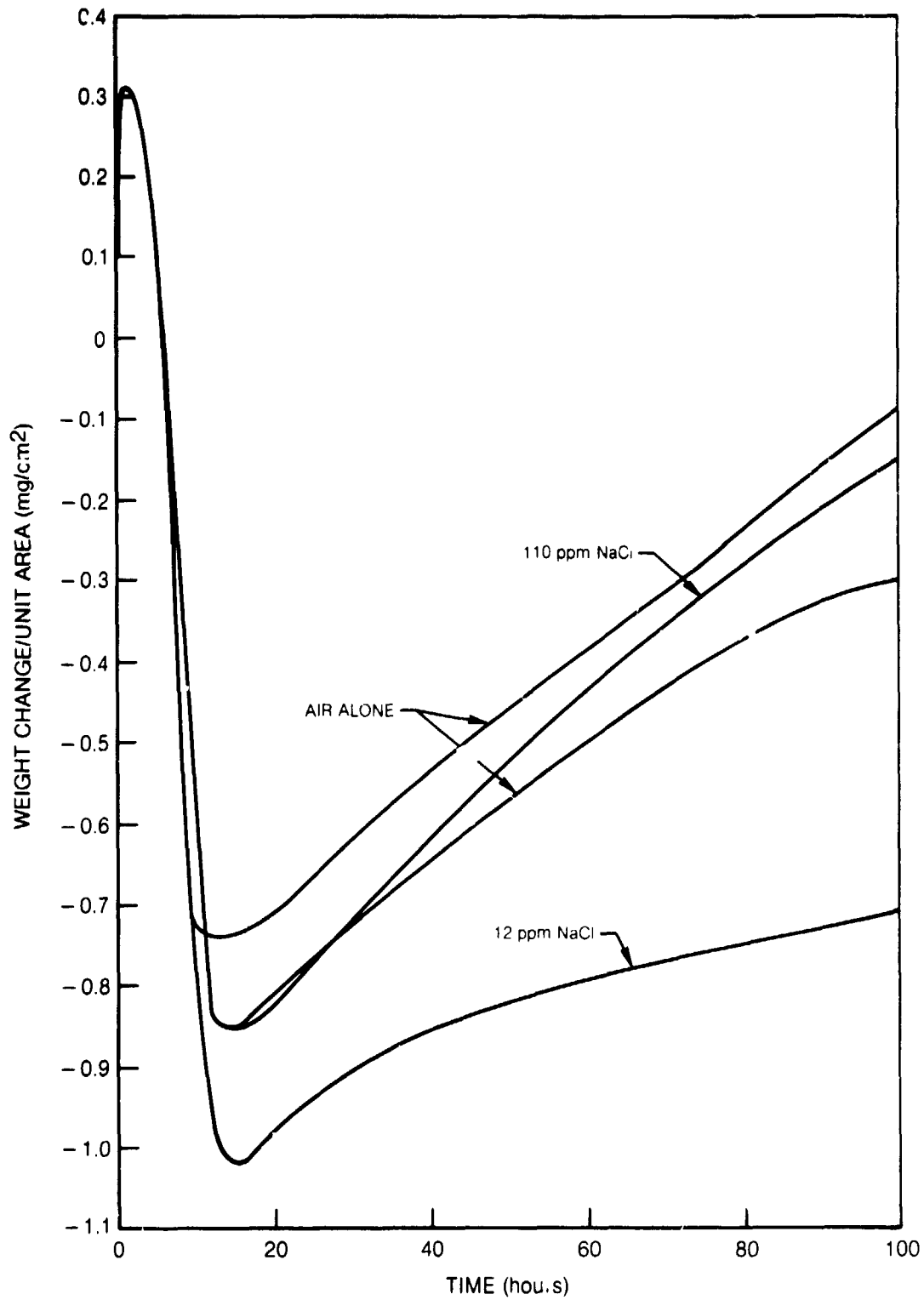


FIG. 28 Thermogravimetric data for sodium sulfate-coated Ni-25Cr oxidized at 1050°C for 100 hours (1.0 mg/cm<sup>2</sup>).

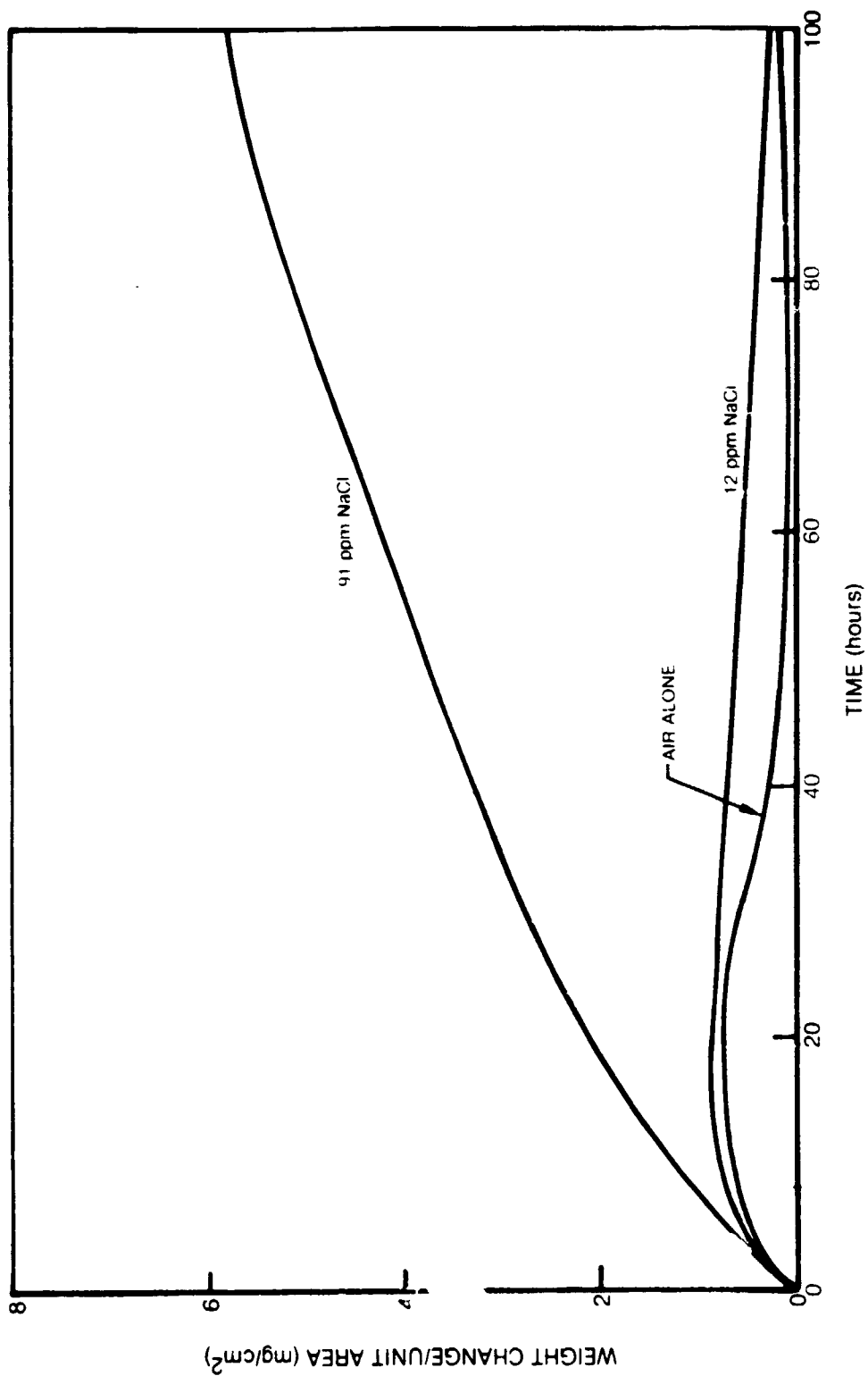
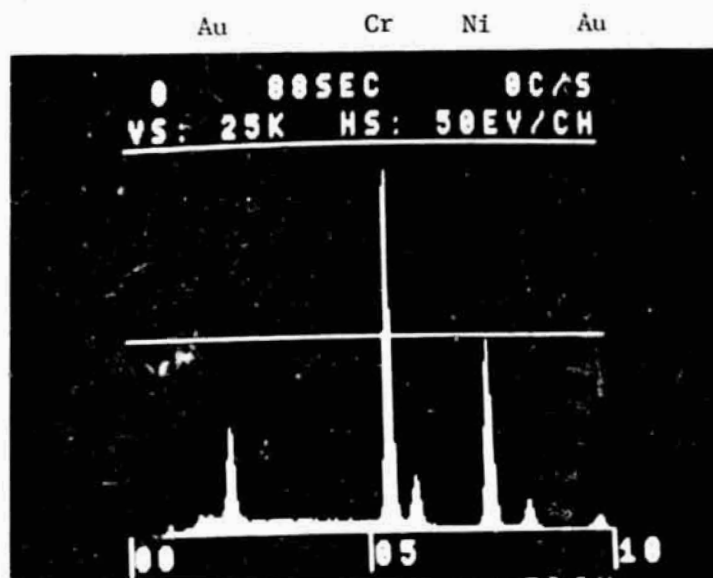


FIG. 29 Oxidation of sodium sulfate-coated (1.0 mg/cm<sup>2</sup>) Ni-25Cr at 900°C.



- a. A. Chromia crystals produced by molten salt effects  
 B. Matrix scale



- b. EDAX of matrix scale

FIG. 30 Chromia crystals (A) growing on a nickel-enriched oxide substrate (B).  $\text{Na}_2\text{SO}_4$  coated ( $1.0 \text{ mg/cm}^2$ ) Ni-25Cr oxidized in air at  $1050^\circ\text{C}$  for 100 hours.

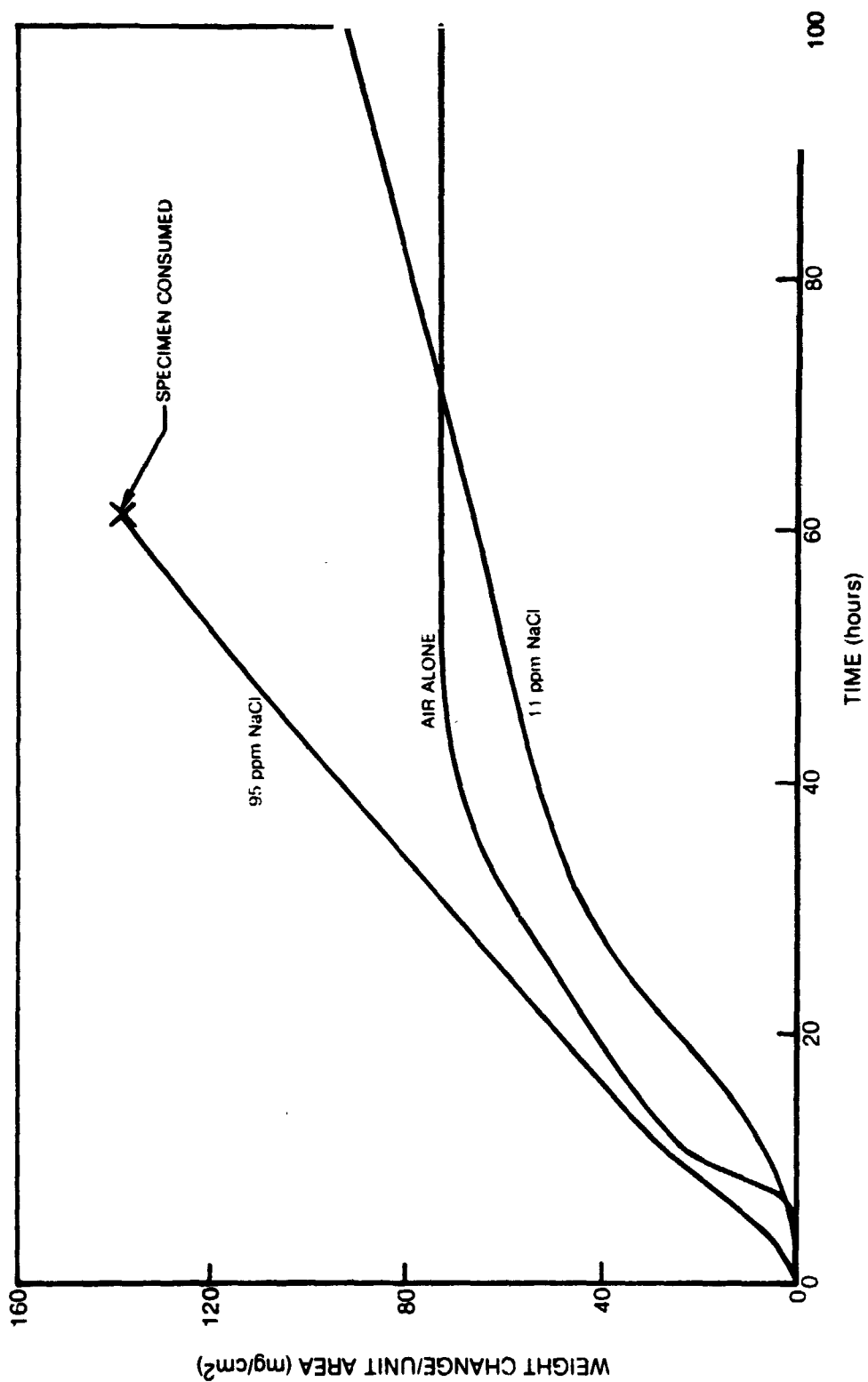


FIG. 31 Oxidation of sodium sulfate-coated (1.0 mg/cm<sup>2</sup>) B-1900 at 900°C.



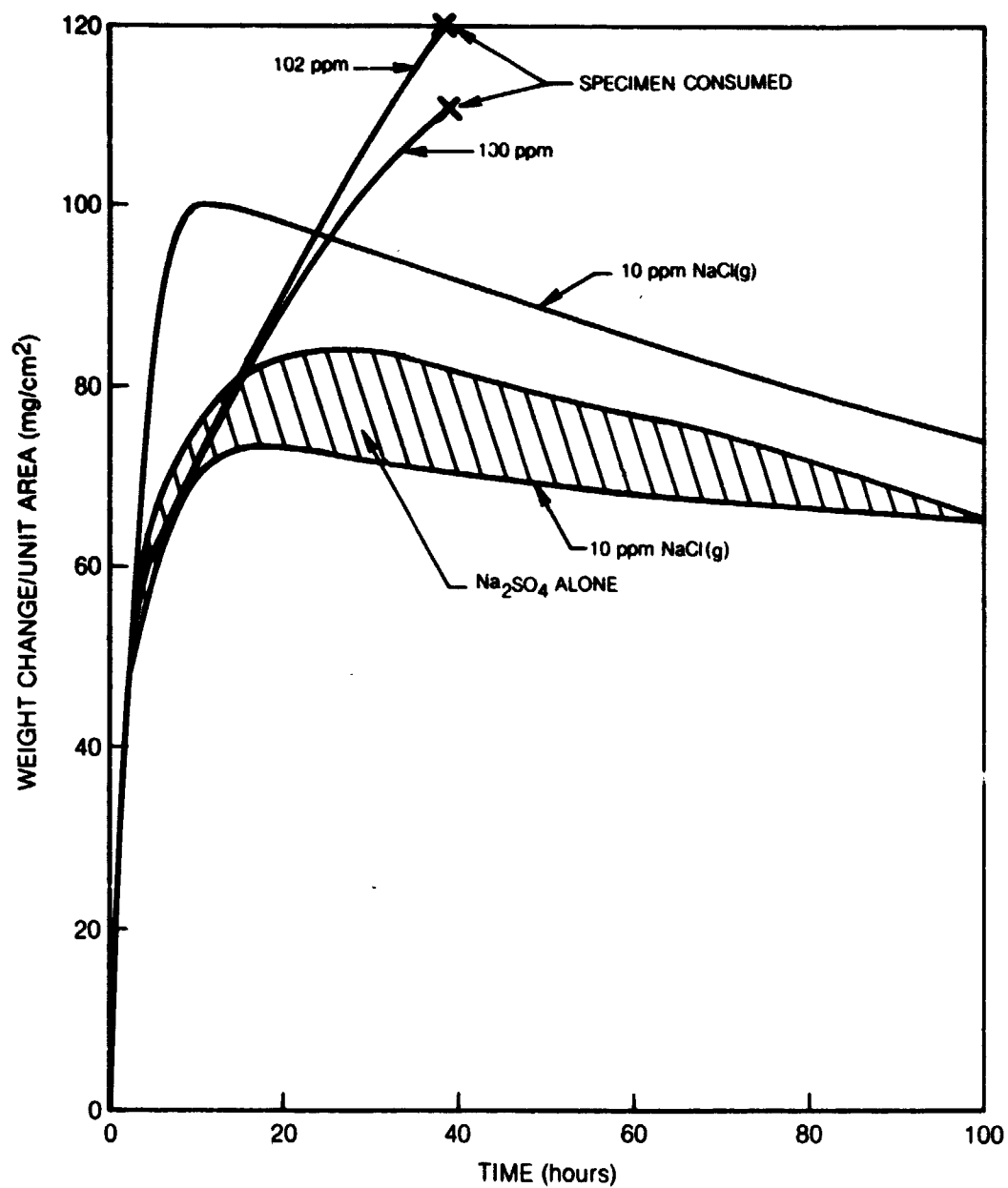


FIG. 32 Thermogravimetric data for sodium sulfate-coated (1.0 mg/cm<sup>2</sup>) B-1900 oxidized at 1050°C.

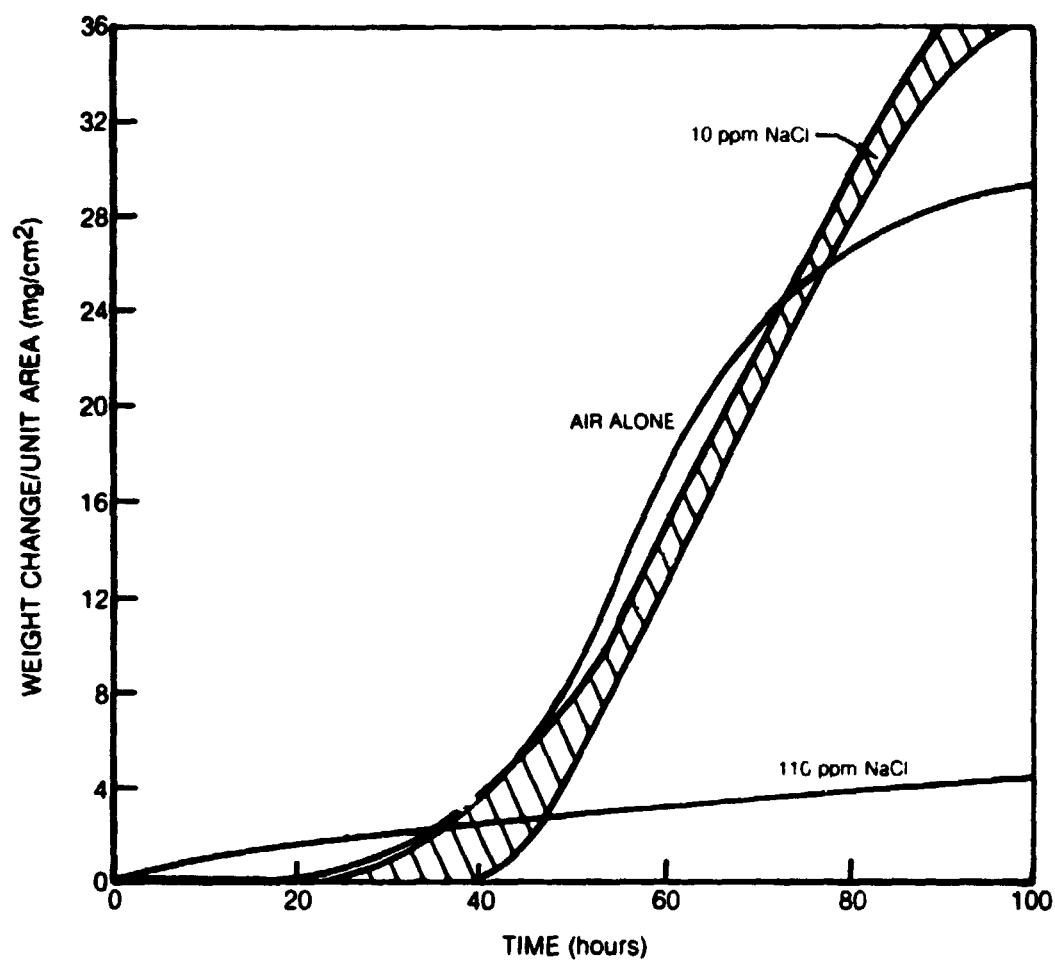


FIG. 33 Oxidation of sodium sulfate/ammonium chromate-coated B-1900 at 900°C in air with and without NaCl vapor present.

Deposit: 3.2 mg/cm<sup>2</sup> (1 part by weight Na<sub>2</sub>SO<sub>4</sub>:: 2.2 parts by weight (NH<sub>4</sub>)<sub>2</sub>Cr<sub>2</sub>O<sub>7</sub>).

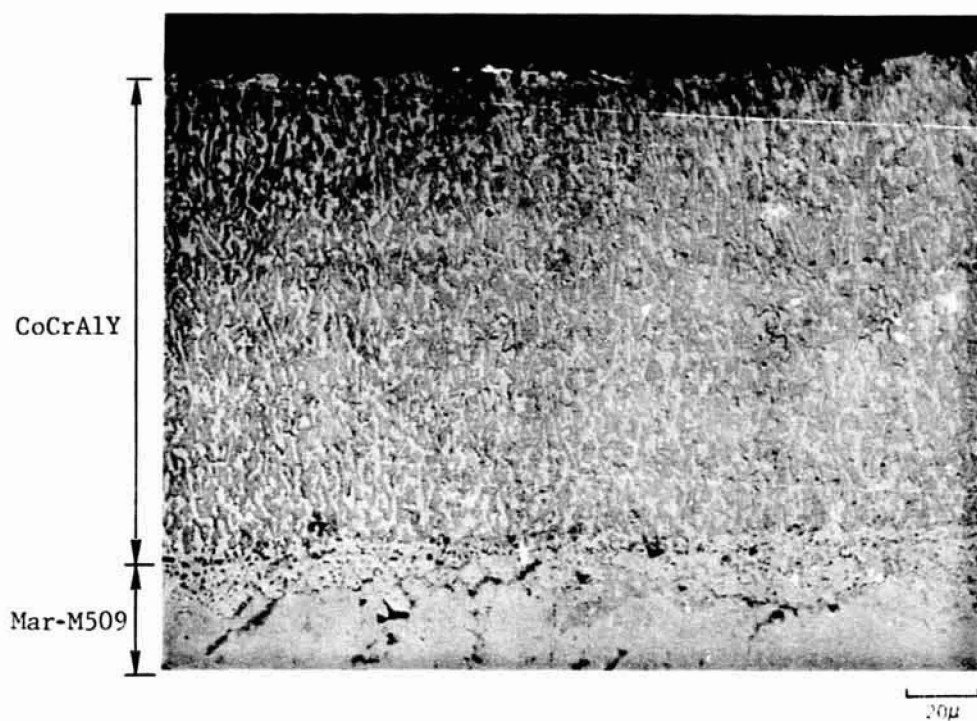


FIG. 34 CoCrAlY-coating oxidized in air at 700°C for 3000 hours.

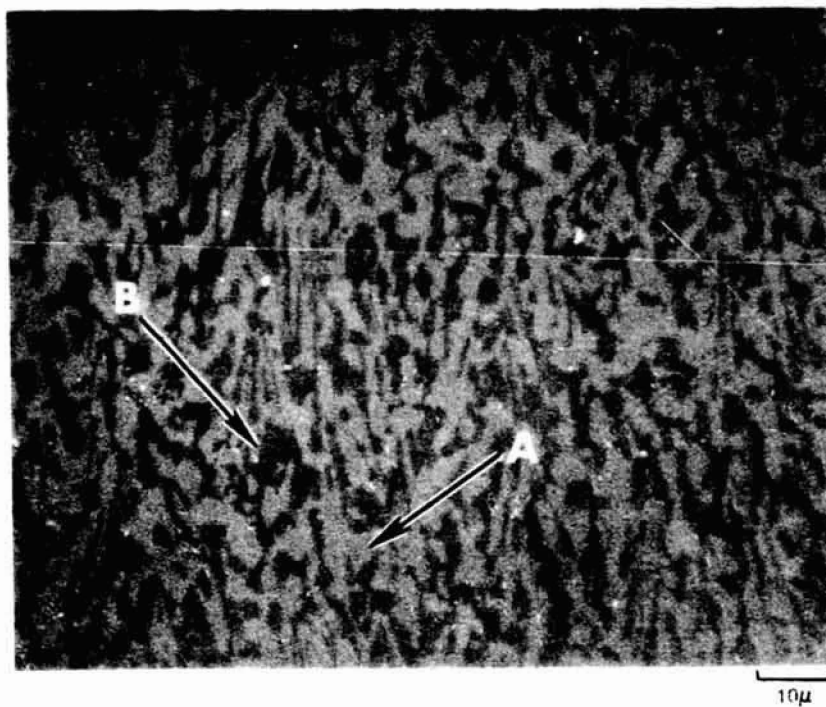


FIG. 35 CoCrAlY-coating (IM 6250), as processed.

- A.  $\alpha$ -Co(Cr,Al) solid solution
- B.  $\beta$ -CoAl

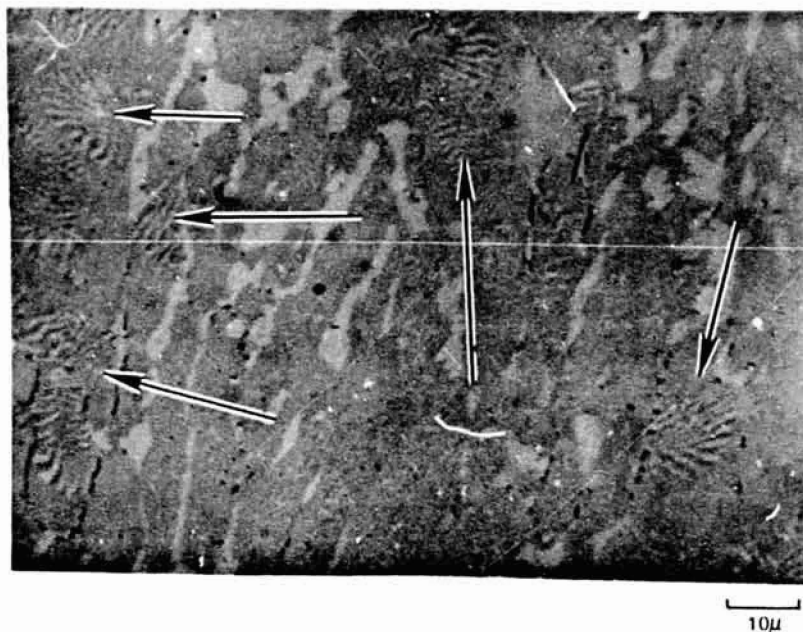


FIG. 36 Discontinuous precipitation effects producing cellular recrystallization (arrows) in CoCrAlY-coating exposed at 1300°C for one minute followed by 60 hours in air at 700°C.

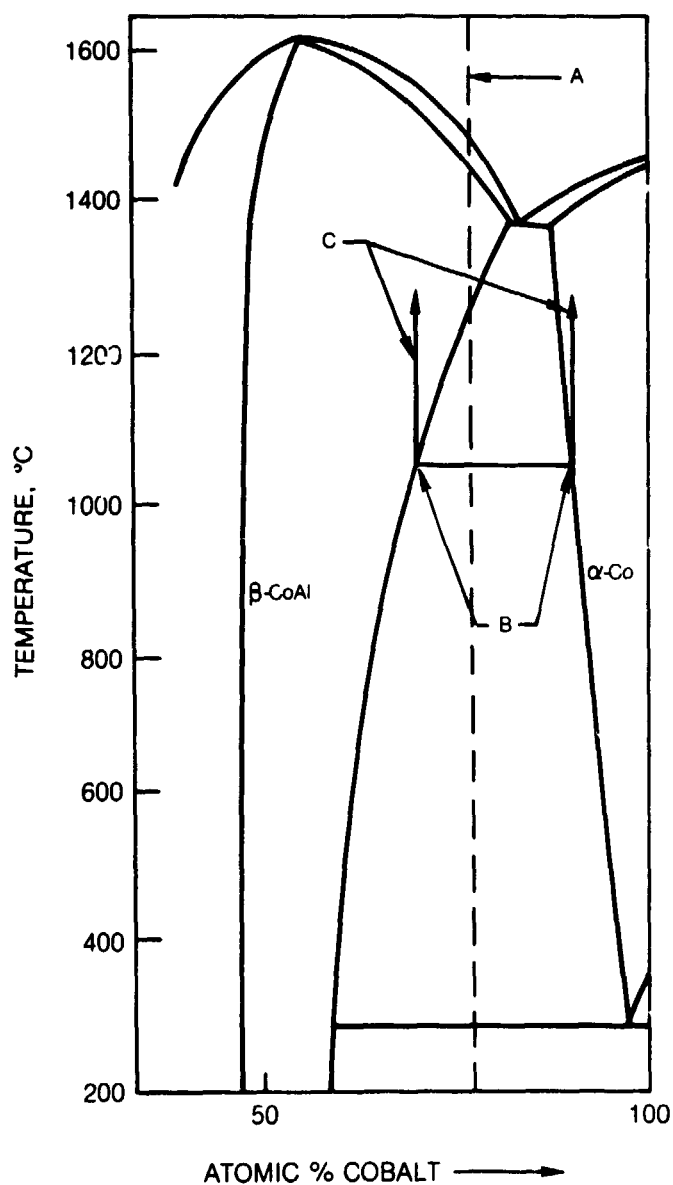


FIG. 37 Partial phase diagram for the aluminum-cobalt system (Ref. 40).

- A. Approximate overall composition of CoCrAlY (neglecting chromium)
- B. Approximate composition of  $\alpha$ -cobalt and  $\beta$ -CoAl after 4 hours 1975°F (1080°C) heat treatment
- C. Effect of thermal spike on the composition of  $\alpha$ -cobalt and  $\beta$ -CoAl.

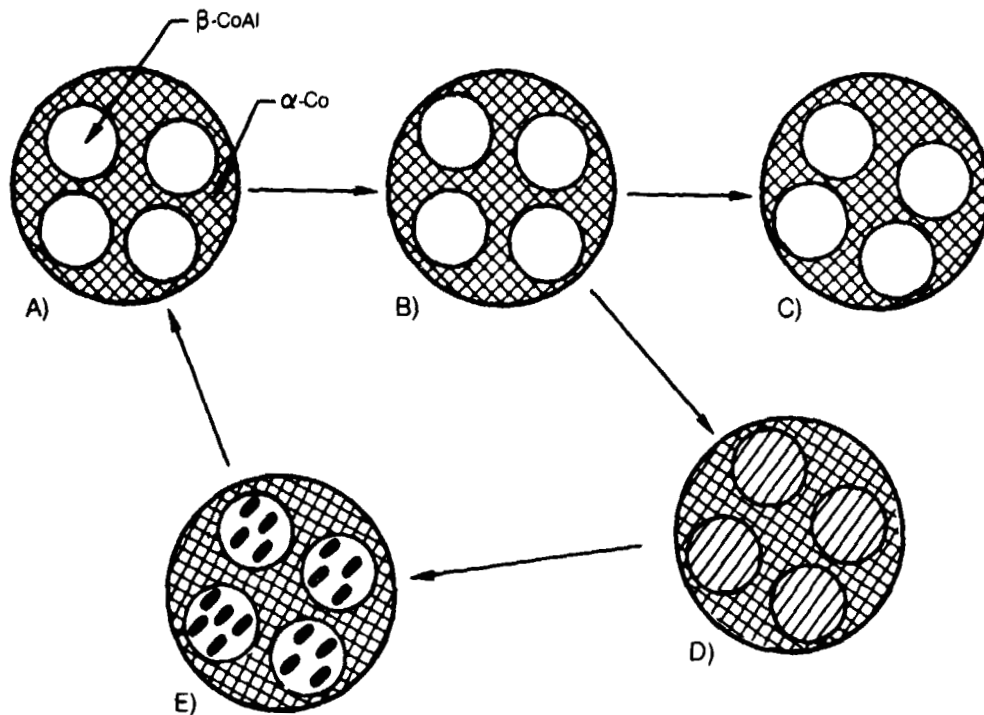


FIG. 38 Effect of thermal history on coating microstructure

#### Thermal History

- A: As-processed CoCrAlY coating microstructure
- B: A-immediately after a thermal transient
- C: B-aged at too low a temperature to effect precipitation
- D: B-aged at an appropriate temperature to produce a lamellar structure via discontinuous precipitation effects
- E: D (or B)-aged at higher temperature results in lamellar structure coarsening
- A: E (or B, C, and D) exposed to too high a temperature will revert to original microstructure, A.

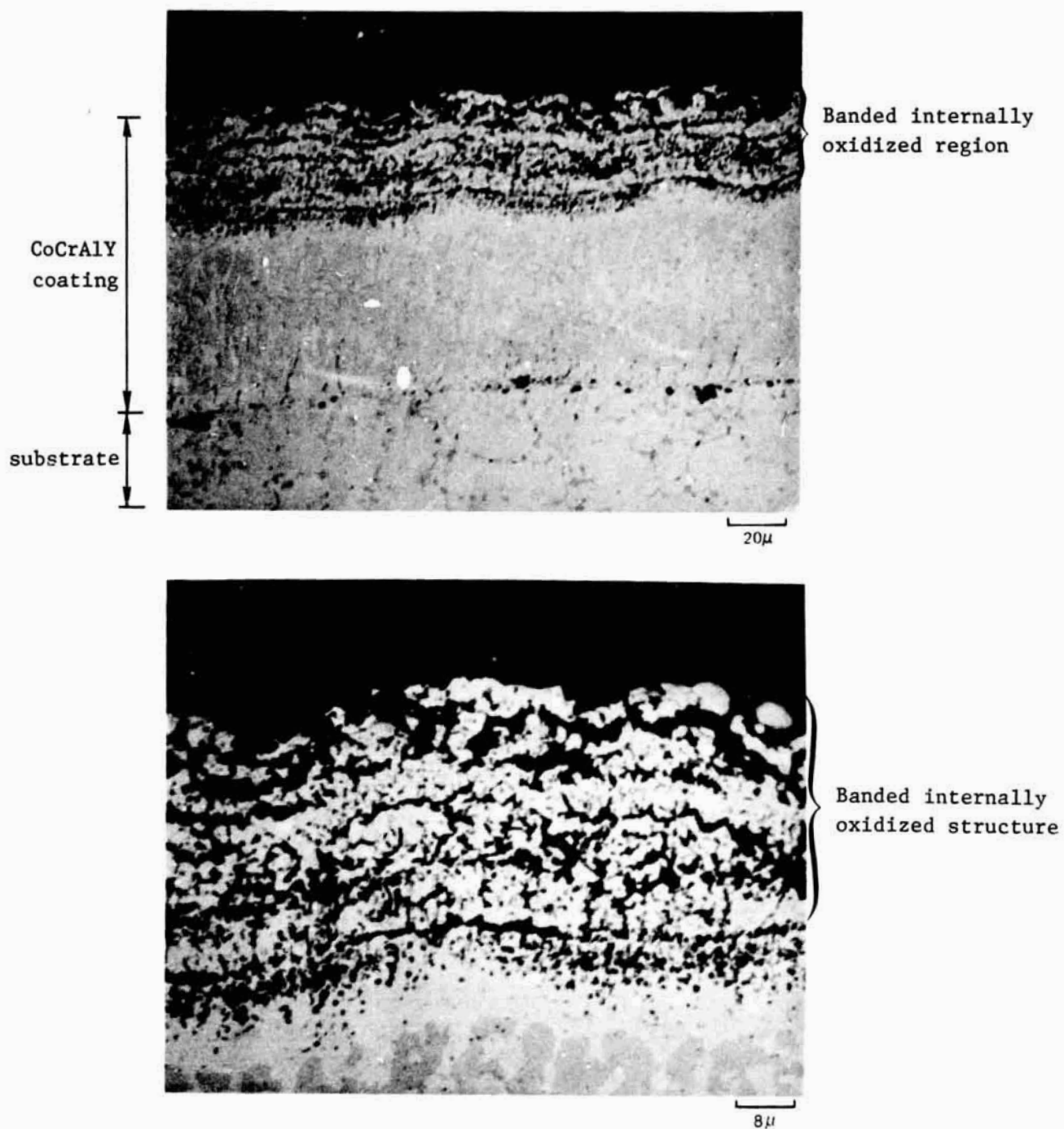


FIG. 39 Banding produced in CoCrAlY coatings by thermal transients and NaCl(g).  
CoCrAlY thermally spiked fifty times and aged at 300°C in air with 100ppm NaCl(g).





FIG. 40 Pitting attack of CoCrAlY after 58 cycles showing the presence of a retained substrate morphology in the oxide pit coincident with the prior  $\alpha$ -Co grains in the CoCrAlY coating (A), prior corrosion front images (B) and  $\beta$ -cobalt islands in the oxide pit (C). (Scanning electron micrograph)



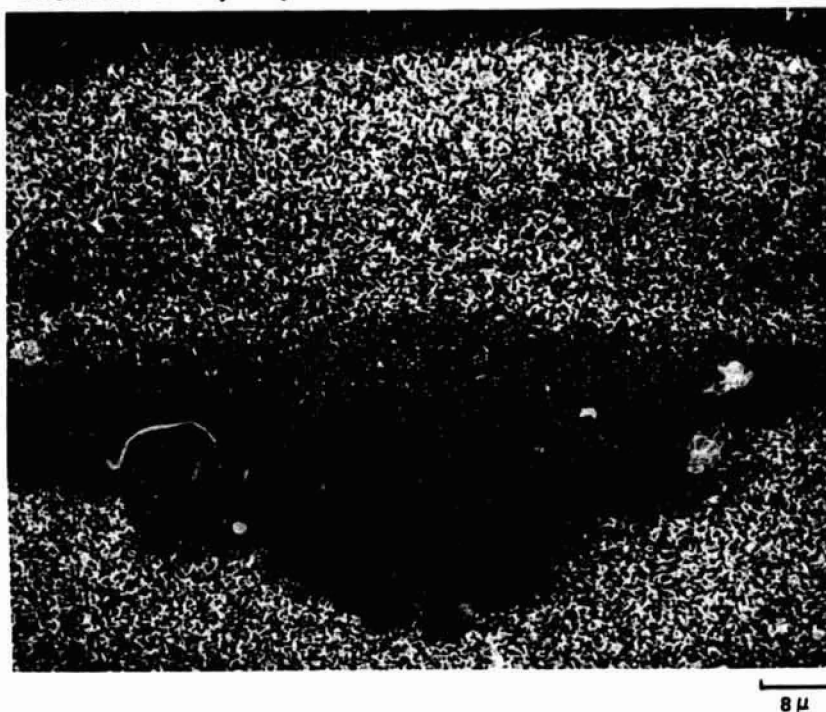
FIG. 41 Pitting Attack of CoCrAlY

Laboratory Test (131 cycles\*)

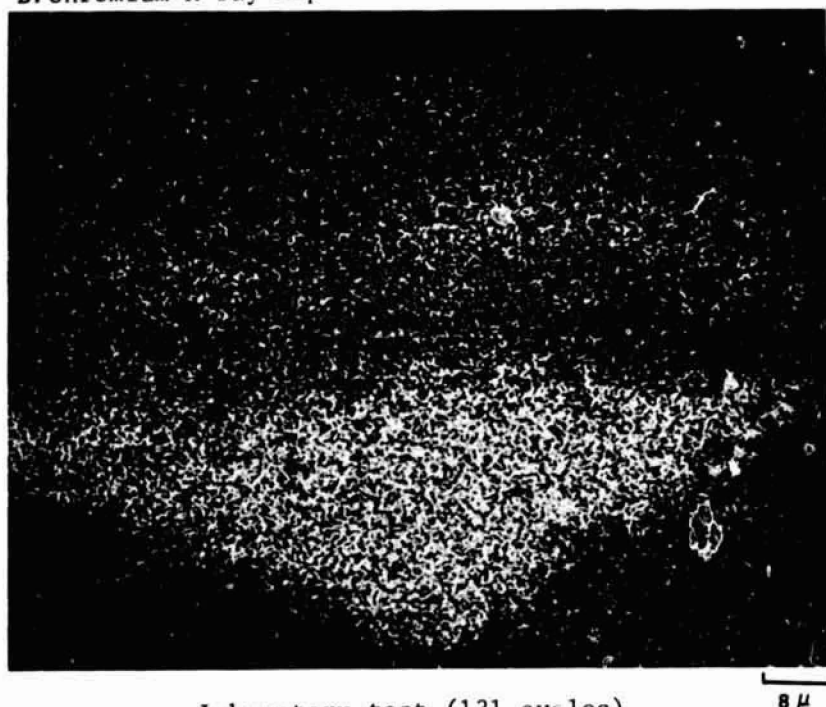
- A.  $\alpha$ -Co(Cr) solid solution
- B.  $\beta$ -CoAl
- C. Islands of  $\alpha$ -cobalt in inner oxide zone
- D. Al-enriched grain, cf. Figure 43
- E. Cr-enriched grain, cf. Figure 43
- F. Al-enriched oxide striations in the inner oxide zone

\*(1 cycle: Exposure at 1300°C in a preheated furnace for 30 seconds with intervening time spent in furnace at 700°C, sodium sulfate (~1 mg/cm<sup>2</sup>) deposits reapplied every 15 cycles, fuel applied each cycle.)

A. Cobalt X-ray Map



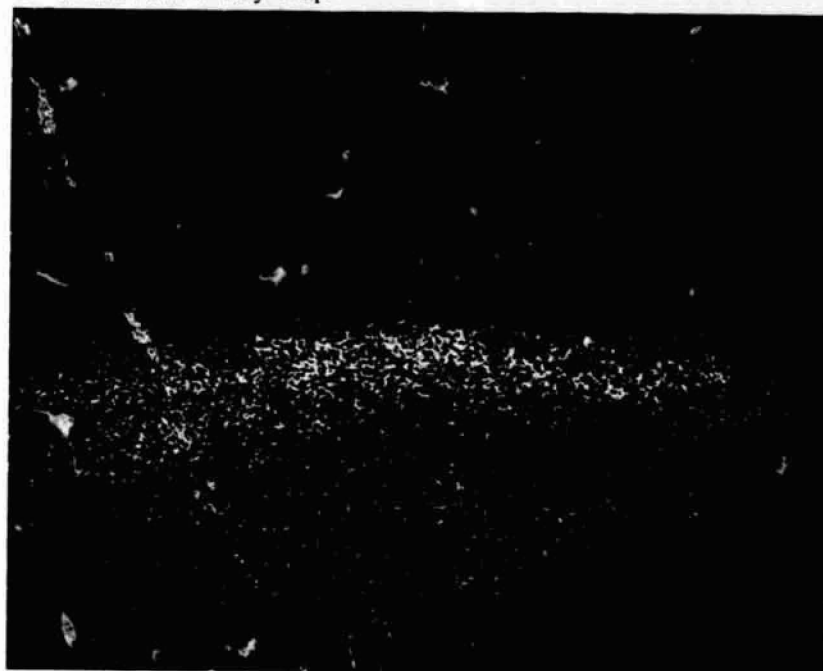
B. Chromium X-ray Map



Laboratory test (131 cycles)

FIG. 41 Pitting attack of CoCrAlY coating.

C. Aluminum X-ray Map



8  $\mu$

D. Sulfur X-Ray Map

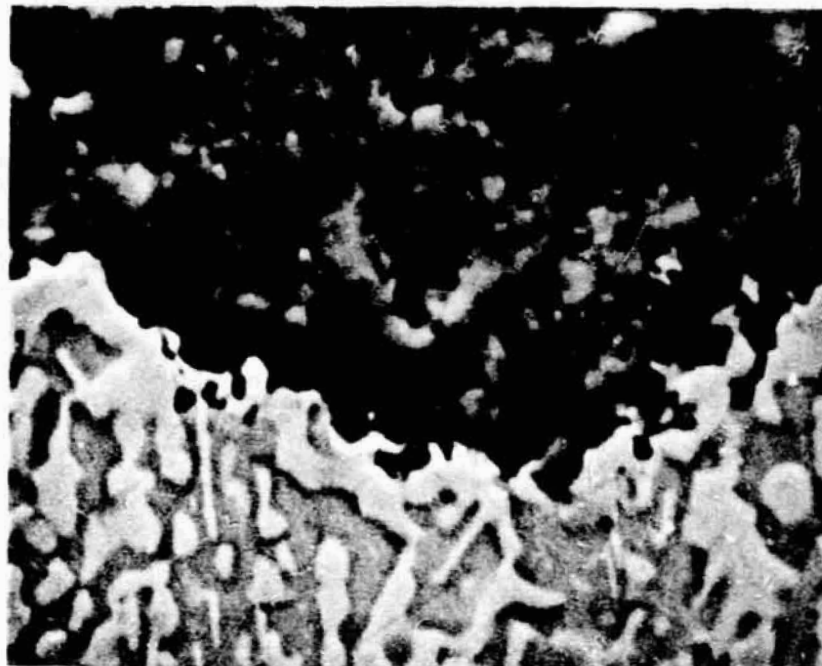


Laboratory test (131 cycles)

8  $\mu$

FIG. 41 Pitting attack of CoCrAl<sup>v</sup> coating.

Scanning electron micrograph

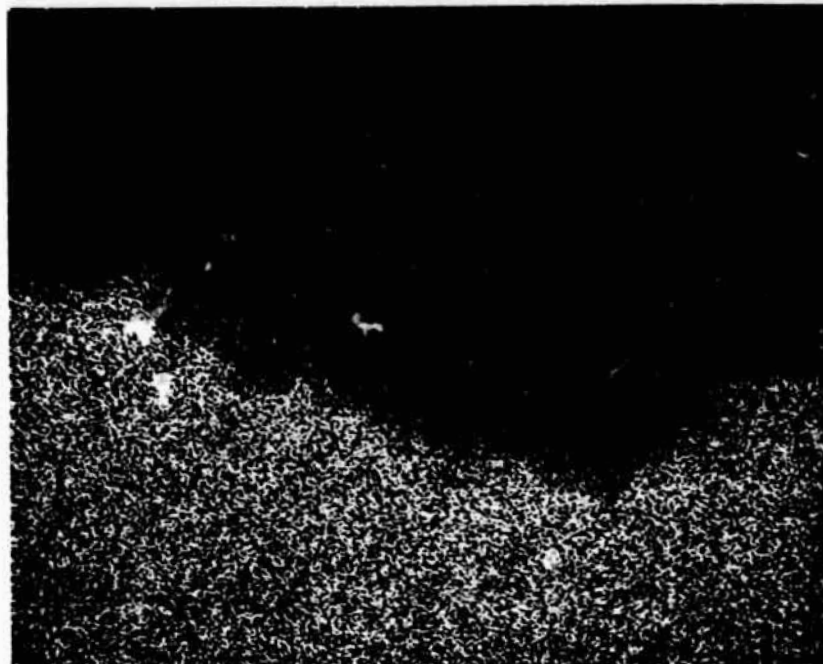


Laboratory test (131 cycles)

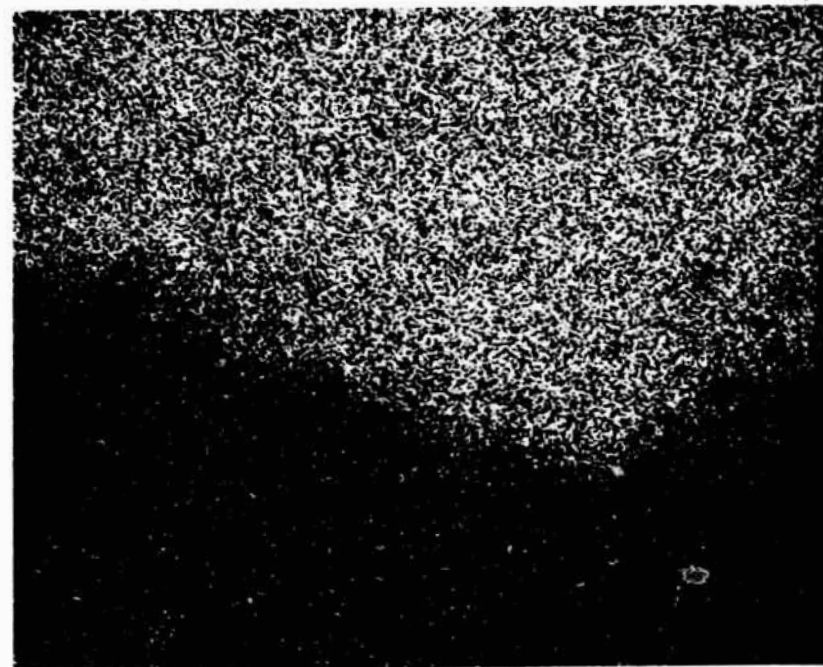
2.5μ

FIG. 42 Metallographic studies of the base of the oxide pit, cf. FIG. 41.

A. Cobalt X-ray Map



B. Chromium X-ray Map



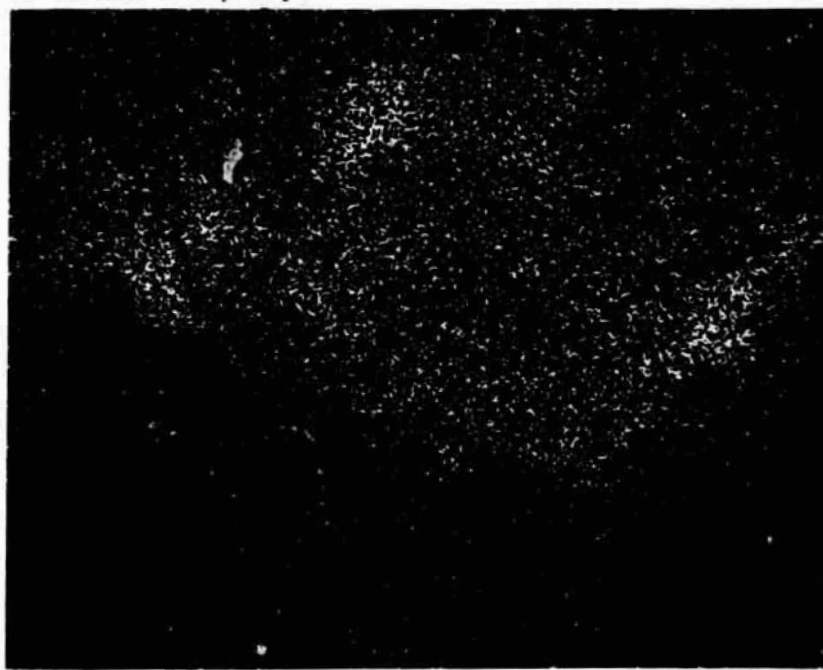
Laboratory test (131 cycles)

FIG. 42 Base of oxide pit, cf. FIG. 41.

C. Aluminum X-Ray Map



D. Sulfur X-ray Map

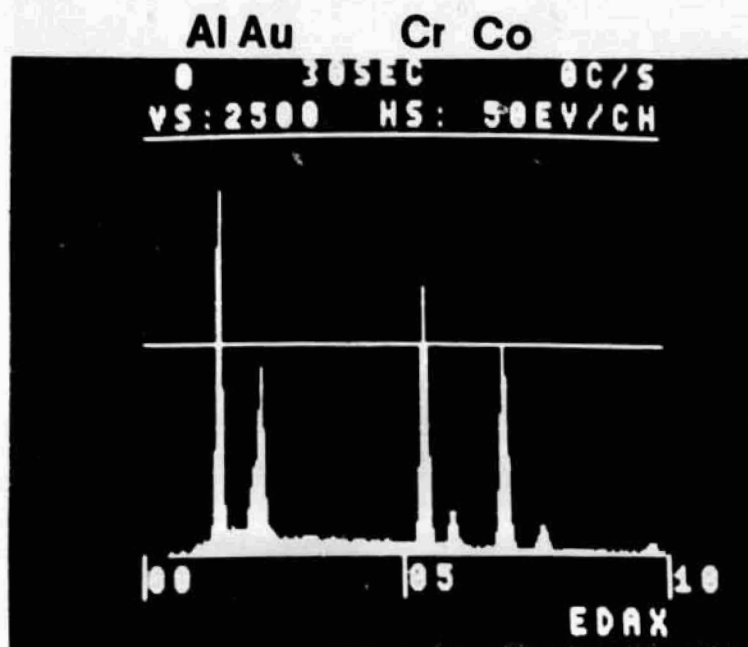


Laboratory test (131 cycles)

2.5μ

FIG. 42 Base of oxide pit, cf. FIG. 41.

A



B

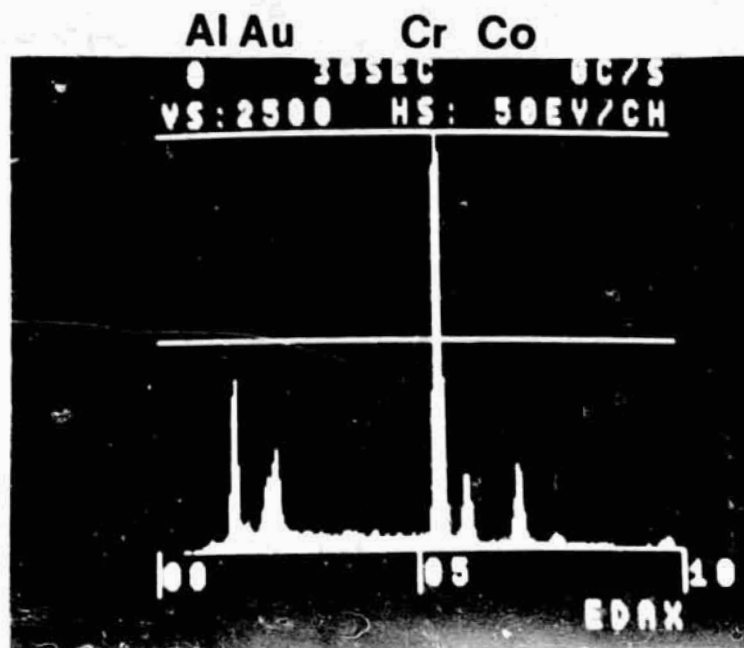


FIG. 43 Energy dispersive X-ray (EDAX) analysis of bi-phasic layer showing: A. Aluminum-rich grain, cf. FIG. 41  
B. Chromium-rich grain, cf. FIG. 41



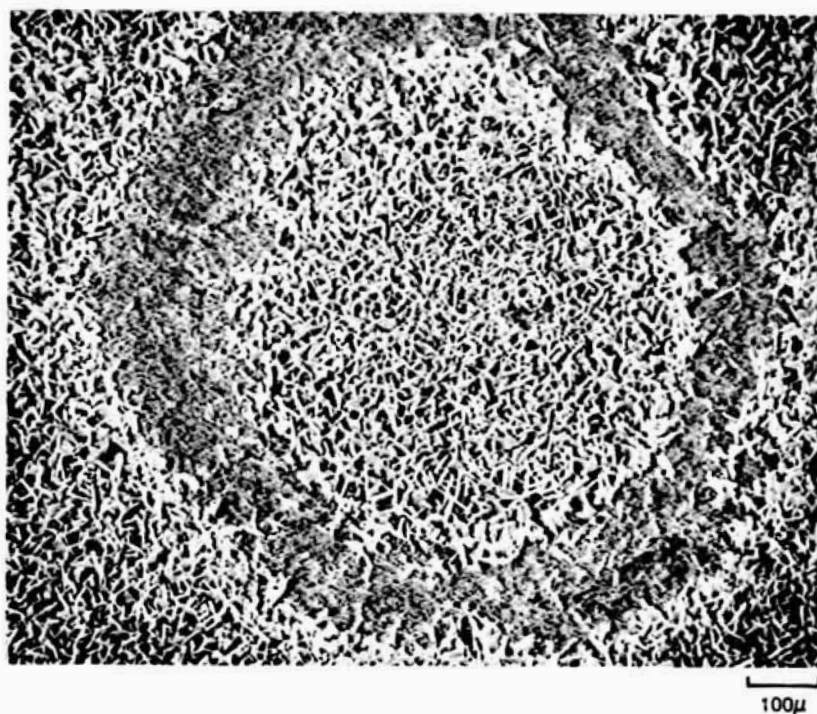


FIG. 44 Morphology of growth colonies of  $\text{Cr}_2\text{O}_3$  crystal platelets.  $\text{Na}_2\text{SO}_4$ -coated ( $0.56 \text{ mg/cm}^2$ ) Ni-25Cr oxidized at  $1050^\circ\text{C}$  for 25 hours, cf. Fig 100 in Ref. 13.

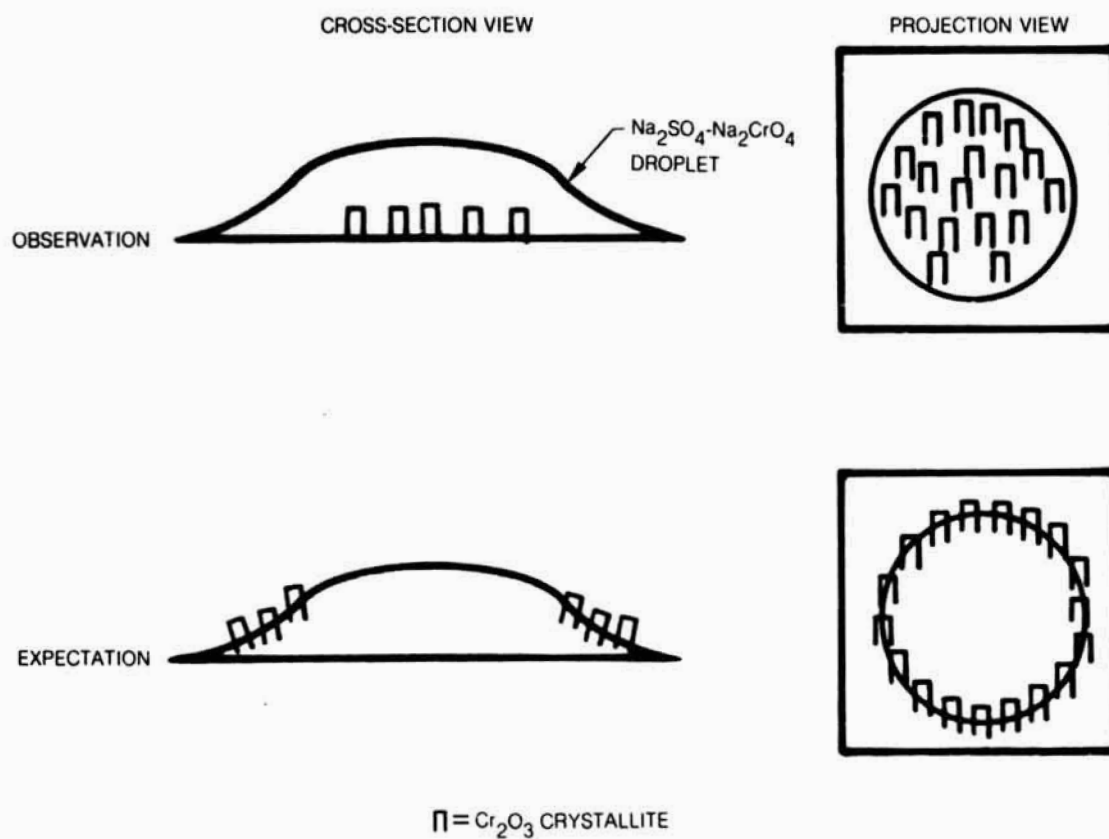


FIG. 45 Expected  $\text{Cr}_2\text{O}_3$  crystal growth from a droplet, cf. FIG. 44

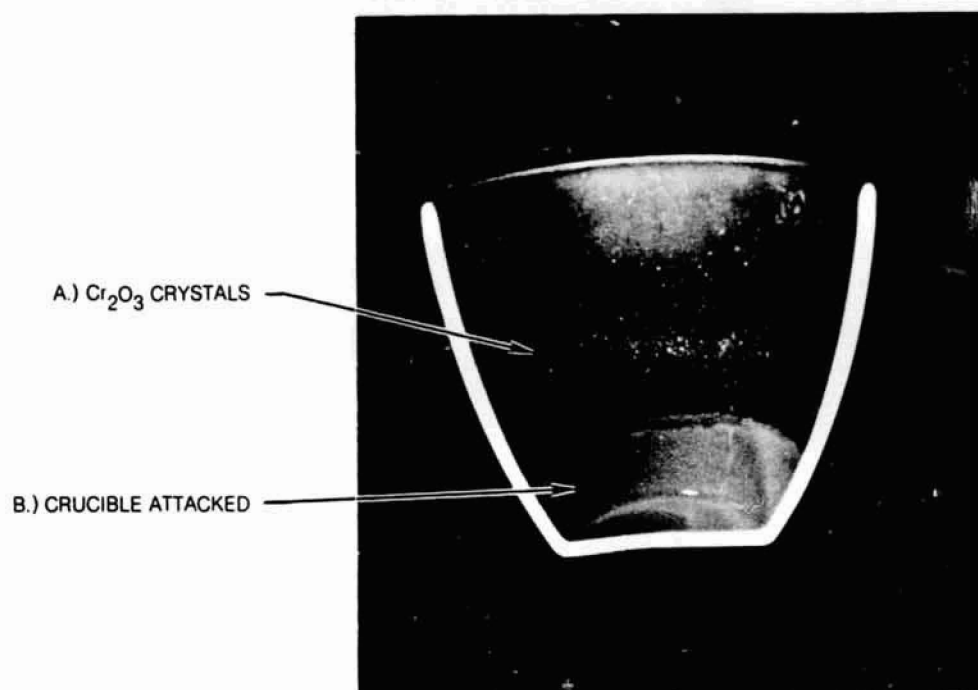
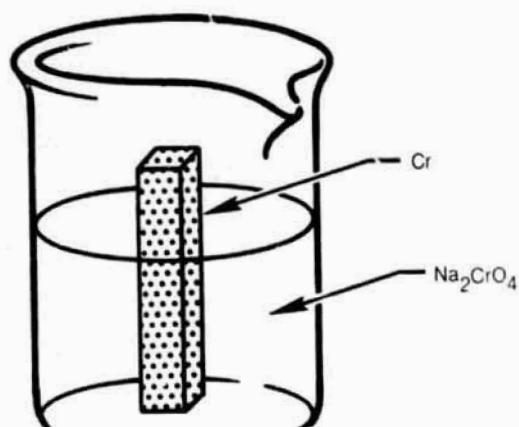


FIG. 46 Production of (A) Cr<sub>2</sub>O<sub>3</sub> crystals by means of (B) an oxide ion sink (a glazed crucible).



1000°C, 1 WEEK Pt CRUCIBLE

SUBMERGED  
SECTION

MENISCUS

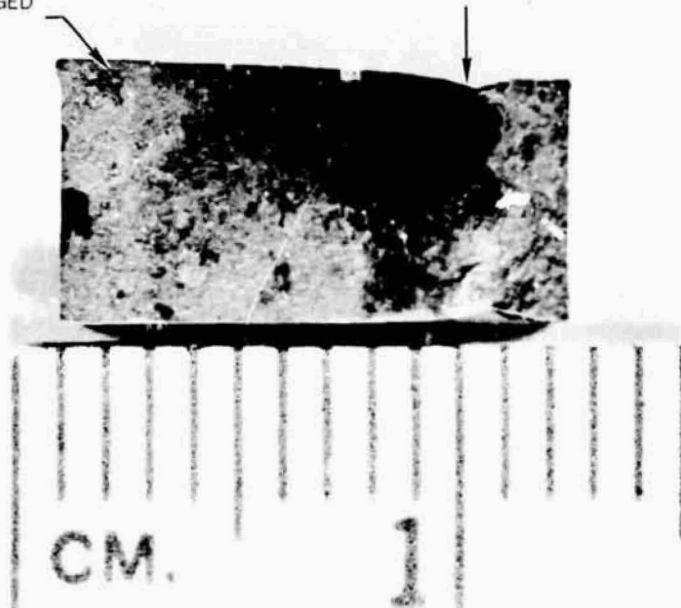
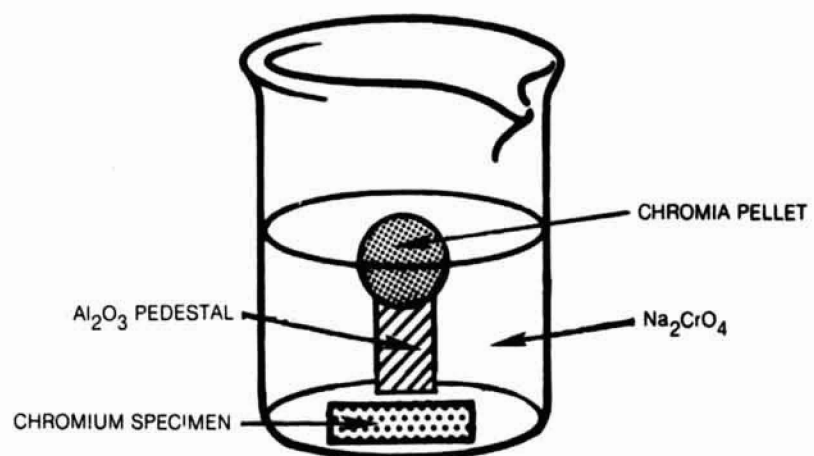


FIG. 47 Chromium partially immersed in Na<sub>2</sub>CrO<sub>4</sub> showing attack at meniscus.



ORIGINALLY SPHERICAL PELLET SHOWING PARTIAL DISSOLUTION EFFECTS AFTER 1 WEEK AT 1000°C

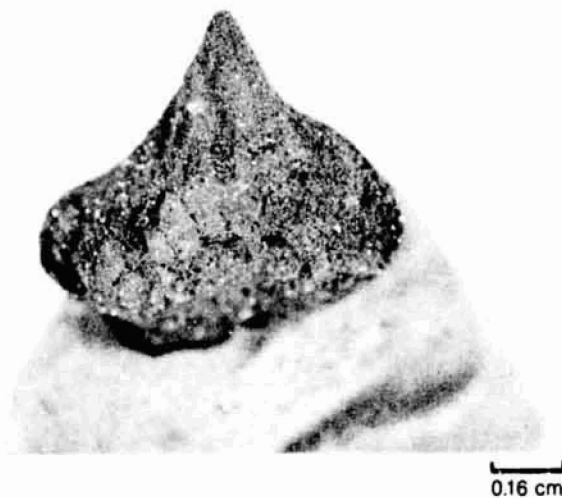


FIG. 48 Chromia pellet serving as oxygen transport medium